

EFFECTS OF SEISMIC SOURCE MODEL PARAMETERS ON THE
PROBABILISTIC SEISMIC HAZARD ASSESSMENT RESULTS

A THESIS SUBMITTED TO
THE GRADUATE SCHOOL OF NATURAL AND APPLIED SCIENCE
OF
MIDDLE EAST TECHNICAL UNIVERSITY

BY
MARJAN VAKILINEZHAD

IN PARTIAL FULFILLMENT OF THE REQUIREMENTS
FOR
THE DEGREE OF MASTER OF SCIENCE
IN
CIVIL ENGINEERING

APRIL 2015

Approval of the thesis:

**EFFECTS OF SEISMIC SOURCE MODEL PARAMETERS ON THE
PROBABILISTIC SEISMIC HAZARD ASSESSMENT RESULTS**

submitted by **MARJAN VAKILINEZHAD** in partial fulfillment of the requirements for the degree of **Master of Science in Civil Engineering Department, Middle East Technical University** by,

Prof. Dr. Gülbin Dural Ünver
Dean, Graduate School of **Natural and Applied Science**

Prof. Dr. Ahmet Cevdet Yalçiner
Head of Department, **Civil Engineering**

Assoc. Prof. Dr. Zeynep Gülerce
Supervisor, **Civil Engineering Dept., METU**

Examining Committee Members:

Prof. Dr. M. Yener Özkan
Civil Engineering Dept., METU

Assoc. Prof. Dr. Zeynep Gülerce
Civil Engineering Dept., METU

Prof. Dr. Kemal Önder Çetin
Civil Engineering Dept., METU

Asst. Prof. Dr. N. Kartal Toker
Civil Engineering Dept., METU

Asst. Prof. Dr. A. Arda Özacar
Geological Engineering Dept., METU

Date: 16.04.2015

I hereby declare that all information in this document has been obtained and presented in accordance with academic rules and ethical conduct. I also declare that, as required by these rules and conduct, I have fully cited and referenced all material and results that are not original to this work.

Name, Last name: Marjan Vakilinezhad

Signature:

ABSTRACT

EFFECTS OF SEISMIC SOURCE MODEL PARAMETERS ON THE PROBABILISTIC SEISMIC HAZARD ASSESSMENT RESULTS

Vakilinezhad, Marjan

M.S., Department of Civil Engineering

Supervisor: Assoc. Prof. Dr. Zeynep Gülerce

April 2015, 81 pages

The inputs to the Probabilistic Seismic Hazard Analysis (PSHA) contain large uncertainties regarding the seismic source model parameters; therefore, the results may vary significantly due to subjective judgment and interpretation of the limited data. The objective of this study is to show the effect of seismic source model on the hazard results by quantifying the difference in the design ground motions for different risk levels at different locations around an active tectonic structure. Analysis showed that the variances in the hazard results obtained by different seismic source models are closely correlated with the location and hazard level. Additionally, sensitivity of the hazard results to the uncertainties involved in each source parameter, especially the source zone boundaries, annual slip rate, maximum and minimum magnitudes, fault width, b-value and scenario weights are analyzed and presented to provide insight on the relative contribution of source or fault parameters to the PSHA results. Finally, design ground motions for other spectral periods obtained by different seismic source models are compared with the Turkish Earthquake Code (TEC, 2007) requirements. The calculated uniform hazard

spectrum (UHS) for almost all sites is lower than the TEC-2007 design spectrum, except for the near field sites. Results indicated that the difference between the spectra decreases as the distance between the site and source increases.

Keywords: Probabilistic Seismic Hazard Analysis, Seismic Source Characterization, Earthquake Catalogue, North Anatolian Fault, 1939 Erzincan Earthquake

ÖZ

SİSMİK KAYNAK MODELİ PARAMATRELERİNİN OLASILIKSAL SİSMİK TEHLİKE ANALİZİ SONUÇLARI ÜZERİNDEKİ ETKİSİ

Vakilenezhad, Marjan

Yüksek Lisans, İnşaat Mühendisliği Bölümü

Tez Yöneticisi: Doç. Dr. Zeynep Gülerce

Nisan 2015, 81 Sayfa

Olasılıksal Sismik Tehlike Analizi'nin (OSTA) önemli girdilerinden biri olan sismik kaynak modellerinin parametrelerinin belirlenmesinde oldukça büyük belirsizlikler söz konusudur. Eldeki limitli verilerin sübjektif olarak yorumlanması sonucunda aynı saha için elde edilen OSTA sonuçları çok değişebilir. Bu çalışmanın amacı, sismik kaynak modelinin değişik lokasyonlarda ve çeşitli risk seviyelerinde yer alan yapılar için tasarımda kullanılacak kuvvetli yer hareketi mertebeleri üzerindeki etkisini nicel olarak göstermektir. Analiz sonuçlarına göre, farklı sismik kaynak modelleri kullanılarak elde edilen OSTA çıktıları birbirlerinden oldukça farklıdır ve bu farklılık sahanın tektonik yapıya olan uzaklığı ve göz önünde bulundurulan tehlike düzeyi ile ilişkilidir. Buna ek olarak, OSTA sonuçlarının sismik kaynak parametrelerine (kaynak geometrisi, yıllık kayma hızı, minimum ve maksimum deprem büyüklüğü, fay düzlemi genişliği, b-değeri ve senaryo ağırlıkları gibi) karşı hassasiyeti analiz edilmiş ve bu parametrelerin sonuca olan görece katkısı incelenmiştir. Son olarak, tüm spektral periyodlar için değişik sismik kaynak modelleri kullanılarak belirlenen tasarım yer hareketleri, Deprem Bölgelerinde Yapılacak Binalar Hakkında Yönetmelik'de (TEC, 2007) önerilen tasarım eğrileri ile

karşılaştırılmıştır. Bu çalışmada hesaplanan neredeyse tüm eşdeğer tepki spektrumu değerleri (faya yakın sahalar hariç) TEC-2007 tasarım değerlerine kıyasla daha düşüktür. Çalışma sonucunda aradaki farkın mertebesinin tektonik yapıya olan uzaklık ile yakından ilişkili olduğu belirlenmiştir.

Anahtar Kelimeler: Olasılıksal Sismik Tehlike Analizi, Sismik Kaynak Modelleri, Deprem Katalođu, Kuzey Anadolu Fay Hattı (KAF), 1939 Erzincan Depremi

To my Beloved Family

ACKNOWLEDGEMENTS

I would like to thank my advisor Assoc. Prof. Dr. Zeynep Gülerce for her guidance, support and understanding during each step in the preparation of this thesis.

I would also like to thank Dr. Norman Abrahamson, for his invaluable guidance in providing the hazard code.

I am very grateful to Dr. Arda Arcasoy for his help during the preparation of digitized active fault maps in ArcGIS software.

Special thanks to Can Acar for his support, at even the most desperate times during the preparation of this thesis.

At last and most important, sincere thanks to my beloved family who did not avoid their support, guidance, understanding and protection at any time during this period.

TABLE OF CONTENTS

ABSTRACT	V
ÖZ.....	VII
ACKNOWLEDGEMENTS	X
TABLE OF CONTENTS:	XI
LIST OF FIGURES:	XIII
LIST OF TABLES:.....	XVI
LIST OF ABBREVIATIONS:.....	XVII
CHAPTERS	
1. INTRODUCTION	1
1.1. Previous PSHA Practice around Turkey in Regional and Global Scale	2
1.2. Previous Studies on the Sensitivity of PSHA Results to Input Source Model	5
1.3. Research Statement.....	8
1.4. Scope.....	9
2. ALTERNATIVE SEISMIC SOURCE CHARACTERIZATION MODELS FOR THE 1939 ERZINCAN EARTHQUAKE RUPTURE ZONE.....	11
2.1. Magnitude Distribution Models for Areal and Planar Seismic Sources	12
2.1.1. Truncated Exponential Model	12
2.1.2. Truncated Normal Model (Characteristic Model)	12
2.1.3. Composite Model (Youngs and Coppersmith, 1985).....	13
2.2. Seismic Source Characterization for 1939 Erzincan Earthquake Rupture Zone	14
2.2.1. Model 1: Areal source geometry with truncated exponential magnitude recurrence model.....	24
2.2.2. Model 2: Planar source geometry including a buffer zone for small-to-moderate magnitude events	25
2.2.3. Model 3: Planar source geometry	26

2.3. Ground Motion Characterization.....	29
2.3.1. TR-Adjusted Abrahamson and Silva (2008) (TR-AS08) Model.....	31
2.4. PSHA Methodology and Software	32
2.5. Comparison of the hazard results using different seismic source characterization models	33
3. EFFECT OF SOURCE MODEL PARAMETERS ON THE PSHA RESULTS	35
3.1. Model 1 - Areal source geometry with truncated exponential magnitude recurrence model	35
3.1.1 Sensitivity analysis for the effect of source boundary.....	36
3.1.2. Sensitivity analysis for the effect of b-value	37
3.1.3. Sensitivity analysis for the effect of maximum magnitude	38
3.1.4 Sensitivity analysis for the effect of minimum magnitude.....	39
3.1.5 Sensitivity analysis for effect of depth of the source zone	41
3.2. Model 2 - Planar source geometry including a buffer zone for small-to- moderate magnitude events	41
3.2.1. Effect of buffer zone dimensions and threshold magnitude	43
3.2.2. Fault model parameters	43
3.3. Model 3 - Planar fault geometry with TE or Composite magnitude distribution.....	47
3.3.1. Sensitivity analysis for the effect of annual slip rate.....	48
3.3.2. Sensitivity analysis for the effect of fault width.....	51
3.3.3. Sensitivity analysis for the effect of scenario weights	51
3.3.4. Sensitivity analysis for maximum and characteristic magnitudes.....	54
3.3.5. Sensitivity analysis for the effect of b-value and M_{min}	55
4. DESIGN GROUND MOTIONS BASED ON DIFFERENT SEISMIC SOURCE MODELS: A COMPARISON WITH TURKISH EARTHQUAKE CODE (2007) REQUIREMENTS	61
5. SUMMARY AND DISCUSSION.....	69
REFERENCES.....	73

LIST OF FIGURES

FIGURES

Figure 1.1: Seismic source regionalization for Turkey.....	3
Figure 1.2: Fault segmentation model proposed for the Marmara region	3
Figure 1.3: Area source model geometry colored by tectonic regimes	4
Figure 1.4: Accelerations calculated to have a 90 percent probability of not being exceeded during time periods of 10, 50, 250, and 1000 yr.	6
Figure 1.5: Accelerations calculated to have a 90 per cent probability of not being exceeded during various time periods at sites on a line perpendicular to the center of a 300-km-long fault.....	7
Figure 1.6: Annual ground motion exceedances a) calculated at a site for two alternative source zone scenarios and b) calculated for a site 10 km away from the center of a 280 km long fault using different M_{max} and b-values.	8
Figure 2.1: Rupture zones of the consecutive 1939-1943 earthquakes on North Anatolian Fault Zone. Stars show the approximate locations of epicenters	15
Figure 2.2: Slip distribution along the rupture zone of the 1939 Erzincan earthquake	15
Figure 2.3: Creep distribution graphics measured by various researches according to the segments of the 1939 Erzincan Earthquake rupture.....	16
Figure 2.4: Sub-Segments of the 1939 rupture zone of NAF	18
Figure 2.5: Comparison of rupture scenarios and weighted average scenario including Weichert (1980) error bars.....	19
Figure 2.6: Slip vectors along the NAF by various studies.	20
Figure 2.7: The Niksar-Erzincan segment of the NAF. The sub-segments and associated slip rates are indicated on the map.....	22
Figure 2.8: The catalogue completeness analysis for the earthquake catalog.	23
Figure 2.9: 10-km buffer zone around the 1939 earthquake rupture zone fault that is used as the areal source for Model 1 and the seismicity in the region.....	24

Figure 2.10: 5-km Buffer zone used for the Model 2 of this study and seismicity in the region.	26
Figure 2.11: Different magnitude recurrence models for the weighted combination of the rupture scenarios of Niksar-Erzincan segment of NAF.....	29
Figure 2.12: Hazard curves for Models 1, 2, 3a, 3b, and 3c of this study.	34
Figure 3.1: Effect of changing the source zone boundaries (using buffer zones of 5-10-15 km around the fault line) on the hazard for 2% and 10% chance of exceeding in 50 years.	37
Figure 3.2: hazard curves for different b-values (ranging between 0.4-1.2)	38
Figure 3.3: hazard curves for different maximum magnitudes (ranging between 7.2 and 8.2)	39
Figure 3.4: hazard curves for different minimum magnitudes (4, 4.5, and 5).....	40
Figure 3.5: Annual exceedance of various levels of PGA calculated for $M_{\min}= 4.0$ and $M_{\min}= 5.0$	41
Figure 3.6: Sensitivity of the hazard to different parameters of areal source zone: (a) b-value, (b) M_{\max} , (c) M_{\min} and (d) depth.	42
Figure 3.7: Effect of changing the buffer zone boundaries (buffer zones of 5-10-15 km around the fault line) on the hazard	44
Figure 3.8: Effect of changing the slip rates (ranging between 15 to 24 mm/yr) on the hazard.	45
Figure 3.9: Effect of changing the fault width (ranging between 8 and 20 km) on the hazard.....	45
Figure 3.10: Effect of changing the scenario weights on the hazard.....	46
Figure 3.11: Effect of changing the characteristic magnitude (ranging between 7.2 and 8.2) on the hazard.....	46
Figure 3.12: Sensitivity of the hazard to different parameters of Model 2: (a) annual slip rate, (b), fault width (c) scenario weighing factors, and (d) M_{char}	47
Figure 3.13: Effect of changing the slip rates (ranging between 15 and 24 mm/yr) on the hazard for Model 3a with $R_{\text{rup}} = 5$ km for figures (a), (c), (e) and $R_{\text{rup}} = 50$ km for figures (b), (d) and (F).	49
Figure 3.14: Effect of changing the slip on the hazard for Model 3b with $R_{\text{rup}} = 5$ km for figures (a), (c), (e) and $R_{\text{rup}} = 50$ km for figures (b), (d) and (F).	50

Figure 3.15: Effect of changing the fault width of Model 3a (ranging between 8 km and 20 km) on the hazard	52
Figure 3.16: Effect of changing the fault width of Model 3b (ranging between 8 km and 20 km) on the hazard	52
Figure 3.17: Effect of changing the scenario weights of Model 3a on the hazard....	53
Figure 3.18: Effect of changing the scenario weights of Model 3b on the hazard ...	53
Figure 3.19: Effect of changing the M_{max} of Model 3a on the hazard.	54
Figure 3.20: Effect of changing the M_{char} of Model 3b on the hazard.....	55
Figure 3.21: Effect of changing the b value on the hazard at a site with (a) $R_{rup} = 5$ km and (b) $R_{rup} = 50$ km and M_{min} at a site with (c) $R_{rup} = 5$ km and (d) $R_{rup} = 50$ km for Model 3a.....	55
Figure 3.22: Effect of changing the b value on the hazard at a site with (a) $R_{rup} = 5$ km and (b) $R_{rup} = 50$ km and M_{min} at a site with (c) $R_{rup} = 5$ km and (d) $R_{rup} = 50$ km for Model 3b.....	56
Figure 3.23: Sensitivity of the hazard to different parameters of Model 3a.	58
Figure 3.24: Sensitivity of the hazard to different parameters of Model 3b.....	59
Figure 4.1: Location of the selected sites with respect to the first, second, third and fourth seismic zones depicted in Seismic Zoning Map of Turkey.....	63
Figure 4.2: The procedure used in developing the UHS.....	64
Figure 4.3: UHS for the (a): Site 20, (b): Site 8, (c): Site 7, (d): Site 9, (e): Site 18, (f): Site 6, (g): Site 17, (h): Site 22	66
Figure 4.4: UHS for the sites located within the boundaries of (a): Zone 1, (c): Zone 2, (e): Zone 3, (g): Zone 4 for Model 3b and, (b): Zone 1, (d): Zone 2, (f): Zone 3, (h): Zone 4 for Model 1.....	67
Figure 4.5: UHS for Site 19, 20 and 21 of this study.....	68

LIST OF TABLES

TABLES

Table 2.1: Segment geometry, assigned slip rate and characteristic magnitude for each segment.....	20
Table 2.2: Maximum likelihood estimation of the regional “b-value”	23
Table 2.3: Maximum likelihood estimation of the zone specific “b-value”	25
Table 2.4: 1939 Earthquake Rupture Zone with associated scenarios and assigned weights..	28
Table 3.1: Parameters assigned to source zones with different source boundaries. .	36
Table 3.2: Activity rates used in the analyses for different minimum magnitudes ..	40
Table 4.1: Closest distance to the fault and seismic zones of the selected sites	62

LIST OF ABBREVIATIONS

GEM	Global Earthquake Model
GMPE	Ground Motion Prediction Equation
GSHAP	Global Seismic Hazard Assessment Program
LL	Lower Limit
LLNL	Lawrence Livermore National Laboratory
NAF	North Anatolian Fault
NGA	Next Generation Attenuation
PSHA	Probabilistic Seismic Hazard Assessment
SHARE	Seismic Hazard Harmonization in Europe
TE	Truncated Exponential
TEC	Turkish Earthquake Code
UHS	Uniform Hazard Spectra
UL	Upper Limit

CHAPTER 1

INTRODUCTION

The inputs to the Probabilistic Seismic Hazard Analysis (PSHA) contain large uncertainties regarding the seismic source model parameters; therefore, the results may vary significantly due to subjective judgment and interpretation of the limited data. Bender and Perkins (1993) stated that “different analysts may make very different interpretations and selections” and “seismic hazard estimates obtained for a single site may vary significantly” based on the examples by EPRI/SOG (1987) and Lawrence Livermore National Laboratory (LLNL) (Bernreuter et al. 1987, 1989). Bender and Perkins (1993) observed a factor of two to factor of five times difference between the median hazard estimates of the same sites when they compared the results of LLNL and EPRI/SOG studies. Since the beginning of 1990’s, the number of PSHA studies conducted both in global and regional scale increased exponentially; however, the differences between the estimations of proponent modelers are still large (e.g., Probabilistic Seismic Hazard Analysis for Swiss Nuclear Power Plant Sites (PEGASOS)) and the ways to “reasonably” capture this epistemic uncertainty is still a subject of debate.

In the PSHA framework, it is possible to identify, quantify and combine the uncertainties in the size, location, and occurrence rate of earthquakes, uncertainties in the seismogenic source geometry, and variability of the ground motion as a function of the size and location of earthquakes (Kramer, 1996). Currently, there are many software packages available for hazard analysis (Seisrisk III, EZFrisk, etc.) and the analysts can implement the seismic source and ground motion models easily using the embedded data in the software to give estimates of the design ground motions at any site. Nevertheless, the hazard analysts should be utterly familiar with all aspects of the PSHA to develop a common sense on the sensitivity of the hazard

outcome to different source models and model parameters to be able to provide “reasonable” hazard estimates. Identification of the input parameters with the highest impact on the hazard may help reducing the calculation time and, more importantly, help the analyst to determine the range and logic tree weights of the source model parameters to be included in the logic tree.

1.1. Previous PSHA Practice around Turkey in Regional and Global Scale

The PSHA studies conducted for Turkey were limited with the initiative nation-wide works of Erdik et al. (1985) and Gülkan et al. (1993) before the 1999 Kocaeli and Düzce earthquakes. Several researchers published estimates of seismic hazard and risk for the Marmara Region and for Istanbul after these events (e.g. Atakan et al. 2002; Erdik et al. 2004; Crowley and Bommer 2006; Kalkan et al. 2009). The approaches used in in these studies for seismotectonic modeling were consistent with the global PSHA practice. In some regions like Eastern United States, the association of earthquakes with tectonic structures is uncertain; therefore, recorded earthquakes are often used to delineate source zones. For these regions, the earthquake catalogues are the largest contributor to the uncertainty in seismic source characterization models. On the other hand, paleoseismic recurrence intervals and geologic slip rates have been used to estimate the seismic activity of the faults in areas like Western United States (Bender and Perkins, 1993). In many parts of the world, particularly those without known faults, using predefined areal source zones is still the standard of practice (Abrahamson, 2006). Seismic source characterization was typically based on earthquake catalogue data using areal sources in early seismic hazard assessment studies (Erdik et al. 1985; Gülkan et al. 1993; Atakan et al. 2002) and the magnitude distributions of these areal sources (Figure 1.1) were modeled with truncated exponential frequency-magnitude relationship.

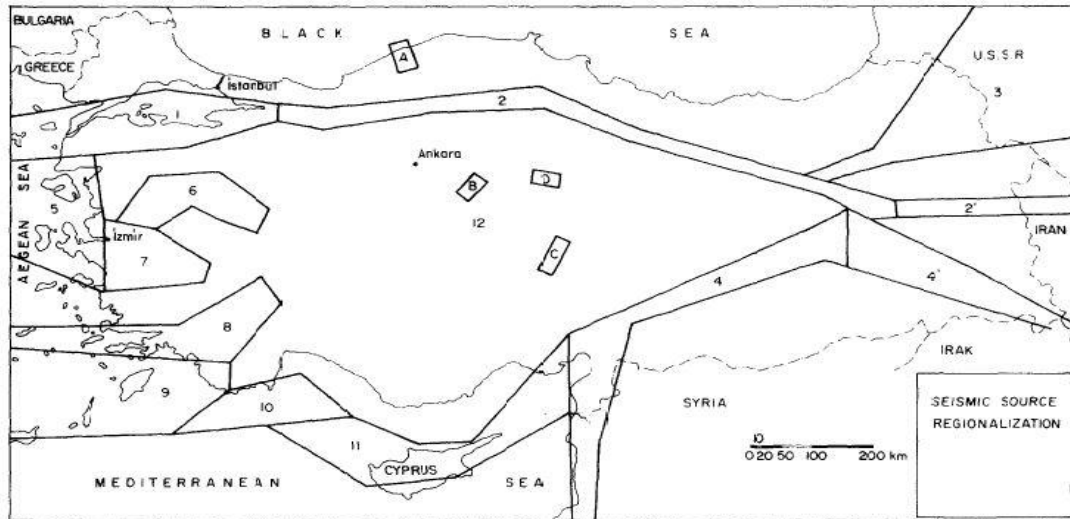


Figure 1.1: Seismic source regionalization for Turkey (After Erdik et al., 1985)

In relatively recent studies (Erdik et al. 2004; Crowley and Bommer 2006; Kalkan et al. 2009), seismic sources were modeled by defining linear fault segments with the assumption that the seismic energy along these fault segments was released by characteristic events (Figure 1.2). The magnitude distribution functions of these linear sources were considered to be fully characteristic (truncated normal distribution). In addition, a background source representing the small-to-moderate magnitude earthquakes (magnitudes between 5 and 6.5-7 depending on the study) were added to the source model and the earthquake recurrence of the background source was modeled using a truncated exponential magnitude distribution model.

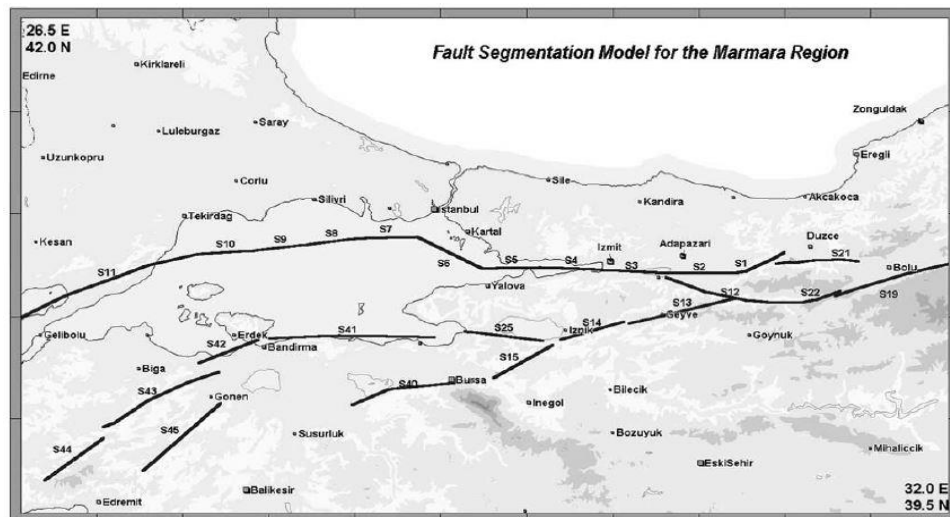


Figure 1.2: Fault segmentation model proposed for the Marmara region (After Erdik et al., 2004)

In Turkey, the major active tectonic structures such as North Anatolian Fault (NAF) and East Anatolian Fault (EAF) systems have clearly defined geometries, rupture histories, long term geological slip rates, etc., however even in the recent large-scaled studies like Global Seismic Hazard Assessment Program (GSHAP) (Grunthel et al., 1999), Seismic Hazard Harmonization in Europe (SHARE) (<http://www.efehr.org:8080/jetspeed/portal/hazard.psml>, last accessed at March 10, 2015) and Global Earthquake Model (GEM) (<http://www.globalquakemodel.org/what/regions/middle-east/>, last accessed at March 10, 2015), areal source zones (with or without the addition of planar fault sources for characteristics events) are preferred to represent the seismicity around these well-studied tectonic structures. The seismotectonic model proposed by the SHARE Project is quite different than the model used by Erdik et al. (2004) as shown in Figure 1.3. Although there is a good change of adopting the results of current large-scaled PSHA projects in earthquake zoning maps and earthquake codes of Turkey, effect of the designated source model (planar fault models as shown in Figure 1.2 or areal source models as shown in Figure 1.3) on the hazard results were not yet discussed properly by quantifying the differences in the hazard curves and design ground motions for different risk levels.

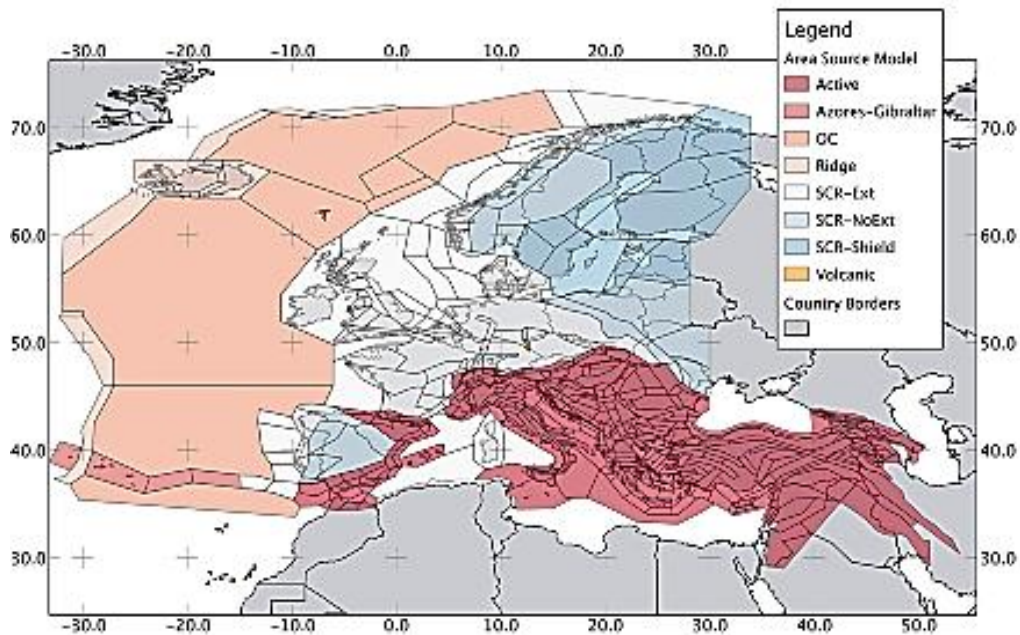


Figure 1.3: Area source model geometry colored by tectonic regimes (Taken from the probabilistic seismic hazard assessment for Euro-Mediterranean region as proposed by the SHARE project - <http://www.share-eu.org>, last accessed 20 March 2015)

One important headline of the ongoing debate of seismo-tectonic modeling in Turkey is the missing or uncertain fault characteristics and data that are crucial for a complete moment-balanced PSHA framework. While building the planar source models for different segments of North Anatolian Fault (NAF), several assumptions and/or simplifications had to be made for assigning the annual slip rate to each segment (especially for parallel fault branches), defining the source geometry in terms of fault length, fault width and segmentation points, and matching the seismic sources with catalog seismicity (e.g. Gülerce and Ocak 2013; Gülerce et al., 2015). These choices may have a great influence on the hazard outcome depending on the sensitivity of the PSHA results to the model parameters and the location of the analyzed site with respect to the seismic source. A quantitative study showing the effects of source model parameters of NAF Zone on the obtained hazard results is not available in the current literature.

1.2. Previous Studies on the Sensitivity of PSHA Results to Input Source Model

Unfortunately, most of the PSHA studies are published as consultancy reports and are not open to public; therefore, experience from previous practice is not effectively transferred to current PSHA works. The published works on the effect of parameter uncertainties in PSHA results for regions other than Turkey are also limited. McGuire (1977) and McGuire and Shedlock (1981) studied the East Coast of United States and San Francisco Bay Area to demonstrate the variations in seismic-hazard calculations resulting from statistical uncertainty in the assumed models and their parameters. McGuire (1977) showed that MM (Modified Mercalli) intensities for a chosen risk level are generally insensitive to the manner in which the region of study is divided into seismic sources; however, they are sensitive to the assumed largest event which can occur. Later, McGuire and Shedlock (1981) proposed that the largest uncertainty arose from the ground motion prediction model and seismogenic depth of the fault plane if a planar fault model is employed in PSHA.

Following works of Bender (1986, 1987) and Bender and Perkins (1993) were dedicated to modeling the effect of source zone boundaries for areal seismic sources and uncertainties in seismic source characterization parameters by means of sensitivity studies. Figure 1.4 shows the acceleration levels having a 90 percent

probability of not being exceeded during exposure times of 10, 50, 250, and 1000 years at several sites near a single arbitrary (60 km × 60 km) square areal source zone. Analyzed sites were 1 km apart on a line perpendicular to a boundary of the zone, extending from the center of the zone to 30 km beyond the boundary. Bender (1986) showed that uniform hazard ground motions change abruptly at source zone boundaries, with the result that predicted acceleration levels may differ considerably at sites a few kilometers apart near a boundary (e.g., changes of 50 to 80 per cent or more at sites 20 km apart). Bender (1986) performed another set of PSHA for several sites that are close to an arbitrary 300 km-long fault model as shown in Figure 1.5. The abrupt changes in the design ground motions on the source zone boundary were not observed when a fault model is defined.

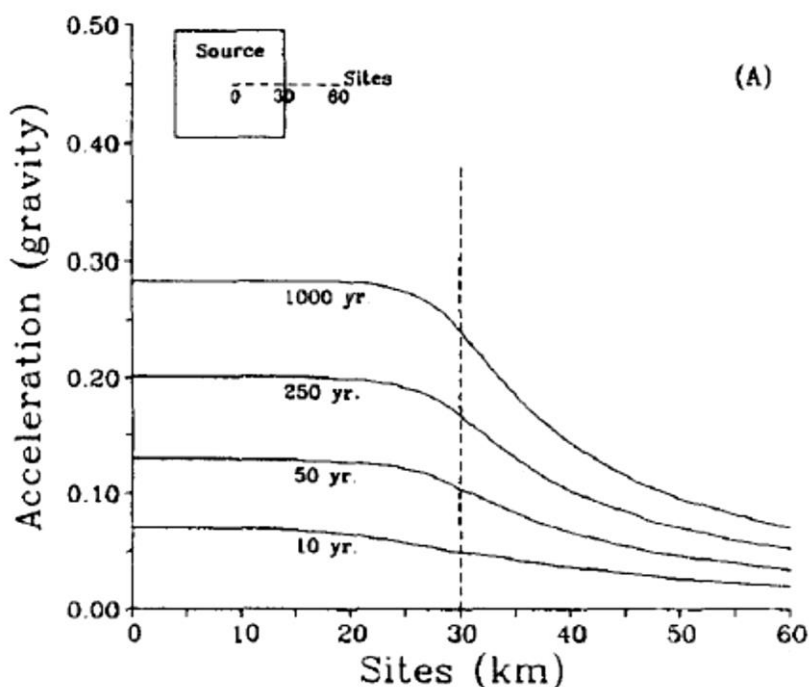


Figure 1.4: Accelerations calculated to have a 90 percent probability of not being exceeded during time periods of 10, 50, 250, and 1000 yr. The dashed line at 30 km corresponds to a boundary of the source zone (After Bender, 1986).

Bender and Perkins (1993) compared the hazard curves at the same site using a 260x260 km square areal source zone and 340 km long fault zone in Figure 1.6(a). Results indicate that the design ground motions (here only peak ground acceleration,

PGA) for near field sites will decrease significantly if an areal source is defined instead of a planar fault zone.

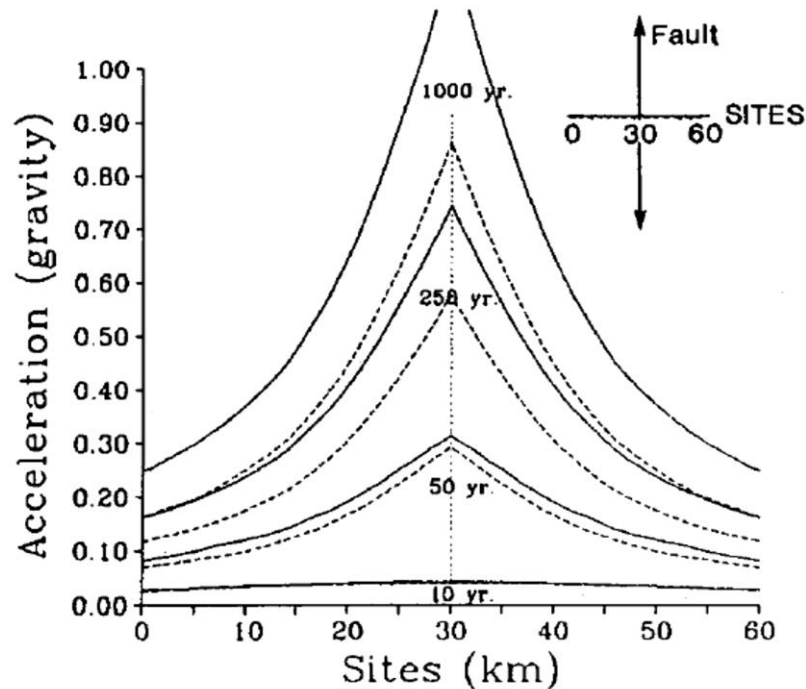


Figure 1.5: Accelerations calculated to have a 90 per cent probability of not being exceeded during various time periods at sites on a line perpendicular to the center of a 300-km-long fault (After Bender, 1986).

For a defined planar source zone, the effect of assigned maximum magnitude (M_{max}) and b-value were evaluated by Bender and Perkins (1993) as shown in Figure 1.6(b). For these analyses, they assumed a triangular distribution between 0.7 and 1.1 for the b-value but M_{max} has a uniform distribution between 7.3 and 8.5. Analysis results showed that the design ground motions are significantly sensitive to the changes in the source model parameters. However, this sensitivity is not quantified separately for M_{max} and b-value. Effect of other parameters, such as minimum magnitude, analyzed by Bender and Perkins (1993) are compared with the results obtained in this study and presented in Chapter 3. This study is inspired from the remarkable work of Bender and Perkins (1993); however, the sensitivity analyses are conducted in a systematic manner. For each set of sensitivity analysis, only one parameter is modified in a “reasonable” or “usual” range of values and all other parameters are kept constant if possible.

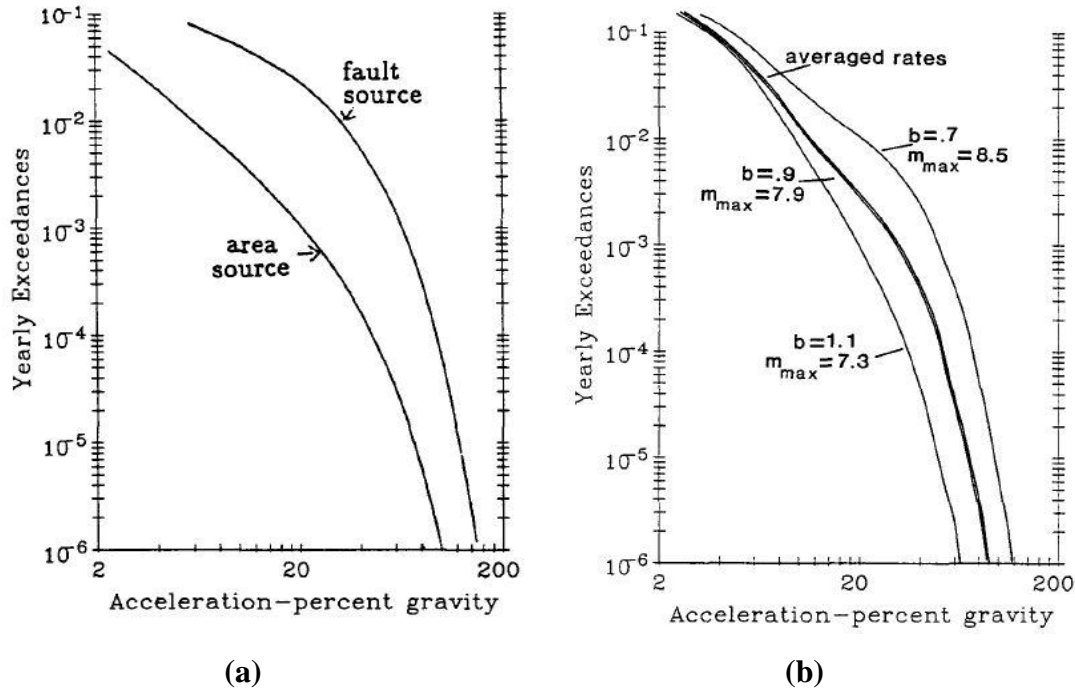


Figure 1.6: Annual ground motion exceedances a) calculated at a site for two alternative source zone scenarios and b) calculated for a site 10 km away from the center of a 280 km long fault using different M_{max} and b -values. (After Bender and Perkins, 1993)

1.3. Research Statement

The primary objective of this study is to show the effect of designated source model on the hazard results by quantifying the differences in the hazard curves and design ground motions for different risk levels at different locations around the NAF system. 1939 Erzincan earthquake rupture zone is selected as the basis for this study since it is a well-studied segment of the NAF zone with documented rupture extends, slips, and segmentation models (Barka, 1996; Emre et al., 2010 and 2013); however no PSHA study is published for this region for more than 20 years. Four different seismic source models are developed by using areal or planar source geometries (or a combination of both) and by employing different magnitude distribution models based on the widespread applications in the current PSHA practice. Significant and systematic differences in the design ground motions obtained by employing different seismic source models clearly demonstrate the need of defining planar source zones and selecting suitable magnitude recurrence models for accurate estimation of ground motions, especially in the near-fault areas.

One of the most valid arguments in preferring the simplified areal source zones for active tectonic structures instead of planar fault geometries is the missing fault parameters or data such as fault width (or seismogenic depth), annual slip rate, recurrence characteristics, and segmentation models. While building the planar source models, several assumptions and/or simplifications have to be made to define the fault parameters and the associated uncertainty. This study, also aims to provide some insight on the effect of source or fault parameters on the final hazard outcome by presenting series of sensitivity analyses for source zone boundaries, annual slip rate, maximum and minimum magnitudes, fault width, b-value and scenario weights. Several arbitrary sites starting from 1 kilometer away from the rupture zone up to 100 kilometers away from the source are selected for the analysis to capture the effect of site location. Effects of the parameter uncertainties are evaluated by comparing the hazard curves with the base case hazard curve for each source model defined for 1939 Erzincan earthquake rupture zone. Hopefully, these analyses will reveal the important missing parameters of the NAF system that requires further research and multi-disciplinary collaboration in terms of PSHA in the near future.

1.4. Scope

The scope of this thesis can be summarized as follows:

Chapter 1 presents the problem significance and research statement with an emphasis on the limitations of the previous literature related to PSHA practice of the region in local and global scales.

In Chapter 2, four separate seismic source characterization models developed for the same source as input to PSHA analysis are discussed in details. Source geometry, segmentation points, slip rates and moment accumulation in each sub-segment, magnitude recurrence relations and activity rates are presented within the content of this chapter. Chapter 2 also contains a brief introduction to the PSHA framework and ground motion prediction models.

Within Chapter 3, the effect of source model parameters on the PSHA results for each source model are investigated by comparing the hazard curves for several locations with the hazard curves of base case models provided in Chapter 2.

Chapter 4 includes the PSHA analyses for different sites that are carefully selected to allow comparison with Turkish Earthquake Code (TEC, 2007) zones. Uniform Hazard Spectrum (UHS) for selected sites are constructed and compared with TEC-2007 design spectrum.

Chapter 5 includes a comprehensive summary of the study and discussion of the results.

CHAPTER 2

ALTERNATIVE SEISMIC SOURCE CHARACTERIZATION MODELS FOR THE 1939 ERZINCAN EARTHQUAKE RUPTURE ZONE

Probabilistic Seismic Hazard Assessment (PSHA) can be described as a four-step procedure:

- I. Identification of the geometry of seismic sources, which are capable of producing damage to engineering structures.
- II. Defining the magnitude recurrence models for seismic sources.
- III. Estimation of resulting distribution of ground motion intensity in terms of earthquake magnitude, distance etc. and its variability for each scenario.
- IV. Construction of the hazard curve and selection of the design ground motion parameters.

The first two steps are critical in PSHA since the magnitude, location and frequency estimation for future earthquakes depends on this information. In these steps, the source geometry in terms of length, width, dip and strike angles of the fault plane must be accurately defined. In addition, the segmentation points of the faults must be identified and used to define the fault rupture model. Finally, the earthquake recurrence relations must be modeled with the help of geological information and associated historical events (Reiter, 1990).

General seismo-tectonic features of the NAF system, especially the rupture zone of 1939 Erzincan Earthquake are carefully studied and summarized in this chapter. Contribution of this information for building the seismic source model as well as estimation of activity rates and recurrence relations are also discussed in details. Last two steps of the PSHA procedure require a careful review of suitable ground motion prediction equations (GMPEs) for the region and numerical integration of the hazard integral. Details of the selected GMPEs, applied PSHA methodology, and the software used for the numerical integration are provided at the end of this chapter.

2.1. Magnitude Distribution Models for Areal and Planar Seismic Sources

In the PSHA framework two types of sources can be described; areal sources and planar sources. Areal sources are defined based on the spatial distribution of the seismicity of the region and generally used in regions with less-known or unknown faults. However, planar fault sources can be used in regions where accurate seismo-tectonic information on the fault geometry is available. Each seismic source generates a range of earthquakes with different magnitudes. The relative number of different magnitude earthquakes is described by the magnitude distribution models. Typical magnitude distributions functions that are used in PSHA are briefly described below.

2.1.1. Truncated Exponential Model

The basic and the most common magnitude recurrence relation is the exponential model proposed by Gutenberg and Richter (1944);

$$\text{Log}_{10}N = a - bM \quad 2.1$$

In Equation 2.1, M is the earthquake magnitude; N is the cumulative number of earthquakes greater than M; and the constants “a” and “b” are regression parameters. “a” represents the activity rate (measure of the occurrence rate of earthquakes in the region) and b is the slope of the line that represents relative frequency of different magnitude earthquakes. Since there is a maximum magnitude that the source can produce and a minimum magnitude for engineering interest, the G-R distribution is usually truncated at both ends and renormalized so that it integrates to unity. The truncated exponential distribution function is shown in Eq.2.2 and 2.3.

$$f_m^{TE}(M) = \frac{\beta \exp(-\beta(M - M_{min}))}{1 - \exp(-\beta(M_{max} - M_{min}))} \quad 2.2$$

$$\beta = \ln(10) \times b \quad 2.3$$

2.1.2. Truncated Normal Model (Characteristic Model)

Youngs and Coppersmith (1985) proposed that the truncated exponential distribution is suitable for large regions or regions with multiple faults but in most cases does not work well for fault zones. Instead, individual faults may tend to rupture at what have

been termed as “characteristic” size events. The alternative magnitude distribution for this case is the “characteristic model” proposed by Schwartz and Coppersmith (1984). According to the characteristic model, due to the geometry of the fault, once a fault begins to rupture in large earthquakes, it tends to rupture the entire fault segment and produce similar size earthquakes. In other words, the faults or fault segments generate earthquakes that, in terms of distribution, are highly populated in a small range near the maximum magnitude. After this model was introduced, there were several discussions comparing this characteristic model to the previous models (Wesnousky, 1994; Kagan, 1996) that argued the suitability of each model for major fault lines. It is notable that the characteristic model does not consider the small-to-moderate magnitude earthquakes on a fault.

2.1.3. Composite Model (Youngs and Coppersmith, 1985)

A third model was proposed by Youngs and Coppersmith in 1985 that combines the truncated exponential and characteristic magnitude distributions. This composite model relies on both geological and seismological basis and uses the characteristic earthquake magnitude for large magnitude earthquakes and exponential model for small to moderate magnitude earthquakes. The key feature of this well-known model that widely used for PSHA evaluations is the relative size of the released seismic moments for small to moderate and large magnitude events. Due to the constraints of the model, 94% of the accumulated seismic moment is released by the characteristic events and the rest by small-to-moderate events on the exponential tail. The equation of the composite magnitude distribution model is given below:

$$f_m^{YC}(M) = \begin{cases} \frac{1}{1+c_2} \times \frac{\beta \exp(-\beta(\bar{M}_{char}-M_{min}-1.25))}{1-\exp(-\beta(\bar{M}_{char}-M_{min}-0.25))} & \text{for } \bar{M}_{char}-0.25 < M \leq \bar{M}_{char}+0.25 \\ \frac{1}{1+c_2} \times \frac{\beta \exp(-\beta(M-M_{min}))}{1-\exp(-\beta(\bar{M}_{char}-M_{min}-0.25))} & \text{for } M_{min} < M \leq \bar{M}_{char}-0.25 \end{cases} \quad 2.4$$

Where,

$$c_2 = \frac{0.5\beta \exp(-\beta(\bar{M}_{char} - M_{min} - 1.25))}{1 - \exp(-\beta(\bar{M}_{char} - M_{min} - 0.25))} \quad 2.5$$

and M_{char} is the characteristic earthquake magnitude.

Magnitude distribution models only represent the relative rate of different magnitude earthquakes. In order to calculate the absolute rate of events, the activity rate $N(M_{\min})$, the rate of earthquakes above the minimum magnitude, should be used. For areal sources, $N(M_{\min})$ may be calculated by using the seismicity within the defined area. For planar fault sources, the activity rate is defined by the balance between the accumulated (Equation 2.6) and released (Equation 2.7) seismic moments as shown in Equation 2.8. The accumulated seismic moment is a function of the annual slip rate (s) in cm/years, area of the fault (in cm^2) and the shear modulus of the crust (μ in dyne/cm^2). Hanks and Kanamori (1979) proposed that the released seismic moment is related to the magnitude of the earthquake as shown in Equation 2.7.

$$M_0 = \mu AD \quad 2.6$$

$$\log_{10} M_0 = 1.5M_w + 16.05 \quad 2.7$$

$$N(M_{\min}) = \frac{\mu AS}{\int_{M_{\min}}^{M_{\max}} f_m(M_w) 10^{1.5M_w + 16.05} dM} \quad 2.8$$

Ultimately the magnitude distribution and the activity rate are used to calculate the magnitude recurrence relation $N(M)$ as shown in Equation 2.9.

$$N(M) = N(M_{\min}) \int_{M_{\min}}^{M_{\max}} f_m(M_w) dM \quad 2.9$$

2.2. Seismic Source Characterization for 1939 Erzincan Earthquake Rupture Zone

On 26 December 1939, a destructive earthquake with estimated magnitude of 7.8 (surface magnitude, $M_s=7.8$ (Ambraseys and Finkel, 1988)) ruptured the 360-km long Niksar-Erzincan segment of NAF extending from the Erzincan Basin on the east to Amasya on the west (McKenzie, 1972; Barka, 1996; Stein et al., 1997; Gürsoy et al., 2013) (Figure 2.1). The epicenter was located at approximately 10 km northwest of Erzincan according to Dewey (1976). In the following years after the 1939 Erzincan earthquake, many field surveys have been carried out by different researchers in the area. Ketin (1948) had studied the 1939 earthquake and following events over a ten year period and was the first researcher who identified this fault as an active right-lateral strike-slip fault. However, detailed mapping studies of the surface rupture have not been undertaken in the region except for the key works of Barka (1996) and Emre et al. (2010). Recently, a limited part of the surface rupture

zone between Susehri-Erzincan near the towns of Resadiye and Koyulhisar are investigated by Gürsoy et al. (2013).

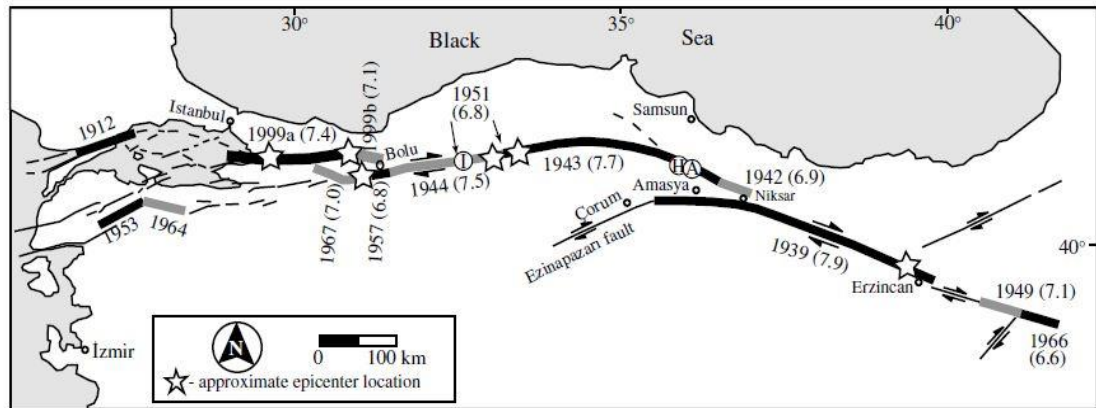


Figure 2.1: Rupture zones of the consecutive 1939-1943 earthquakes on North Anatolian Fault Zone. Stars show the approximate locations of epicenters (After Hartleb et al., 2003).

Barka (1996) has assembled a record of 27 dextral slips and presented the slip distribution along the rupture zone of the 1939 Erzincan earthquake as shown in Figure 2.2. Based on the slip distribution, Barka (1996) proposed a 5-segment model for the 1939 Erzincan earthquake rupture zone. The 5 geometrically distinct segments and their lengths from east to west are: (1) the 60-km long Erzincan segment, (2) the 65-km long Mihar-Tümekear segment, (3) the 45-km long Ortaköy-Susehri segment, (4) the 100-km long Kelkit Valley segment, and (5) the 90-km long Eziñepazarı segment as shown in Figure 2.2.

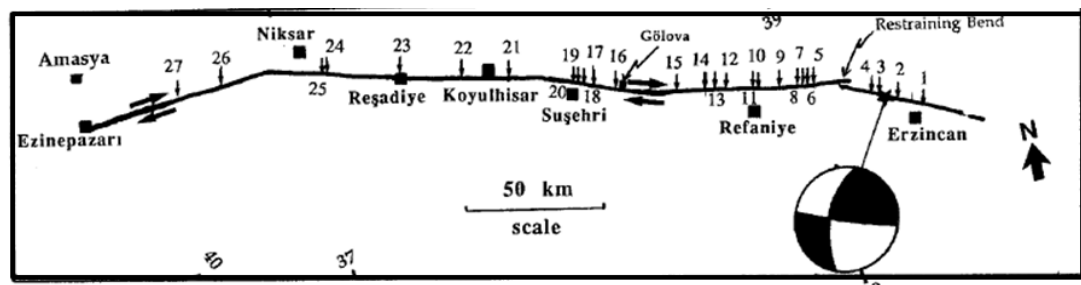


Figure 2.2: Slip distribution along the rupture zone of the 1939 Erzincan earthquake (After Barka, 1996)

Detailed observations at 20 different points are conducted using palaeoseismological techniques together with channel excavations between Niksar and Koyulhisar, the most morphologically prominent and narrowest part of the NAF by Gürsoy et al. (2013). Results obtained by Gürsoy et al. (2013) indicate that the right lateral

displacements decrease from southwest to northeast for the segments of the 1939 Erzincan earthquake rupture zone (Figure 2.3).

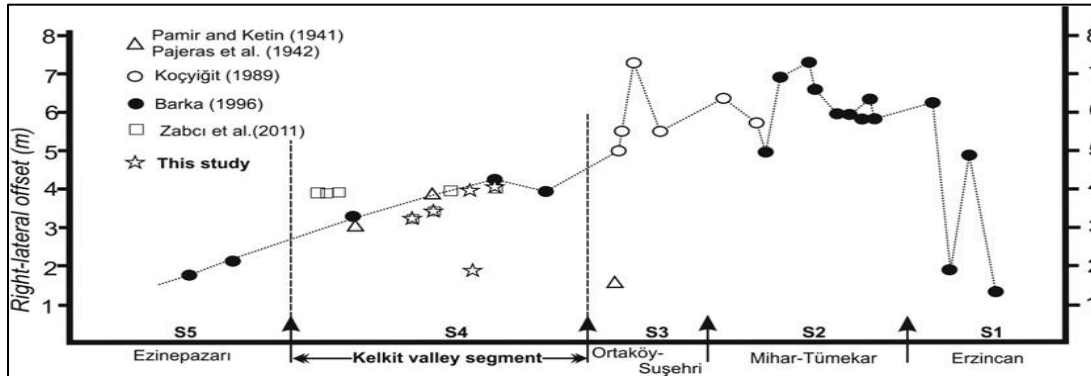


Figure 2.3: Creep distribution graphics measured by various researches according to the segments of the 1939 Erzincan Earthquake rupture (After Gürsoy et al., 2013)

Emre et al. (2010) performed a field study on the fault geometry and revised the slip data associated with this event based on detailed field mapping and slip measurements. The 1939 rupture is also divided into five fault segments based on slip distribution and fault geometry by Emre et al. (2010): the Erzincan, Refahiye, Susehri, Resadiye and Ezinepazari segments from east to west. Length of segments varies from 42 to 90 km. Collected slip data by Emre et al. (2010) from 95 measurements revealed that the amount of average slip varies between 2.30 to 8.8 m. and the slip distribution is not uniform along the entire rupture zone. Emre et al. (2010) claims that the total length of the surface rupture associated with the 1939 earthquake is 330 km and the amount of slip along the entire 1939 rupture is larger than that given by previous studies. Therefore, the magnitude of the 1939 event could be revisited based on the empirical laws of surface slip and magnitude. These findings were reflected in the Updated Active Fault Maps of Turkey published by The Mineral Research and Exploration (2012).

For this study, the rupture zone of 1939 earthquake mapped in Çorum (No:30), Divriği (No:41), Erzincan (No:44), Giresun (No:40), Sivas (No:36), and Tokat (No:35) sheets of the Updated Active Fault Map of Turkey (MTA, 2012) are accessed and digitized using WGS84 datum system and the GIS software, ArcGIS. In these maps, the 1939 Erzincan earthquake rupture zone is divided into 8 sub-segments as shown in Figure 2.4. Following the segmentation models provided by Barka (1996) and Emre et al. (2010) some of these sub-segments are combined into

single segments: sub-segments 1A and 2 are combined and denoted as the Erzincan Segment; sub-segment 3 shown in Figure 2.4 is the Mihar-Tümekekar Segment; sub-segments 4 and 5 are combined and denoted as the Ortaköy-Suşehri Segment; sub-segments 6 and 7 are combined as the Kelkit Valley Segment and finally the sub-segments 8A and 9 are combined into the Ezinepazarı Segment.

In order to see the effect of combining smaller segments into larger segments, the moment balance achieved by the 5-segment model and 2-segment model are shown in Figure 2.5(a) and 2.5(b), respectively. In order to develop the 2-segment model, the sub-segments 1A, 2, 3, 4, 5 shown in Figure 2.4 are combined to form Segment-1 and for Segment-2, sub-segments 6, 7, 8A and 9 are combined. Figure 2.5(a) shows that reducing the segment lengths increases the relative rate of small-magnitude events and provides a better fit to the associated seismicity. When the segments are longer, relative rates of small-magnitude events decrease, but large-magnitude events increases as shown in Figure 2.5(c). Figure 2.5 (c) also indicates that the 2-segment model (black line) has a closer fit to large magnitude catalog events (black dots) while the 5-segment model covers small magnitude events as well as large events.

The width of the fault zone is back calculated by the area–magnitude relations proposed by Wells and Coppersmith (1994) shown in Eqn. 2.10, as 14 km.

$$M_{char} = 3.98 + 1.02 \log(RA) (\pm 0.23) \quad 2.10$$

where RA is the rupture area. Segment geometry and calculated mean characteristic earthquake magnitude for each segment is presented in Table 2.1.

For different segments of NAF, the long term geological slip rates have been reported between 10 to 20.5 mm/year based on different geological and seismological methods (Barka, 1996; Stein et al., 1997; McClusky et al., 2000; Reilinger et al., 2006; Tatar et al., 2011; Yavaşoğlu et al., 2011). Figure 2.6 shows the GPS vectors provided by Tatar et al. (2011) along the NAF Zone. The short term slip rates proposed by recent works of McClusky et al. (2000) and Reilinger et al. (2006) for central and western part of NAF are slightly higher than the geological slip rates.

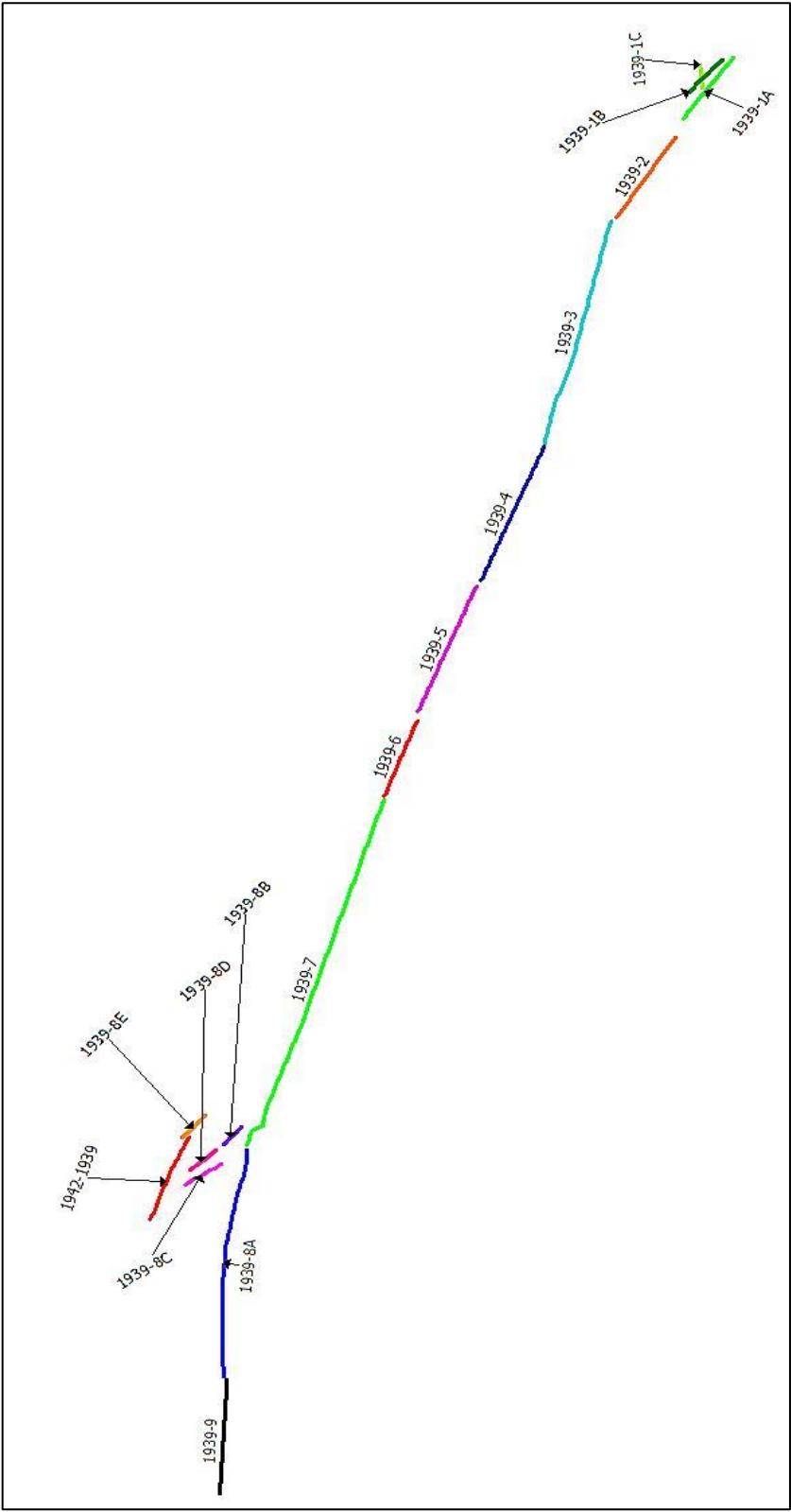
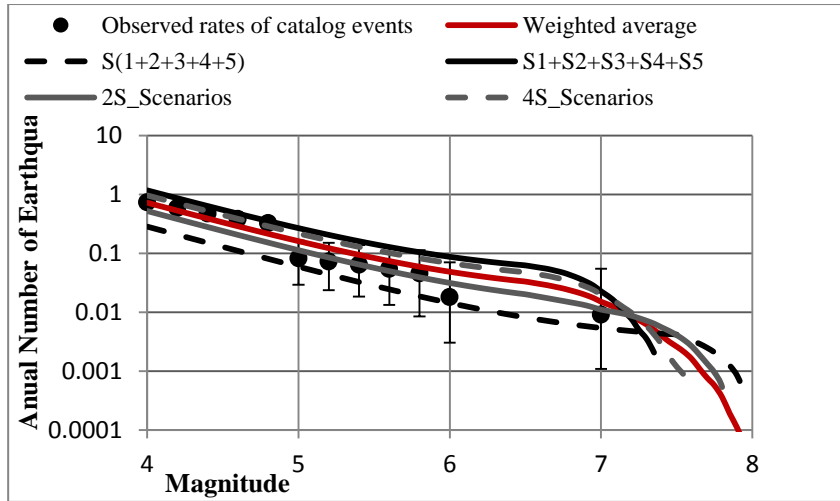
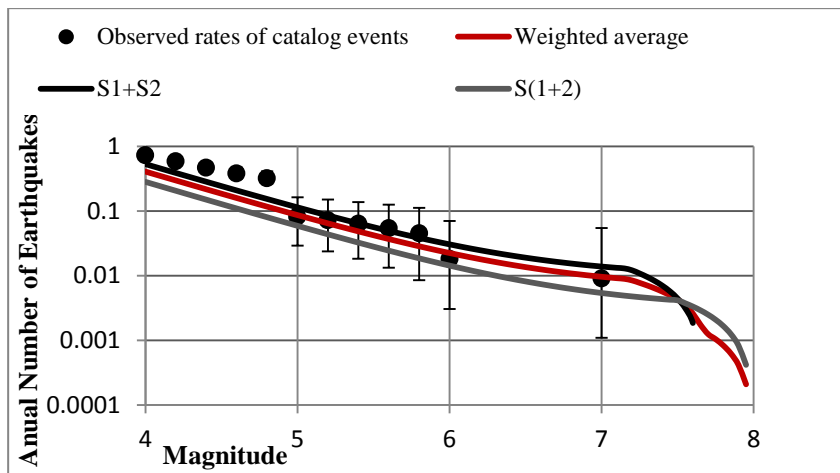


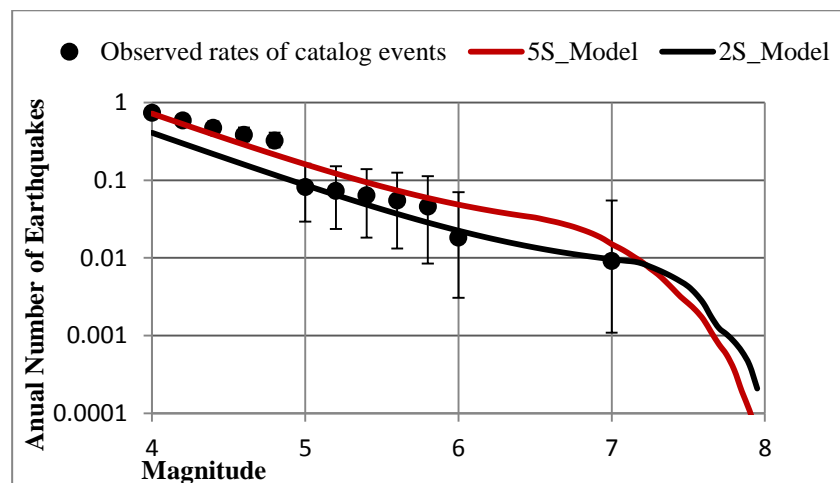
Figure 2.4: Sub-Segments of the 1939 rupture zone of NAF (After MTA, 2012)



(a)



(b)



(c)

Figure 2.5: Comparison of rupture scenarios and weighted average scenario including Weichert (1980) error bars for (a): the 5-Segment model, (b): the 2-Segment model and (c): between weighted average scenario of two different models.

Table 2.1: Segment geometry, assigned slip rate and characteristic magnitude for each segment

No	Segment Name	Length (km)	Width (km)	Slip rate (mm/year)	Characteristic Earthquake (M_{char})
1	Erzincan	37.04	14	17	6.75
2	Mihar-Tümekekar	50.06	14	18	6.88
3	Ortakoy-Suşehri	61.16	14	19	6.97
4	Kelkit Valley	97.28	14	20	7.18
5	Ezinepazarı	73.97	14	8	7.05

Tatar et al. (2011) calculated a locking depth of 12.5 ± 3.5 km and an average slip rate of 20.1 ± 2.4 mm/year for the eastern part of the NAF Zone by using GPS measurements which is consistent with the slip rates achieved by geological observations (Hubert-Ferrari, 2002; Hartleb, 2003; Hubert-Ferrari et al., 2009).

Modeling results of Tatar et al. (2011) and Gürsoy et al. (2013) show a westward increase in the slip rates from 16.3 ± 2.3 mm/year to 24.0 ± 2.9 mm/year on the NAF over a 400 kilometer distance.

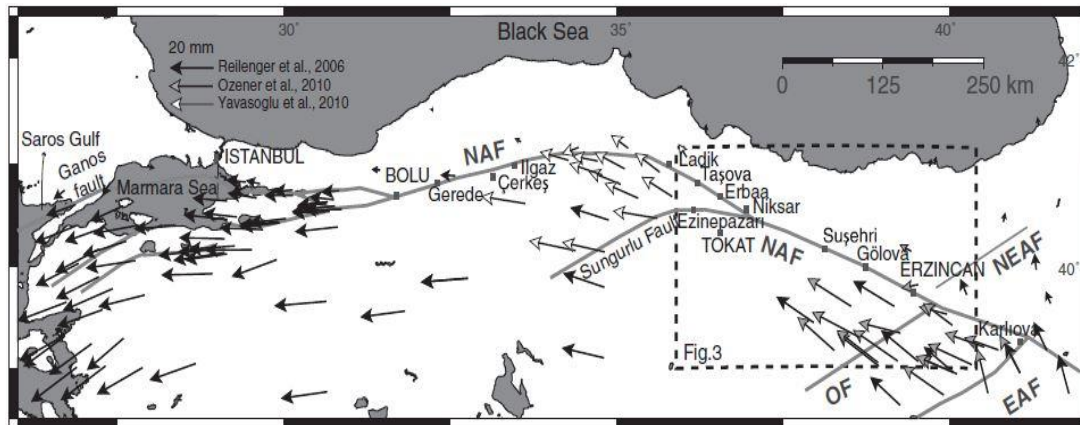


Figure 2.6: Slip vectors along the NAF by various studies. (After Tatar et al. 2011)

The values mentioned in these studies are estimated for the whole NAF system, without considering the parallel fault segments. However, the Ezinepazarı segment of the 1939 earthquake rupture zone lies parallel to the rupture zones of 1942-1943 earthquakes and the Esencay-Merzifon branch of NAF, thus the slip rate must be distributed between these parallel branches. Yılar (2014) assigned a slip rate of 8 mm/year to the Ezinepazarı segment to be consistent with the values proposed by Erturaç and Tüysüz (2012) (6.5 to 10 mm/year). Same value for the Ezinepazarı segment is directly adopted in this study. For the other segments of 1939 earthquake

rupture zone, annual slip rates between 17-20 mm/year is used in a westward increasing manner as suggested by Tatar et al. (2011). Finally, the assigned slip rates are checked in order to achieve a good fit between cumulative historical data and the proposed model for 1939 Erzincan earthquake (Figure 2.11). Slip rates assigned to each segment is shown in Table 2.1.

Another key factor in characterization of the seismic sources for seismic hazard analysis is the analysis of the seismicity associated with the fault. The Integrated Homogeneous Turkish Earthquake Catalog that includes the earthquakes between years 1900-2010 (Kalafat et al., 2011) is employed to define the seismicity in the region (regional seismicity is considered as the seismicity within the red rectangle shown in Figure 2.7). The main shock-aftershock classification of the instrumental catalog was performed and the aftershocks were removed from the dataset using the Gardner and Knopoff (1974) methodology. The remaining dataset after declustering consists of 471 events with magnitudes between 4.0 and 7.7 (Table 2.2). Catalog completeness analysis is performed in order to determine the complete time intervals for different magnitude earthquakes. Cumulative number of earthquakes larger than specific magnitude levels is plotted vs. years in order to examine the completeness of the catalog data. As demonstrated in Figure 2.8 for different cut-off magnitudes, the breaking points for the linear trends in the cumulative number of events were examined and a significant breaking point on the slope was observed at approximately 34 years before 2010 for magnitudes smaller than 4.5 and 5.0. Therefore, the catalog was assumed to be complete for 34 years for $M_w \leq 4.5$ and $M_w \leq 5.0$ events. Although the larger magnitude plots in Figure 2.8 suffer from the lack of data due to the truncation of the catalog, the catalog is assumed to be complete for the greater magnitudes for the whole time span (1900-2010).

Using the modified maximum likelihood method of Weichert (1980) (Eq.2.11) that considers the completeness of the catalog for different magnitude bins, the b-value is calculated as 0.7 for the region as shown in Table 2.2. In Equation 2.11, M_i is the mean magnitude of each interval, R_i is the rate of events and M_{min} is the minimum magnitude.

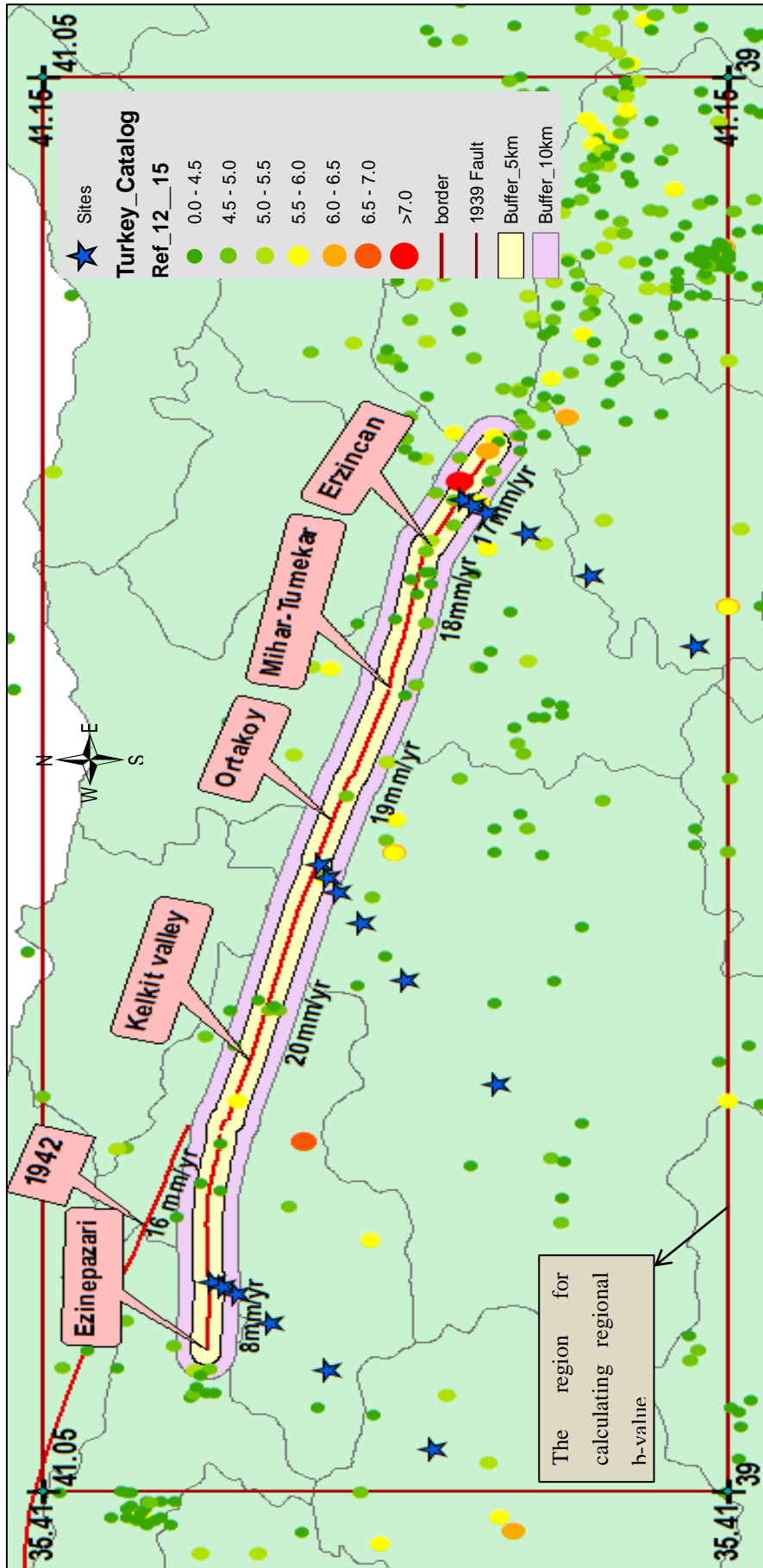


Figure 2.7: The Niksar-Erzincan segment of the NAF. The sub-segments and associated slip rates are indicated on the map. The analyzed site locations are shown with stars. Buffer zones employed for different source models are shown by shaded areas on the map.

$$b = \frac{1}{\left(\frac{\sum M_i \cdot R_i}{\sum R_i} - M_{\min} \right) \times \ln 10}$$

2.11

Table 2.2: Maximum likelihood estimation of the regional “b-value”

Upper Bound	Lower Bound	Mw	# of events	Complete Time Intervals (Years)	Rate	RxM	
4	4.25	4.125	91	34	2.68	11.04	
4.25	4.5	4.375	68	34	2.00	8.75	
4.5	4.75	4.625	85	34	2.50	11.56	
4.75	5	4.875	81	34	2.38	11.61	
5	5.25	5.125	52	110	0.47	2.42	
5.25	5.5	5.375	35	110	0.32	1.71	
5.5	5.75	5.625	30	110	0.27	1.53	
5.75	6	5.875	11	110	0.10	0.59	
6	6.25	6.125	10	110	0.09	0.56	
6.25	6.5	6.375	3	110	0.03	0.17	
6.5	6.75	6.625	4	110	0.04	0.24	
6.75	7.75	7.25	1	110	0.01	0.07	
Total:			471	Total:		10.89	50.26
						b-value= 0.7	

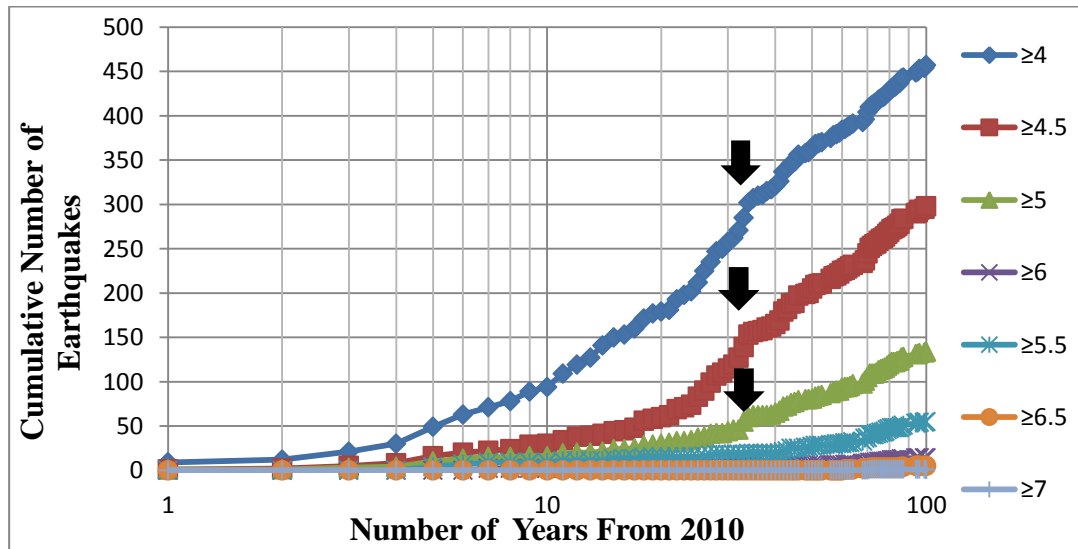


Figure 2.8: The catalogue completeness analysis for the earthquake catalog.

After the compilation of the seismo-tectonic database, the next logical step is the definition of the source model geometry and selection of the magnitude recurrence model that properly describes the source behavior. In order to evaluate the effect of

source model on the hazard results, 3 different source models that are widely used in the practice are applied to Niksar-Erzincan segment of NAF zone in this study.

2.2.1. Model 1: Areal source geometry with truncated exponential magnitude recurrence model

Most PSHA studies assume that the future earthquakes will occur in clearly defined, seismically homogenous areal source zones. For the areas that the geological and paleoseismological information about the active faults are limited, the PSHA practice completely depends on the seismicity within defined source zones. The first model in this study includes a single areal source around the 1939 Erzincan earthquake rupture zone as shown in Figure 2.9. Compatible with the current practice, truncated exponential (TE) magnitude recurrence model is employed for this source zone. The maximum magnitude (M_{max}) value is chosen to be 7.7 based on the magnitude of 1939 Erzincan earthquake and $M_{min}=4.5$ is used to represent the minimum magnitude of the probable lower bound for damaging earthquakes. Geometry of the source zone is defined by a 10 km buffer zone drawn around the fault line. The recurrence parameters for the source are determined by using the modified maximum likelihood method of Weichert (1980) that considers the completeness of the catalog for different magnitude bins. In order to calculate the zone-specific b-value for this areal source, the catalog events in the buffer around the fault and the previously determined catalog completeness intervals are used as shown in Table 2.3. The zone specific b-value for this areal source is calculated as 0.72 using Equation 2.11.

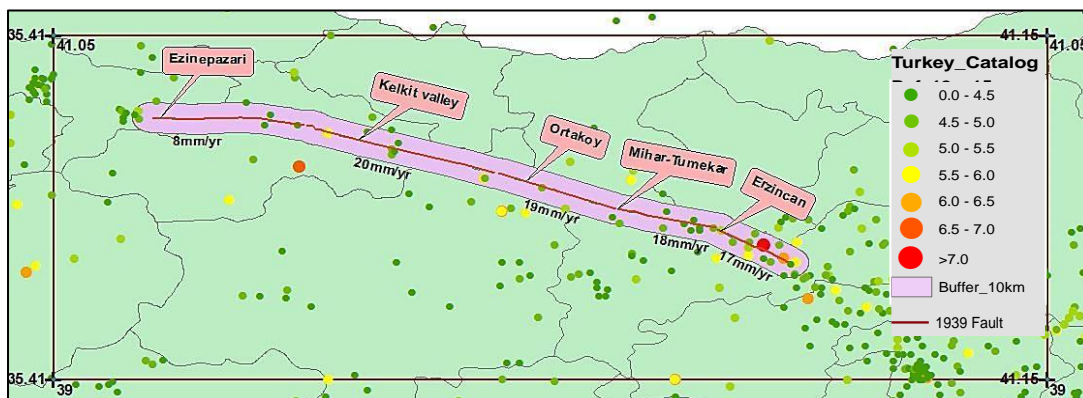


Figure 2.9: 10-km buffer zone around the 1939 earthquake rupture zone fault that is used as the areal source for Model 1 and the seismicity in the region

Table 2.3: Maximum likelihood estimation of the zone specific “b-value”

Lower Bound	Upper Bound	Mw	# of events	Complete time Intervals	Rate	RxM	
4	4.25	4.125	9	34	0.26	1.09	
4.25	4.5	4.375	9	34	0.26	1.16	
4.5	4.75	4.625	9	34	0.26	1.22	
4.75	5	4.875	3	34	0.09	0.43	
5	5.25	5.125	5	110	0.05	0.23	
5.25	5.5	5.375	1	110	0.01	0.05	
5.5	5.75	5.625	1	110	0.01	0.05	
5.75	6	5.875	3	110	0.03	0.16	
6	6.25	6.125	3	110	0.03	0.17	
6.25	6.5	6.375	1	110	0.01	0.06	
6.5	6.75	6.625	0	110	0.00	0.00	
6.75	7.75	7.25	1	110	0.01	0.07	
Total			45	Total		1.02	4.69
						b= 0.72	

2.2.2. Model 2: Planar source geometry including a buffer zone for small-to-moderate magnitude events

Another common practice in PSHA is to assign a characteristic-earthquake distribution for faults and to incorporate an exponential distribution in some aspect of the modeling (e.g., Working Group on California Earthquake Probabilities (WGCEP), 2003; Erdik et al., 2004; Petersen et al., 2008; Field et al., 2009). These source models include a truncated normal model for faults and/or fault segments centered on the mean characteristic magnitude (M_{char}), but smaller magnitude events below a certain threshold magnitude (generally $M=6.5$) within the buffer zone around the fault are modeled using the TE model. This approach is applied to the 1939 earthquake rupture zone using a buffer area of 5 km drawn around the fault (Figure 2.10). Homogenous spatial distribution of the earthquakes within the buffer zone is assumed and the upper and lower bounds of the truncated exponential model are selected as 4.5 and 6.5, respectively.

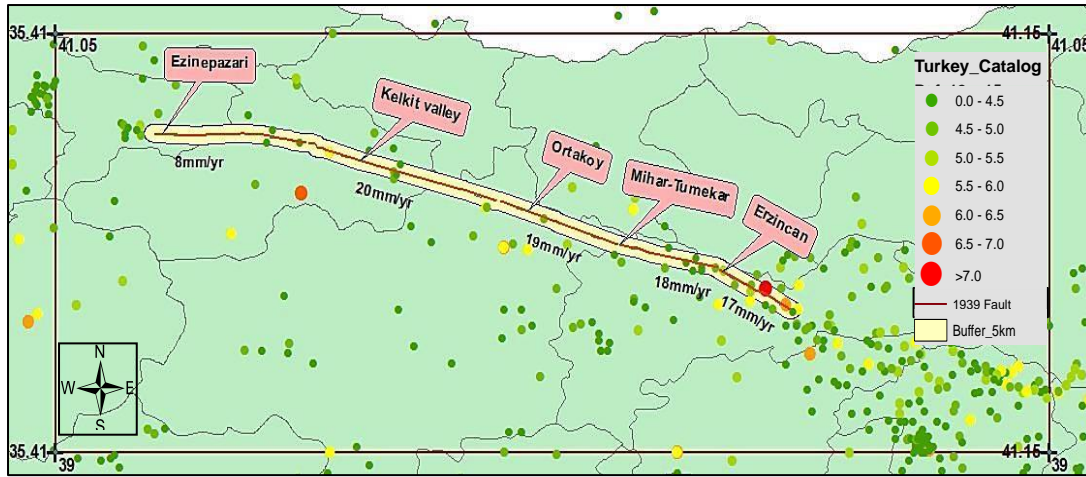


Figure 2.10: 5-km Buffer zone used for the Model 2 of this study and seismicity in the region.

2.2.3. Model 3: Planar source geometry

The faults are defined in this model as planar features without additional background zones, therefore all seismicity including small events are associated with the fault. For defining the planar sources the fault segmentation model and the seismicity associated with the fault must be carefully examined. The approach proposed by the WGCEP-2003 SF Bay Area Model is adapted in this study. The WGCEP-2003 model is primarily based on the characterized faults that are divided into non-overlapping segments. These segments are considered as the fundamental building blocks for earthquake ruptures on each fault. WGCEP-2003 model defines the segmentation as the breaking up of a fault along its length into several smaller faults, each capable of producing large earthquakes. A source is defined as a single segment or combination of multiple adjacent fault segments that are possible to rupture together. Finally the rupture scenario is defined as any combination of sources that illustrates a possible failure mode (Gülerce and Ocak, 2013). As shown in Table 2.4, five non-overlapping segments, 15 seismic sources and 16 rupture scenarios are defined for the 1939 Erzincan earthquake rupture zone. The sources that ruptured during a particular scenario are represented by 1 and the sources that are not ruptured are denoted by 0 in Table 2.4. For a complete fault rupture model, a weight is assigned to each rupture scenario, the weighted average of the rupture scenarios is calculated and the cumulative recurrence rates of events attributed to that particular fault are compared to rupture model to evaluate the assigned weights in moment balanced PSHA. Assuming that the events within a 5-km buffer zone around the

fault can be associated with the fault (as shown in Figure 2.10), a smaller set of earthquakes is selected to be used in balancing the seismic moment.

Appropriateness of the selected magnitude recurrence model and the accuracy of the model parameters such as the annual slip rate or M_{\max} shall be tested by the relative frequency of the seismicity associated with the source in moment-balanced PSHA. This critical procedure is provided in Figure 2.10 for the 1939 Erzincan earthquake rupture zone. In Figure 2.11, the black dots stand for the cumulative annual rates of earthquakes from the instrumental catalogue assigned to the source and the error bars represent the uncertainty introduced by unequal periods of observation for different magnitudes (Weichert, 1980). The M_{\max} is selected as 7.7 due to the estimated moment magnitude of the 1939 earthquake. If the TE model with $M_{\max}=7.7$ is used, it led to a much higher rate of small-to-moderate magnitude earthquakes than has been observed as shown by the purple line in Figure 2.11. A similar phenomenon is observed for Hayward Fault by Stirling et al. (1996), and for other faults by Ishibe and Shimazaki (2012) and Hecker et al. (2013). According to Hecker et al. (2013), assigned M_{\max} may be increased to resolve the discrepancy in the rate of small-to-moderate-magnitude earthquakes. If M_{\max} of the TE model is increased to 8.5, the rates of earthquakes predicted by the recurrence model will be within the close bound of the rate of associated earthquakes (green line in Figure 2.11). However, the technical basis for the quite high maximum magnitude value needs to be justified. Red line in Figure 2.11 shows that the composite magnitude recurrence model (Youngs and Coppersmith, 1985) has a closer fit to the observed rates. Both the composite model and the large magnitude TE model predictions are close to each other and the observed seismicity rates whereas the predictions of TE model is almost 5 times higher than it should be. This difference is observed since approximately 25% of the seismic moment is released by small-to-moderate magnitude earthquakes and the rest is (75%) released by the large earthquakes in TE model. On the other hand, 94% of the accumulated seismic moment is released by characteristic events and the rest of the seismic moment is released by small-to-moderate magnitude earthquakes on the exponential tail due to the constraints of composite magnitude distribution model. On the large magnitude edge of the curve the difference is small and not easy to capture by eye (75/94), however on the small magnitude part the difference is very high (25/6, approximately 4-5 times higher).

Table 2.4: 1939 Earthquake Rupture Zone with associated scenarios and assigned weights. The first column shows different scenarios. Segments that will rupture in each scenario are indicated by 1. The last column shows the weights assigned to each scenario.

Sources	1	2	3	4	5	6	7	8	9	10	11	12	13	14	15	Weights
Segments	1	2	3	4	5	1+2	2+3	3+4	4+5	1+2+3	2+3+4	3+4+5	1+2+3+4	2+3+4+5	1+2+3+4+5	
Scenario (1)	1	1	1	1	1	0	0	0	0	0	0	0	0	0	0	0.1
Scenario (2)	0	0	0	0	0	0	0	0	0	0	0	0	0	0	1	0.13
Scenario (3)	1	0	0	0	0	0	0	0	0	0	0	0	0	1	0	0.055
Scenario (4)	1	1	0	0	0	0	0	0	0	0	0	1	0	0	0	0.055
Scenario (5)	1	1	1	0	0	0	0	0	1	0	0	0	0	0	0	0.055
Scenario (6)	0	0	0	0	0	1	0	0	0	0	0	1	0	0	0	0.055
Scenario (7)	0	0	1	0	0	1	0	0	1	0	0	0	0	0	0	0.055
Scenario (8)	0	0	1	1	1	1	0	0	0	0	0	0	0	0	0	0.055
Scenario (9)	0	0	0	0	1	1	0	1	0	0	0	0	0	0	0	0.055
Scenario (10)	0	0	0	0	0	0	0	0	1	1	0	0	0	0	0	0.055
Scenario (11)	0	0	0	1	1	0	0	0	0	1	0	0	0	0	0	0.055
Scenario (12)	0	0	0	0	1	0	0	0	0	0	0	0	1	0	0	0.055
Scenario (13)	1	0	0	0	1	0	0	0	0	0	1	0	0	0	0	0.055
Scenario (14)	1	0	0	0	0	0	1	0	1	0	0	0	0	0	0	0.055
Scenario (15)	1	0	0	1	1	0	1	0	0	0	0	0	0	0	0	0.055
Scenario (16)	1	1	0	0	1	0	0	1	0	0	0	0	0	0	0	0.055
	Σ															1

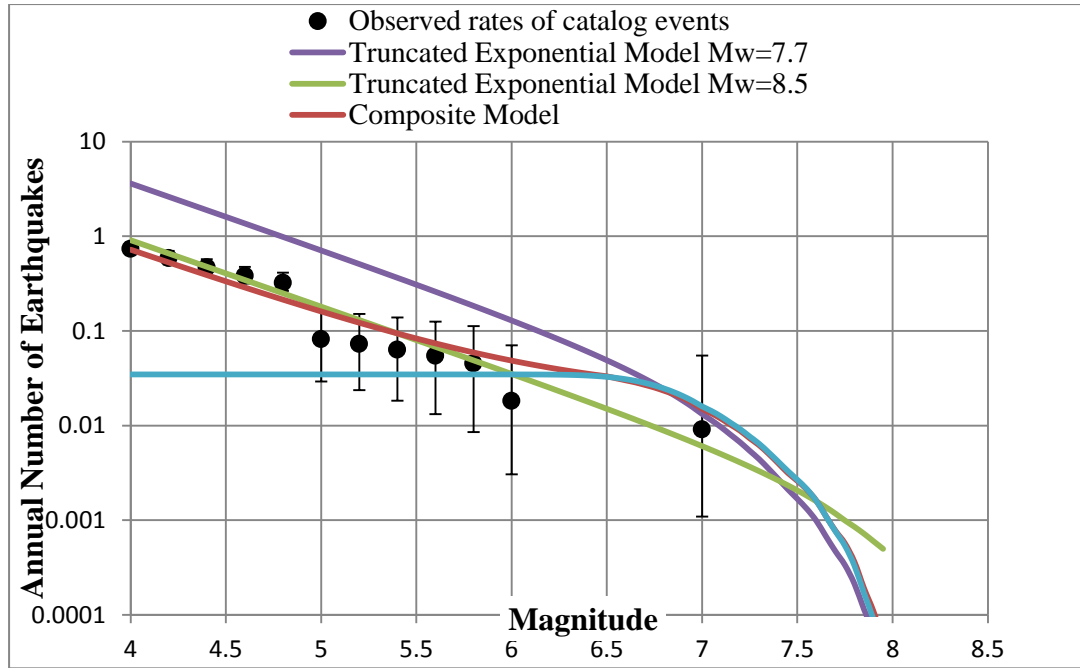


Figure 2.11: Different magnitude recurrence models for the weighted combination of the rupture scenarios of Niksar-Erzincan segment of NAF. Black dots represent the cumulative rates of associated events

Following the current practice, both alternatives are included in this study: in Model 3a the - planar source geometry is combined with TE magnitude recurrence model ($M_{max} = 7.7$) and in Model 3b the planar source geometry with composite magnitude recurrence model is employed.

2.3. Ground Motion Characterization

One of the main steps in PSHA is selection of proper ground motion prediction equations (GMPEs). GMPEs, commonly known as attenuation relationships, predict the level of ground shaking at any site or location based on the earthquake magnitude, source to site distance, local soil conditions, fault mechanism, and other parameters. In both deterministic and probabilistic seismic hazard analysis, GMPEs are competently used to estimate the strong ground motion due to earthquake scenarios from each source for peak ground motion values and elastic response for various spectral ordinates. Nevertheless, GMPEs introduce the biggest uncertainty in the hazard calculations and they have a major effect on the total hazard at the site, despite their confirmed capabilities to predict the level of hazard (Yılmaz, 2008).

More and more GMPEs are derived as national, regional and global databases of strong-motion records expand; therefore, proper selection of ground motion prediction equations among the global and regional alternatives is one of the

important steps in PSHA. Sticking only to the global or local models may create a bias on the results since each group has its own advantages and disadvantages. Local GMPEs are developed from the regional databases; consequently, they are expected to reflect the regional differences better than the global models. However, because of their smaller dataset, local models generally do not extrapolate well to the larger magnitude events. When compared to regional models, global GMPEs represent some important features such as short distance and style of faulting scaling or hanging wall effects more realistically (Bommer et al, 2010). On the other hand, global models may not represent the regional differences as good as local models and the applicability of the global models for the intended region should be evaluated before applying them in the PSHA framework.

The Next Generation Attenuation (NGA) GMPEs are the most widely used global GMPEs around the world. Pacific Earthquake Engineering Research Center initiated the NGA Project as an effort to develop new ground-motion prediction relations between 2004 and 2008. Five sets of GMPEs were developed for shallow crustal earthquakes in the western United States and similar active tectonic regions by teams working independently but interacting with one another throughout the development process as outputs (Abrahamson and Sival (2008) model, Boore and Atkinson (2008) model, Campbell and Bozorgnia (2008) model, Chiou and Youngs (2008) model, and Idriss (2008) model). The NGA models are valid for the moment magnitude ranges of 5.0 to 8.5 for strike-slip earthquakes and 5.0 to 8.0 for reverse and normal earthquakes. All models are applicable for a distance range of 0 to 200 km. V_{S30} , average shear-wave velocity in the upper 30 meters of sediments, is used in all models as the parameter for characterizing site effects on ground motions. Earthquake magnitude, style of faulting, depth to top of fault rupture, source-to site distance, site location on hanging wall or foot wall of dipping faults are the other predictive parameters used in the models.

Stafford et al. (2008) explored the consistency between the global pan-European and NGA GMPEs and concluded that the NGA models can be used for the seismic hazard estimation of shallow crustal active seismic regions in Europe. On the contrary, Bommer et al. (2010) stated that for some particular earthquake scenarios there might be considerable differences between the global European and NGA ground motion models. Recent studies by Scasserra et al. (2009), Shoja-Taheri et al.

(2010), and Bradley (2013) tested the applicability of the NGA-W1 GMPEs for Italy, Iran, and New Zealand. These recent efforts showed that differences between the regional datasets and NGA models exist but these differences may be corrected by small adjustments at the NGA models. Gülerce et al. (2014) regionalized the NGA GMPEs to make the predictions consistent with Turkish strong ground motions. The compatibility of the NGA models with the Turkish strong motion database in terms of magnitude, distance and site effects scaling was evaluated and after certain modifications, a new set of Turkey-specific versions of the NGA GMPEs, the TR-Adjusted NGA-W1 models are proposed by Gülerce et al. (2014). Since evaluating the effects of GMPEs on the hazard results is out of the scope of this study, only one GMPE, TR-Adjusted Abrahamson and Silva (2008) model (Gülerce et al., 2014) is used in the analysis.

2.3.1. TR-Adjusted Abrahamson and Silva (2008) (TR-AS08) Model

Abrahamson and Silva, (2008) is one the five NGA models mentioned in the previous section. In their model, 2754 recordings from 135 earthquakes and the aftershock events among the 3551 recordings from 173 earthquakes are included. AS08 model includes the style of faulting and hanging wall components. Depth to top of rupture and fault dip angle are used in this model in order to define the geometric properties of fault. AS08 includes nonlinear site amplification factors and considers the influence of soil sediment depth. V_{S30} and $Z_{1.0}$ (depth to engineering rock) are the parameters that are used to model the site effects. Magnitude dependent standard deviations are defined in this model. Equation 2.12 presents the functional form of AS08.

$$\ln S_a = f_1(M, R_{rup}) + a_{12} F_{RV} + a_{13} F_{NM} + a_{15} F_{AS} + f_5(PGA_{1100}, VS_{30}) + F_{HW} f_4(R_{jb}, R_{rup}, R_x, W, \delta, Z_{TOR}, M) + f_6(Z_{TOR}) + f_8(R_{rup}) + f_{10}(Z_{1.0}, VS_{30}) \quad 2.12$$

In this equation, S_a is median spectral acceleration, M is the moment magnitude, R_{rup} is rupture distance, F_{RV} and F_{NM} are dummy variables for faulting style, PGA_{1100} , is the rock peak ground acceleration, V_{S30} is the average shear wave velocity in the top 30 meters, R_{jb} is Joyner-Boore distance, R_x is the horizontal distance from top edge of rupture, W is fault width, δ is dip angle of the fault plane, Z_{TOR} is depth to the top

of rupture (in kilometers), $Z_{1.0}$ (in km) is depth to $V_S=1.0$ km/s, a_1 - a_{17} are the regression coefficients.

The TR-Adjusted NGA-W1 GMPEs aim to reflect the regional differences by utilizing the local dataset and to reduce the uncertainties by benefiting the well-constrained pieces of NGA models therefore, only the required pieces of the NGA models were modified for applicability in Turkey. During the regression analysis the dataset including the ground motions recorded from the earthquakes that occurred in Turkey in the last 50 years are used (TSMD, Akkar et al., 2010). The dataset used for comparison includes 1142 recordings from 288 events. By the help of random-effects regression with a constant term, model residuals between the actual strong motion data and NGA model predictions are calculated for a period range of 0.01-10 seconds. The calculated residuals are used to evaluate the differences in the magnitude, distance, and site amplification scaling between the Turkish dataset and the NGA models. Inter-event residuals indicated that the ground motions in the dataset are overestimated by AS08 model. Only small-to-moderate magnitude scaling of the AS08 model is changed in order to preserve the well-constrained large magnitude scaling of the global dataset. No trends in the residuals are observed in the intra-event residuals vs. rupture distance plots up to 100 kilometers; therefore, the distance scaling of the NGA-W1 models is not adjusted. The large distance scaling (between 100 and 200 km) of the AS08 model is modified. An adjustment in the V_{S30} scaling was applied to the AS08 model in order to modify the overestimation at the stiff soil/rock sites. The TR-Adjusted AS08 model is compatible with the regional strong ground motion characteristics and preserves the well-constrained features of the global models; therefore, this model is a suitable candidate for ground motion characterization and PSHA studies conducted in Turkey.

2.4. PSHA Methodology and Software

For estimation of the seismic hazard at a specific site, Cornell (1968) and McGuire (2004) propose a model that formulates the probabilistic approach to calculate the the ground motion levels for corresponding probability of exceedance. In Cornell-McGuire approach, the hazard integral for a single point source is given by:

$$v(A>z) = N_{\min} \cdot \int_M \int_R \int_{\epsilon} f_M(M) f_R(M,R) f_{\epsilon}(\epsilon) P(A>z | M,R,\epsilon) \times dM \quad 2.13$$

where N_{\min} is the annual rate of earthquakes with magnitude greater than or equal to minimum magnitude, M is the magnitude of earthquake, R is the source to site distance; $f_M(M)$ and $f_R(M,R)$ are the probability density functions of magnitude and distance, ϵ is the number of standard deviations above or below the median, $f_{\epsilon}(\epsilon)$ is the probability density function for the epsilon (defined by a standard normal distribution); and $P(A>z | M,R,\epsilon)$ is either 0 or 1. $P(A>z | M, R, \epsilon)$ in this equation selects the scenarios and ground motion combinations that results in events greater than the test level z .

The numerical integration of this integral is performed by the computer code HAZ43b developed by N. Abrahamson (PG&E, 2010). HAZ43 considers the epistemic uncertainties in the source characterization and the GMPEs by means of logic trees and all combinations of the logic tree branches are calculated for each source. Monte Carlo sampling of source characterization uncertainty is used for the total hazard in which, the epistemic uncertainty for each source and full sampling of the GMPEs are combined to be used in developing fractals on the total hazard.

The PSHA is performed for 18 sites; 6 of them are located 1, 5, 10, 25, 50, and 100 kilometers away from the fault on the east, 6 of them located at the same distances from the center, and the last set is located in the same pattern at the west part of the fault as shown by blue stars in Figure 2.7. The analysis was performed assuming rock site conditions ($V_{S30} = 760$ m/s with $Z_{1,0} = 0.034$, $Z_{1,5} = 0.6$, and $Z_{2,5} = 0.64$) for peak ground acceleration (PGA).

2.5. Comparison of the hazard results using different seismic source characterization models

The four alternative source models, for the same fault are incorporated in the PSHA to be able to quantify the differences in the hazard outcome by different modeling approaches. The PSHA is performed for two example sites; a near-fault site ($R_{rup} = 5$ km) and a far-field site ($R_{rup} = 50$ km) assuming rock site conditions ($V_{S30} = 760$ m/s) for peak ground acceleration (PGA). Two horizontal lines in Figure 2.12 show the acceptable risk levels in building codes; 10% chance of exceedance in 50 years (denoted by the black broken line) and 2% chance of exceedance in 50 years

(denoted by the black solid line) for reference. According to Figure 2.12, the differences in the estimated ground motions by different source models are strongly correlated with the source-to-site distance. Figure 2.12(a) shows that the ground motions from the PSHA analyses that employ Models 2, 3a, and 3b are very close to each other both for 475 and 2475 years return periods. The ground motions estimated using Model 3b is lower than Models 2 and 3a for lower hazard levels since the composite magnitude recurrence model is employed in Model 3b, which reduces the relative rates of small-to-moderate magnitude events that dominate the small hazard levels. Rates of small-to-moderate magnitude events are almost equally overestimated if TE model is employed for planar faults (Model 3a) or planar faults are combined with buffer zones (Model 2). Largest hazard numbers are obtained by Model 2 since the rate of moderate magnitude events ($M=6.5-6.6$) introduced by the characteristic magnitude distribution slightly overlaps with the rates introduced by the TE distribution of the buffer zone for short segments. Both for 475 and 2475 years return periods, the estimated ground motions are significantly lower than the other alternatives if the source is modeled by an areal source. For the example near fault site, the 475 years PGA is estimated as 0.2g (half of the Turkish Earthquake Code (2007) requirement) by Model 1; however, the ground motions estimated using the models that incorporate planar sources are between 0.4-0.5g for the same conditions. The differences are not that substantial for the far field site: almost all models ended up providing the same ground motions, especially for 475 years return period as shown in Figure 2.12(b).

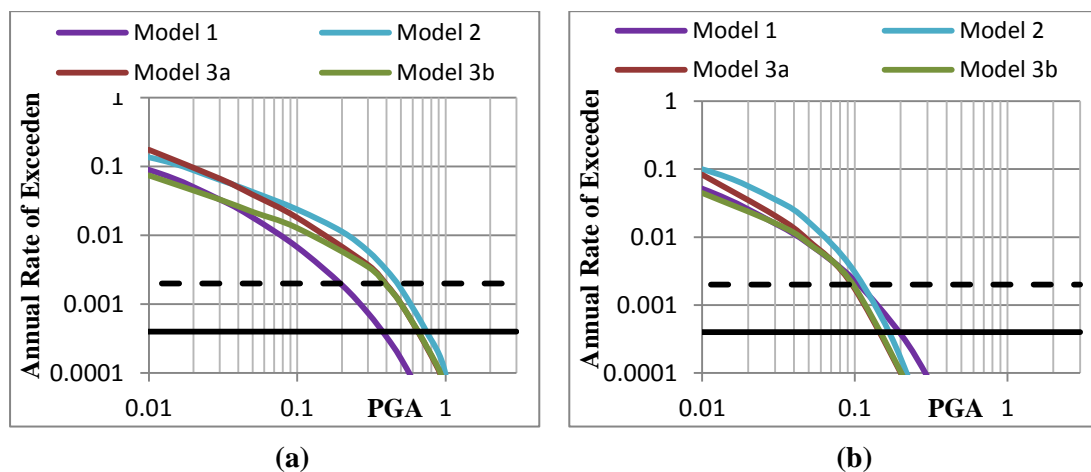


Figure 2.12: Hazard curves for Models 1, 2, 3a, 3b, and 3c of this study. Figure (a) shows the results for near fault ($R=5\text{km}$) and figure (b) shows the results for far field ($R=50\text{km}$) sites. The black broken and solid lines demonstrate the 475 and 2475 year return periods

CHAPTER 3

EFFECT OF SOURCE MODEL PARAMETERS ON THE PSHA RESULTS

In the PSHA framework, it is possible to identify, quantify and combine uncertainties in the size, location and occurrence rate of earthquakes. The PSHA analyst has to choose the correct and most appropriate magnitude recurrence model for each seismic source and then accurately determine the model parameters such as the b-value, slip rate, maximum magnitude and characteristic earthquake magnitude. These choices may have a great influence on the hazard outcome depending on the sensitivity of the PSHA results to the parameter and the location of the analyzed site with respect to the seismic sources. In order to quantify the effect of source characterization parameters on the final hazard outcome, series of sensitivity analysis are conducted for the annual slip rate, minimum magnitude, maximum magnitude or mean characteristic magnitude, fault width, b-value and scenario weights for different models that are presented in Chapter 2. Several arbitrary sites starting from 1 kilometer away from the rupture zone up to 100 kilometers away from the source are selected for the analysis to consider the effect of site location. Effects of the parameter uncertainties are evaluated by comparing the hazard curves with the base case hazard curve for each source model.

3.1. Model 1 - Areal source geometry with truncated exponential magnitude recurrence model

As mentioned before, most PSHA studies assume that the future earthquakes will occur in clearly defined, seismically homogenous areal source zones. In Model 1 an areal source zone is defined around the Niksar-Erzincan segment of NAF Zone and combined with the TE magnitude distribution model. In order to quantify the effect of source zone boundaries together with the effect of catalog seismicity and other

source model parameters, different sensitivity analyses are conducted and presented in this section.

3.1.1 Sensitivity analysis for the effect of source boundary

The first step of defining an areal source zone in PSHA is identifying the source zone boundaries. However, a standard procedure for delineating the source boundaries is not clearly defined: either spatial distribution of recorded earthquakes are used to define seismically homogenous zones or “boxes / buffer zones” with certain distances around a tectonic structure are defined as source zones in the current practice. Distribution of the seismicity in Figure 2.6 does not point out a particular zone of homogenous seismicity; many earthquakes are observed in the close vicinity of the fault line but small-to-moderate magnitude events are also present, especially on the south of the fault line. If a buffer or equal-distanced geometrical shape around the fault is preferred to define the areal source zone, dimensions of this buffer zone could be a subject of debate. Three different source geometries are defined for this model; buffer zones of 5, 10 and 15 km around the fault line (10 km buffer zone is considered as the base case). For each source zone, the magnitude recurrence model parameters (a- and b-values) are re-calculated but the M_{\max} and M_{\min} values are not changed from the values used in the base case. Source parameters and assigned weights are presented in Table 3.1 for each zone.

Table 3.1: Parameters assigned to source zones with different source boundaries.

Buffer Zones	a-value	b-value	M_{\max}	M_{\max} Weights	M_{\min}
±5 km	0.3	0.67	7.7	0.6	4.5
			7.95	0.2	
			8.2	0.2	
±10 km (base case)	0.5	0.72	7.7	0.6	4.5
			7.95	0.2	
			8.2	0.2	
±15 km	0.88	0.72	7.7	0.6	4.5
			7.95	0.2	
			8.2	0.2	

Figure 3.1 shows that changing the source zone boundaries have a considerable effect on the hazard outcome, especially for near-fault sites. For a point that is 10 km

away from the fault, the design ground motions for 475 years return period might change between 0.16g-0.25g depending on the source zone boundary. The effect is less significant for far field sites since the change in 475 years return period ground motions is less than 1%g for different configurations of source zone geometry.

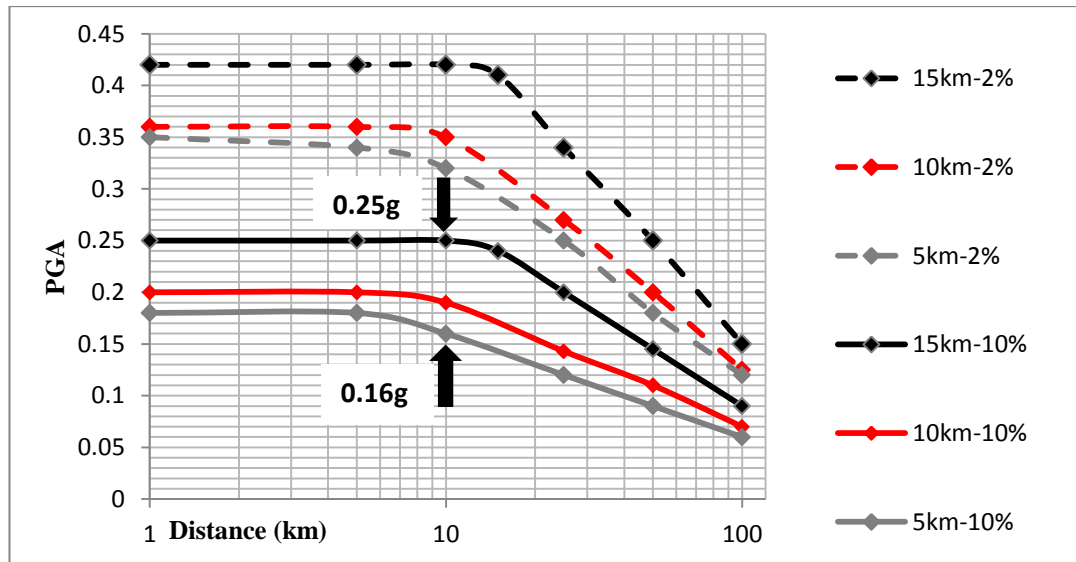


Figure 3.1: Effect of changing the source zone boundaries (using buffer zones of 5-10-15 km around the fault line) on the hazard for 2% and 10% chance of exceeding in 50 years.

3.1.2. Sensitivity analysis for the effect of b-value

The catalogue seismicity plays the most important role in areal source models and many uncertainties are associated with the available earthquake catalogues. First of all, earthquake locations are not precisely known especially for old events, so the number of earthquakes within the areal source zone is uncertain. Sizes of the earthquakes listed in the catalogues may need to be adjusted or converted from different magnitude scales (Bender and Perkins, 1993). To build magnitude recurrence models, completeness intervals for earthquakes in different magnitude ranges are estimated and the aftershock-foreshock classification of the catalogue is performed. These analyses involve certain subjectivity and uncertainty, which have a significant effect on the magnitude recurrence parameters. Finally, the regression method used to estimate the a- and b-values have substantial effect on the result (Aki, 1965). To see the effect of estimated b-value on the hazard results, a sensitivity analysis is performed by changing the b-value from 0.4 to 1.2 for each site shown in Figure 2.6. Sensitivity is limited within this range since the b-values in between 0.4 and 1.2 is not unusual in the practice.

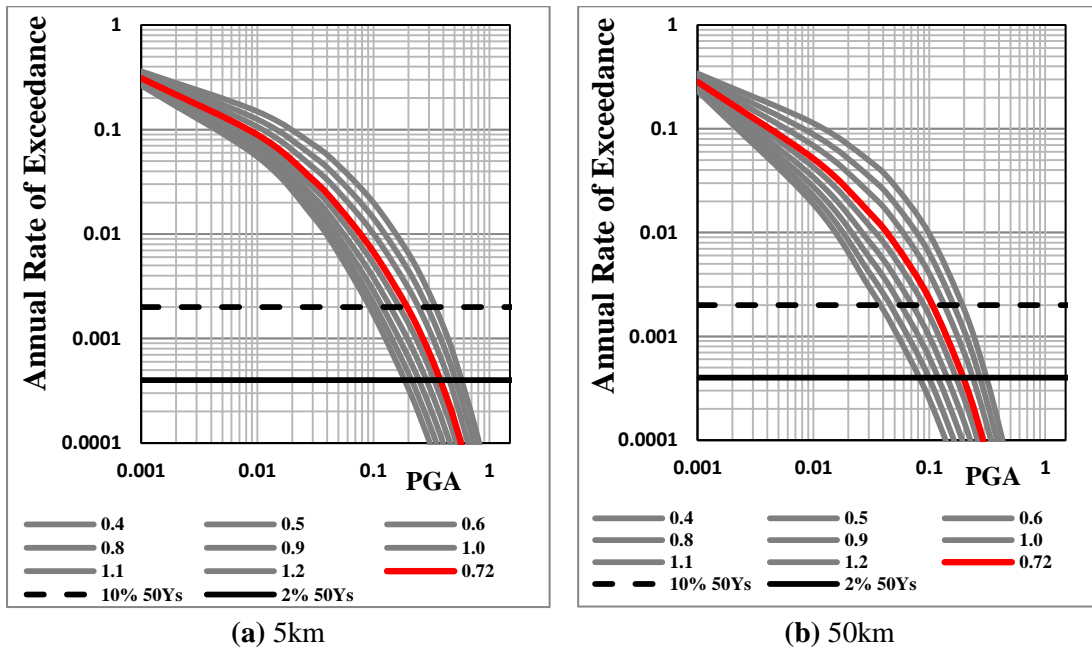


Figure 3.2: hazard curves for different b -values (ranging between 0.4-1.2) at (a) $R_{rup} = 5$ km and (b) $R_{rup} = 50$ km. In figures (a) and (b), the solid red line is the hazard curve for the base case, the broken and solid black lines represent the hazard levels of 10% and 2% chance of exceeding in 50 years.

Figure 3.2(a) and 3.2(b) show the hazard curves for the base case ($b=0.72$, red line) and other configurations for a near fault site ($R_{rup}=5$ km) and a far field site ($R_{rup}=50$ km), respectively. Upper and lower bound values for 10% and 2% chance of exceeding in 50 years for each site are plotted with respect to the distance from the center of the fault in Figure 3.6(a). The effect of b -value on the hazard results are bigger than that of the zone boundary effect and effect of any other parameter shown in Figures 3.6(b-d). The impact is almost 1-1: if the b -value is reduced by approximately 50% (from 0.72 to 0.4), the design ground motions are increased by approximately 50% for all distances and hazard levels.

3.1.3. Sensitivity analysis for the effect of maximum magnitude

For fault sources, M_{char} might be estimated with the help of geological or tectonic considerations; however, selection of the M_{max} value for areal source zones involves serious uncertainties (Bender and Perkins, 1993). Current practice comprises the use of maximum observed magnitude in the instrumental or historical catalogue or suggests a certain increase in the observed value (e.g. by +0.5 magnitude units) for

assigning the M_{\max} value to the source zone. The effect of M_{\max} on the hazard results is evaluated by adding ± 0.5 magnitude units to M_{\max} value of the base case ($M=7.7$) and running the hazard analysis for $M_{\max}=7.2-8.2$. The hazard curves are compared with the base case hazard curve for the near-fault site (Figure 3.3(a)) and for the far-field site (Figure 3. 3(b)). The red line in these figures represents the hazard curve for the base case, the black broken and solid lines represent the 475 and 2475 return periods respectively.

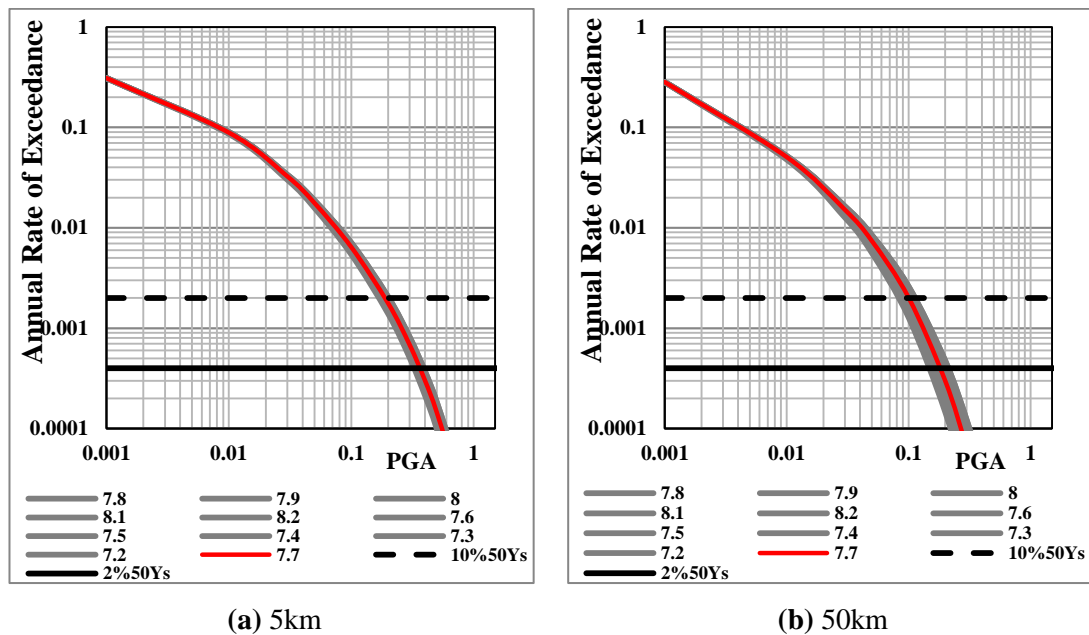


Figure 3.3: hazard curves for different maximum magnitudes (ranging between 7.2 and 8.2), at (a) $R_{rup}=5$ km, and (b) $R_{rup}=50$ km. The solid red line is the hazard curve for the base case, the broken and solid black lines represent the hazard levels of 10% and 2% chance of exceeding in 50 years.

In Figure 3.6(b), upper and lower bound values for 10% and 2% chance of exceeding in 50 years for each site are plotted with respect to the distance from the center of the fault. Figures shows that the effect of this parameter is smaller than that of the b -value but still significant (approximately 15%) for all distances, especially for higher hazard levels. For 475 years return period, increasing M_{\max} by half magnitude units increases the ground motions only by approximately 2%g for all sites.

3.1.4 Sensitivity analysis for the effect of minimum magnitude

Different than the other parameters, the M_{\min} value is generally not estimated using the data in the source zone, but a single value in the range of 3.5 to 5 is chosen arbitrarily. For the sensitivity analysis three different M_{\min} values as 4, 4.5 and 5 are

employed and the corresponding hazard curves are presented in Figure 3.4. All other parameters kept unchanged, but the a-value (the activity rate) is recalculated for each M_{\min} value in these analyses as shown in Table 3.2.

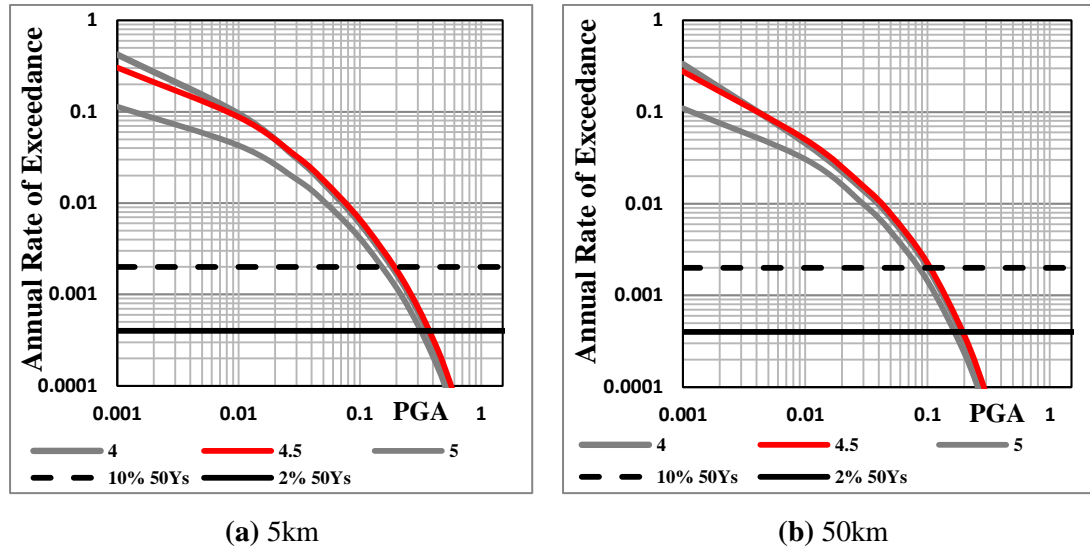


Figure 3.4: hazard curves for different minimum magnitudes (4, 4.5, and 5) at (a) $R_{rup}=5$ km, and (b) $R_{rup}=50$ km. The solid red line is the hazard curve for the base case, the broken and solid black lines represent the hazard levels of 10% and 2% chance of exceeding in 50 years.

Table 3.2: Activity rates used in the analyses for different minimum magnitudes

Minimum magnitude	Re-calculated activity rate
4.0	1.02
4.5 (base case)	0.5
5.0	0.136

The red line in Figure 3.4 represents the hazard curve for the base case ($M_{\min}=4.5$) and the gray lines are the results for $M_{\min}=4$ and $M_{\min}=5$. On the contrary of the general belief, decreasing the M_{\min} value does not decrease the design ground motions by reducing the rate of larger magnitude earthquakes. Similar results were obtained by Bender and Perkins (1993) as shown in Figure 3.5. In Figure 3.6(c), the solid lines show the estimated PGA values for $M_{\min}=4.5$ and broken lines present the PGA values for $M_{\min}=5$ (results of the $M_{\min}=4$ analyses are not shown since they are very close to the values obtained for $M_{\min}=4.5$) for other locations. Analysis results show that the effect of the change in M_{\min} is quite large (approximately 25%) for near-field sites but diminishes as the rupture distance increases.

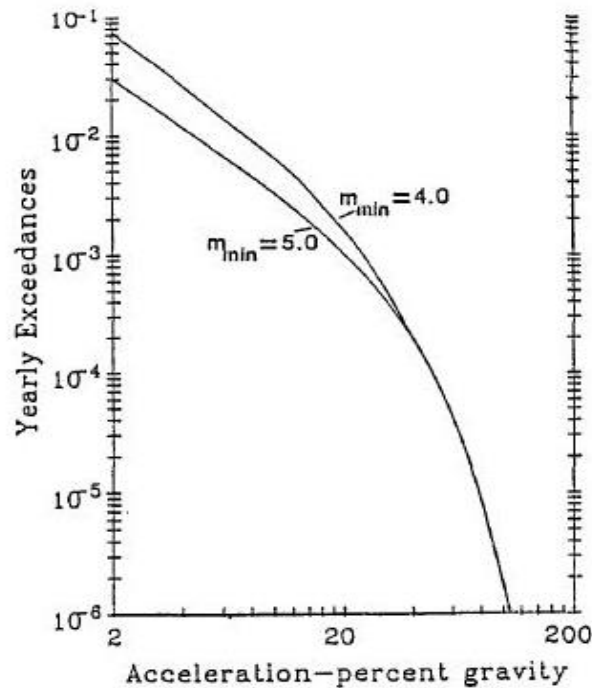


Figure 3.5: Annual exceedance of various levels of PGA calculated for $M_{\min}= 4.0$ and $M_{\min}= 5.0$ (After Bender and Perkins, 1993)

3.1.5 Sensitivity analysis for effect of depth of the source zone

Enough attention is not given to the depth of the areal sources in practice; either the top of the rupture is assumed to be at the surface or a uniform distribution for the depth values is assigned to the source zone. However, this parameter might be critical for deeper earthquake sources, therefore it is evaluated by changing the depth to the top of rupture value from 0 to 20 km (the base case uses 0-14 km to be consistent with the estimated fault width). As shown in Figure 3.6(d), effect of the depth value depends on the location of the site.

If the site is within the areal source zone, then the depth of the source significantly affects the ground motions. As the distance between the source zone boundary and the analyzed site increases, the depth of the source becomes less significant due to the increase in the horizontal distance

3.2. Model 2 - Planar source geometry including a buffer zone for small-to-moderate magnitude events

This source model includes the truncated normal magnitude PDF centered on the M_{char} value for fault segments and the small-to-moderate magnitude events below the

threshold magnitude that are located inside the buffer zone around the fault are modeled using the TE model.

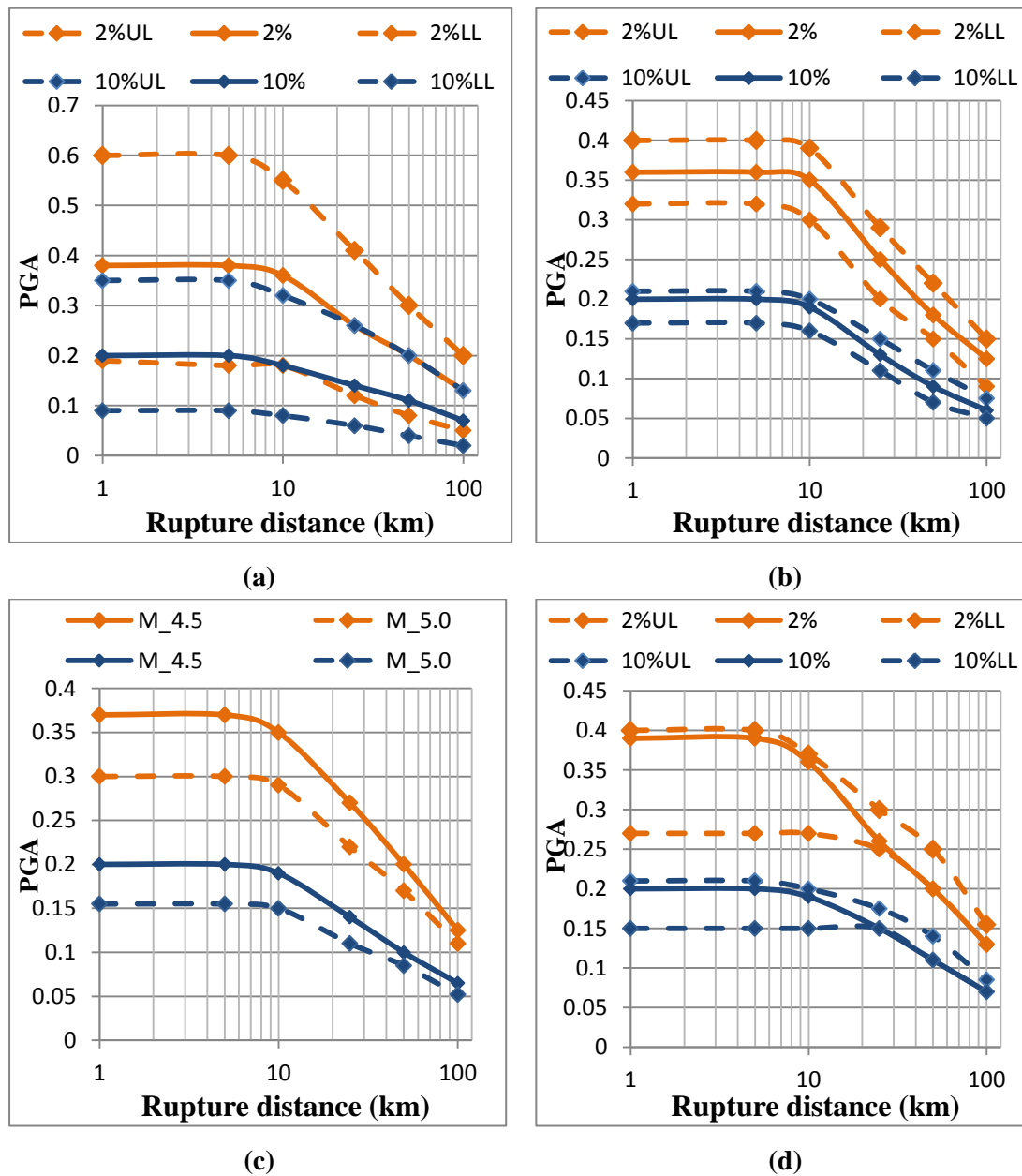


Figure 3.6: Sensitivity of the hazard to different parameters of areal source zone: (a) b -value, (b) M_{max} , (c) M_{min} and (d) depth. The broken orange and blue lines show the upper (UL) and lower (LL) limits on PGA for 2% and 10% chance of being exceeded and the solid lines represent the PGA vs distance values for base case.

The effects of the buffer zone dimensions and the selected threshold magnitude as well as scenario weights, M_{char} , width and slip rate on the hazard results are presented in this section.

3.2.1. Effect of buffer zone dimensions and threshold magnitude

The effect of changing the buffer zone dimensions and the selected threshold magnitude on the hazard results are evaluated in Figure 3.7. Figure 3.7(a-b) show the hazard curves for different buffer zone configurations for a near fault site ($R_{rup}=5$ km) and a far field site ($R_{rup}=50$ km), respectively. Reducing the size of the buffer zone decreases the number of earthquakes within the zone and the activity rate, resulting in smaller ground motions for small hazard levels. The design ground motions with engineering significance (475 and 2475 years return periods), are not affected by the changes in the buffer zone dimensions since the fault model is the dominating contributor of the hazard at these levels.

The threshold magnitude that limits the end of TE magnitude distribution model should be selected carefully in order to prevent the double counting of the rate of moderate magnitude events. As shown in Figure 3.7(c-d), different threshold magnitudes ($M=6, 6.5$ and 7) were employed and the analysis was repeated for the near fault and far field sites. For both sites, the effect of changing the threshold magnitude is insignificant at all hazard levels.

3.2.2. Fault model parameters

Largest contributor of the hazard is the fault model; therefore, the uncertainties in the fault characteristics and parameters have larger impact on the hazard results. In Figure 3.8(a-b), the hazard curves for different slip rates are presented show the sensitivity of the hazard results to the annual slip rate of the fault. Please note that the annual slip rate was varied within reasonable limits for NAF (15 to 24 mm/year) by keeping all other parameters unchanged. Figure 3.12(a) shows that changing the annual slip rate by 15% from the base case model changes the 475 and 2475 years return period PGA approximately by 15% for the near-fault sites. At larger rupture distances, especially for $R_{rup} > 15$ km, the effect of the annual slip rate becomes insignificant.

Sensitivity of the hazard curve to the fault width is evaluated by changing the fault width between 8 and 20 km (Figure 3.9(a-b)). As shown Figure 3.12(b), the effect of fault width on the hazard results is smaller than the effect of other fault parameters. Similar to the depth parameter employed in Model 1, effect is strongly correlated with the location of the site.

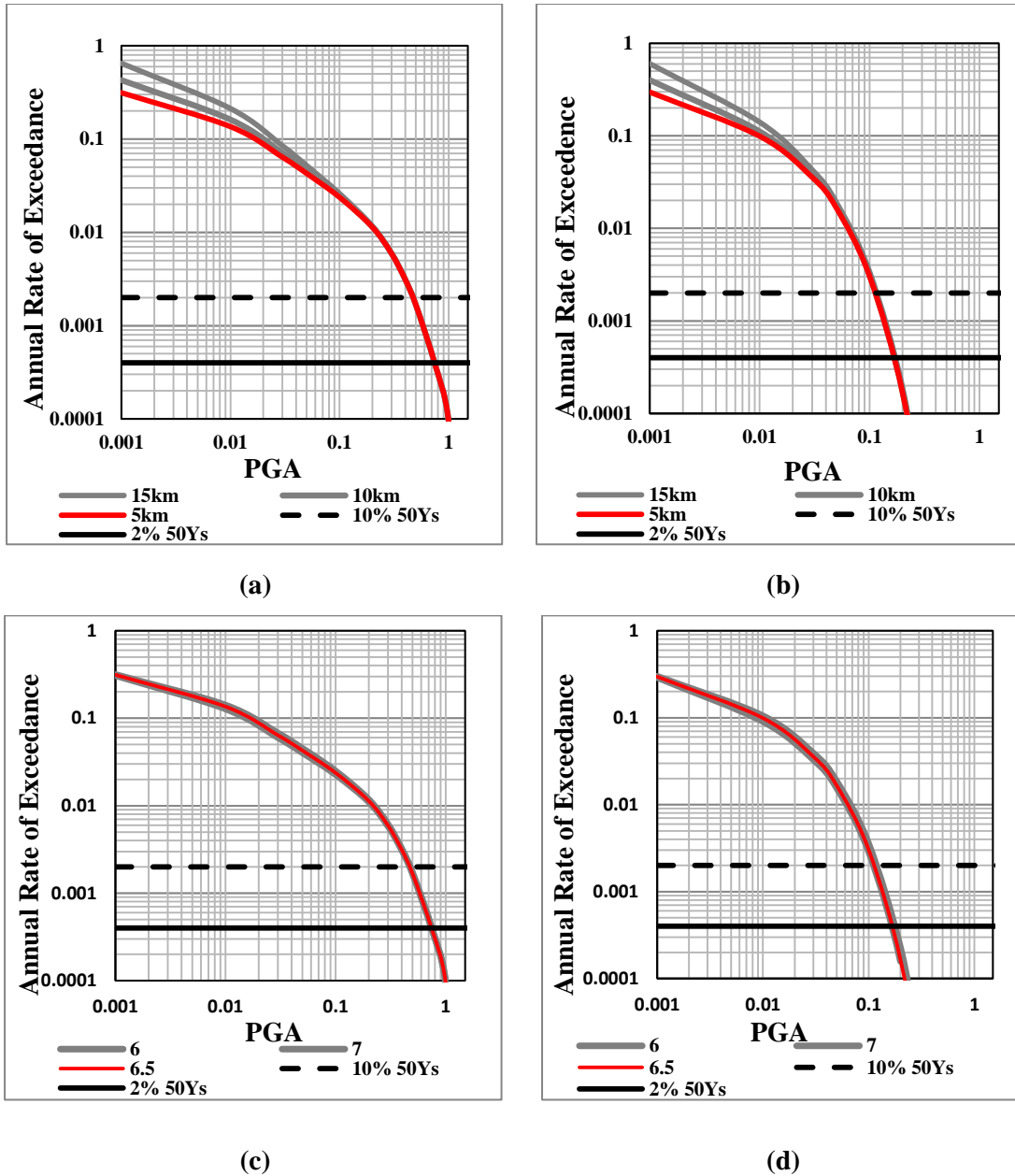


Figure 3.7: Effect of changing the buffer zone boundaries (buffer zones of 5-10-15 km around the fault line) on the hazard at a site with (a) $R_{rup} = 5$ km and (b) $R_{rup} = 50$ km. Hazard curves for different threshold magnitudes at (c) $R_{rup} = 5$ km and (d) $R_{rup} = 50$ km. In these figures the solid red line is the hazard curve for the base case, the broken and solid black lines represent the hazard levels of 10% and 2% chance of exceeding in 50 years.

If the site is inside the buffer zone, then the fault width has a larger effect (approximately 10%) but as the distance between the source and the site increases, the fault width loses its significance on the hazard calculations. Arbitrary combinations of weights for fault rupture scenarios are employed in the logic tree to examine the effect of scenario weighting factors on the hazard for different sites as shown in Figure 3.10 (a-b).

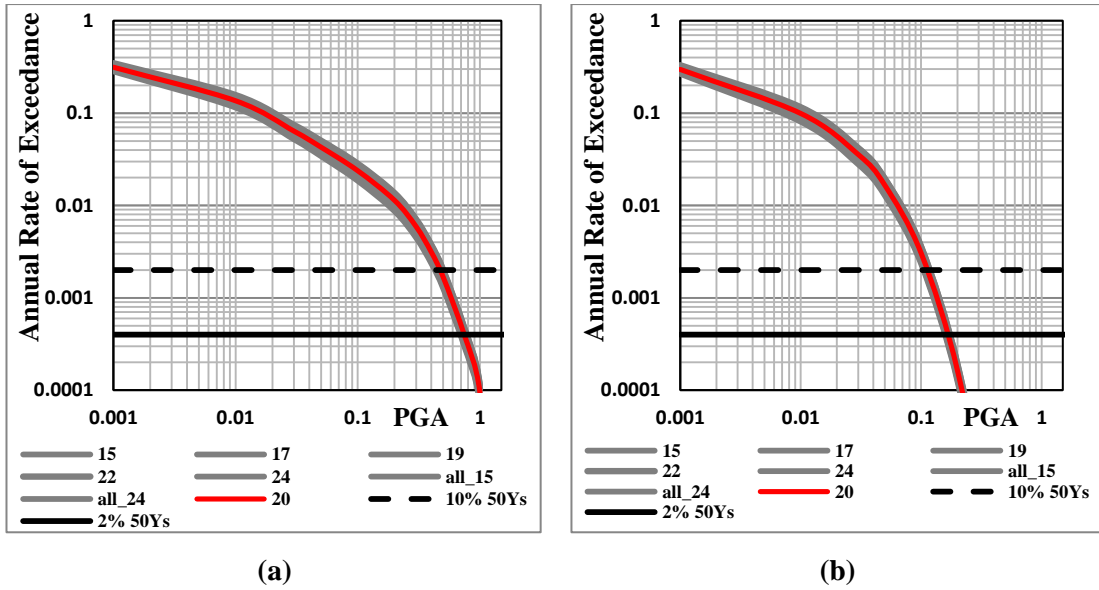


Figure 3.8: Effect of changing the slip rates (ranging between 15 to 24 mm/yr) on the hazard at a site with (a) $R_{rup} = 5$ km and (b) $R_{rup} = 50$ km. In these figures the solid red line is the hazard curve for the base case, the broken and solid black lines represent the hazard levels of 10% and 2% chance of exceeding in 50 years.

The impact of the scenario weights on the hazard curve is substantial, especially in the near fault regions for higher hazard levels, indicating the importance of building the proper fault segmentation models. Figure 3.12(c) shows that the scenario weights may change the 475 and 2475 years design PGA values approximately by 15% for a site that is 5 km away from the fault.

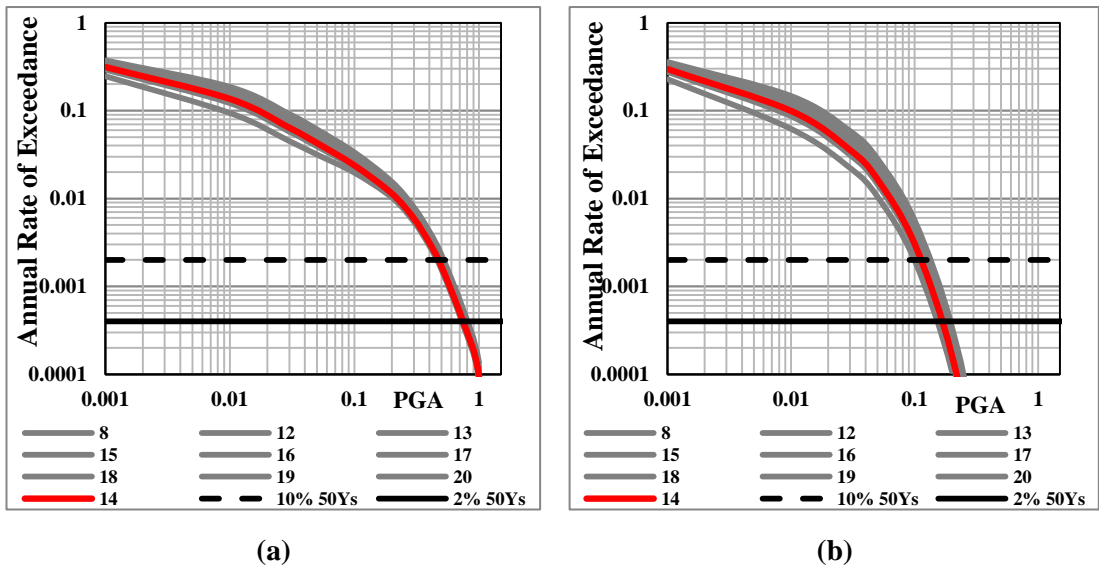


Figure 3.9: Effect of changing the fault width (ranging between 8 and 20 km) on the hazard at a site with (a) $R_{rup} = 5$ km and (b) $R_{rup} = 50$ km. In these figures the solid red line is the hazard curve for the base case, the broken and solid black lines represent the hazard levels of 10% and 2% chance of exceeding in 50 years.

Among the other fault parameters, the impact of the M_{char} on the hazard curve is the largest, especially if the site is located within the buffer zone (Figure 3.12(d)). However, as the source-to site distance increases, the hazard results become almost irrelevant with the M_{char} value.

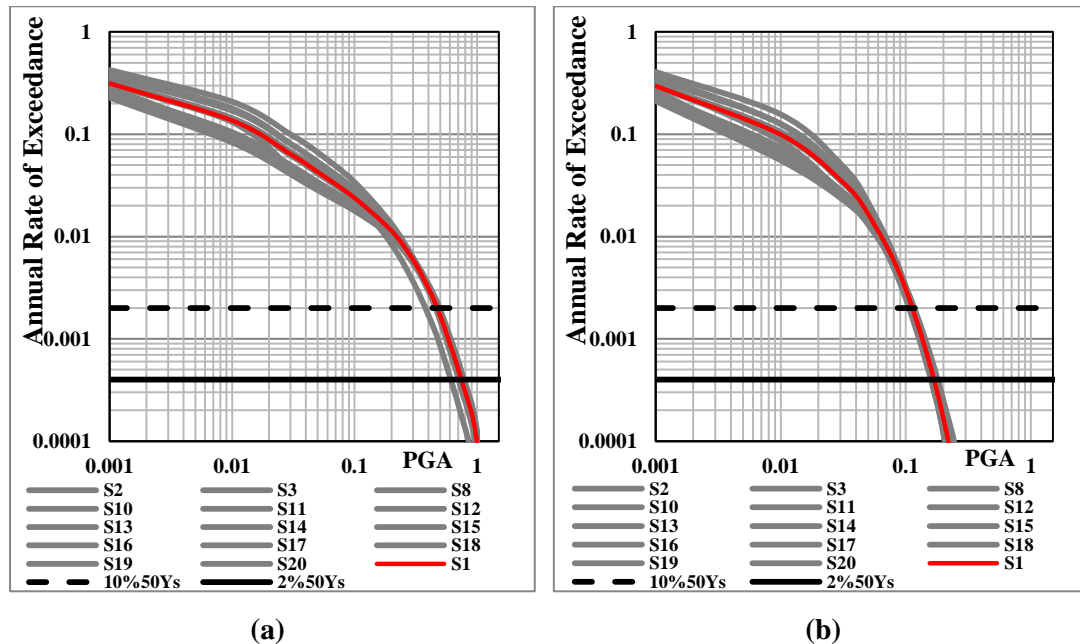


Figure 3.10: Effect of changing the scenario weights on the hazard at a site with (a) $R_{rup} = 5$ km and (b) $R_{rup} = 50$ km.

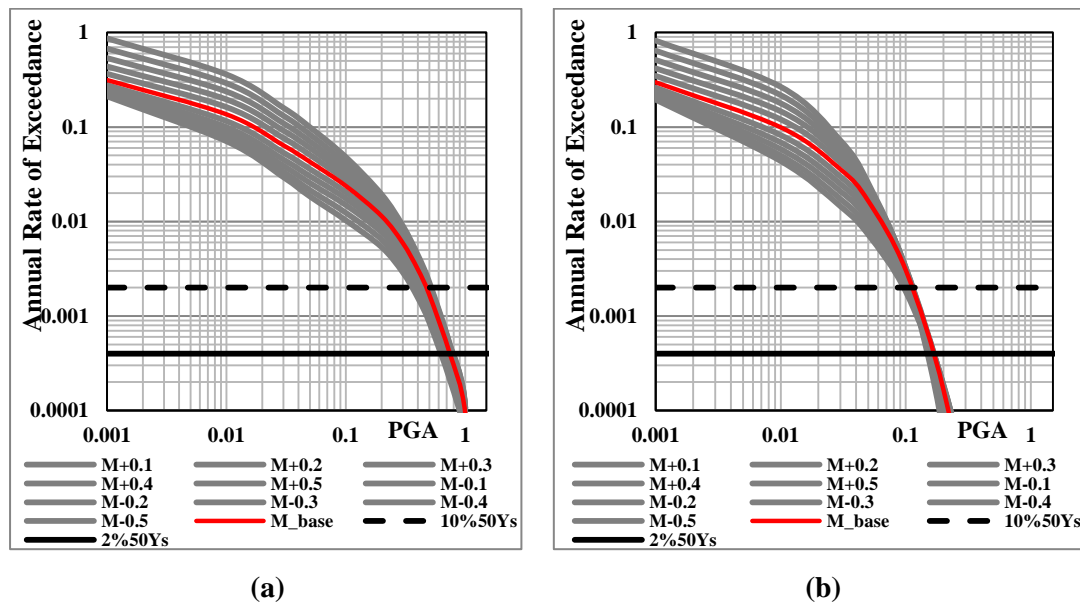


Figure 3.11: Effect of changing the characteristic magnitude (ranging between 7.2 and 8.2) on the hazard at a site with (a) $R_{rup} = 5$ km and (b) $R_{rup} = 50$ km. In these figures the solid red line is the hazard curve for the base case, the broken and solid black lines represent the hazard levels of 10% and 2% chance of exceeding in 50 years.

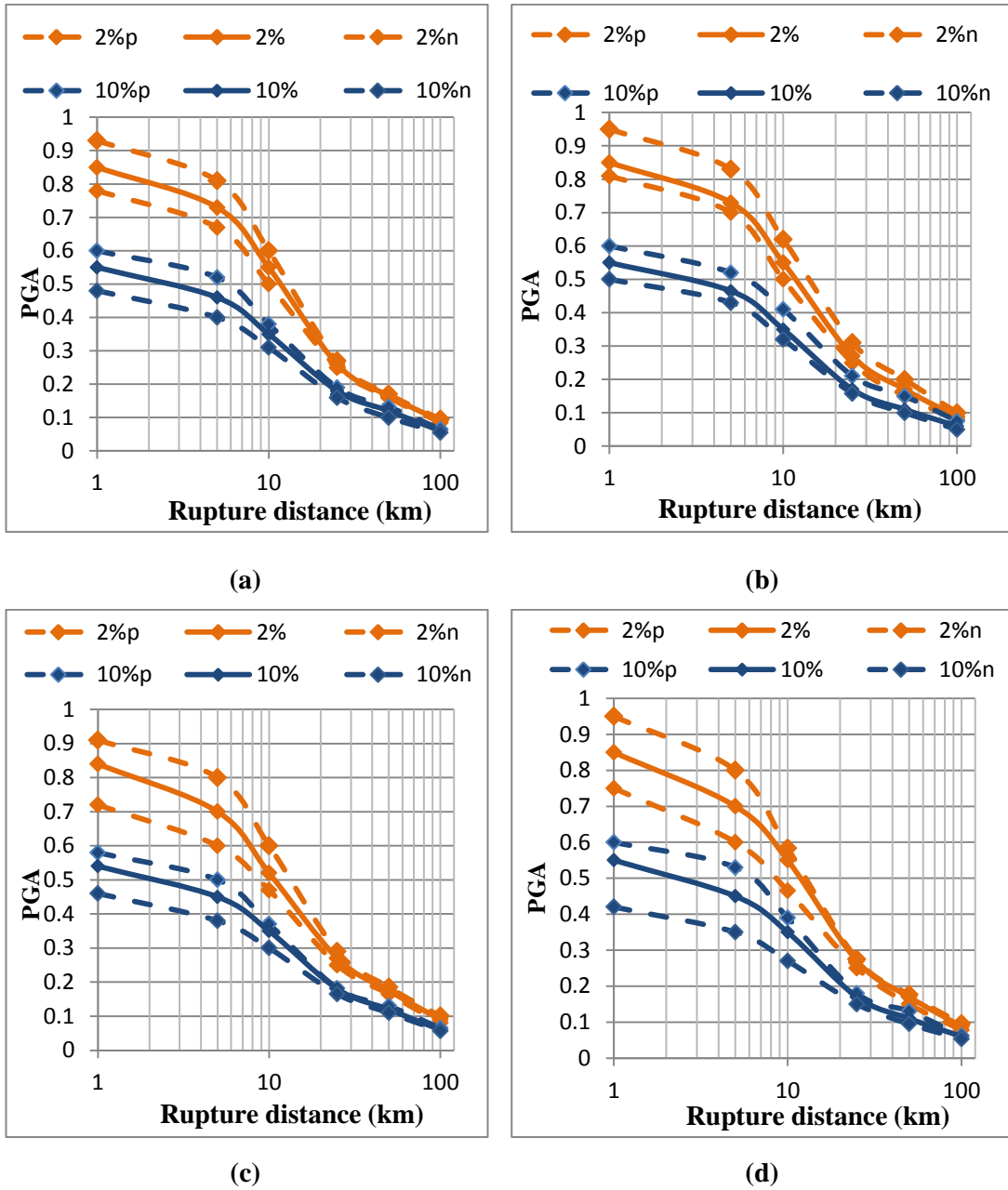


Figure 3.12: Sensitivity of the hazard to different parameters of Model 2: (a) annual slip rate, (b), fault width (c) scenario weighing factors, and (d) M_{char} . The broken orange and blue lines show the upper and lower limits on PGA for 2% and 10% chance of being exceeded and the solid lines represent the PGA vs distance values for base case.

Finally, the effect of the mean characteristic magnitude was evaluated by adding ± 0.5 magnitude units to the M_{char} value of the base case for each source (both to single and multi-segment sources on the same analyses) and comparing the hazard curves with the base case hazard curve (red line in Figure 3.11).

3.3. Model 3 - Planar fault geometry with TE or Composite magnitude distribution

For Model 3 planar fault segments are defined without additional background sources therefore, all seismicity (small, moderate and large events) is represented with the fault model. In Model 3a, the characteristic behavior of NAF is not considered and the TE magnitude recurrence model is adopted. For Model 3b, the Youngs and Coppersmith (1985) composite magnitude recurrence model is preferred. Sensitivity of these two models to different model parameters (annual slip rate, fault width, scenario weights, M_{max} / M_{char} , b-value and M_{min}) is evaluated by comparing the hazard curves for different sites in this section.

3.3.1. Sensitivity analysis for the effect of annual slip rate

Effect of the annual slip rate on the hazard results is investigated by changing the slip rate within reasonable limits for NAF (15-24 mm/year) for Model 3a and Model 3b and the results are compared with the base case in Figure 3.13 (a-f) and Figure 3.14(a-f), respectively. Since the slip rate is not constant over the length of the fault (starts from 17 mm/yr in the easternmost segment, 20 mm/yr in the center and decreases to 8 mm/yr in the far west in Ezinepazari segment) to accurately evaluate the effect of site location, three sets of sites with different distances from the fault (1, 5, 10, 25, 50, and 100 km), located close to the center, east, and west parts of the Niksar-Erzincan Segment are selected and the PSHA results are presented for 18 different sites.

As shown in Figures 3.13 and 3.14, for both models, since the slip rates for the eastern and center sub-segments are close to each other (17 mm/yr and 20 mm/yr) the hazard results for 10% and 2% chance of exceedance are not significantly different for sites located at $R_{rup} = 5$ km of these segments. However, as the distance from the fault increases, the difference rises from 7% to 11% approximately. The difference in hazard results for sites located at the same distance from the fault in center and western end is considerable, especially for Model 3b. This could be explained by the decreased slip rate (8 mm/yr for the Ezinepazari segment) due to the parallel branches of 1939 and 1942-43 ruptures of NAF. This reduction results in lower hazard values for sites located in western end of the fault. Discrepancy in the hazard results would be corrected by including the 1942-1943 rupture zone models in the hazard runs.

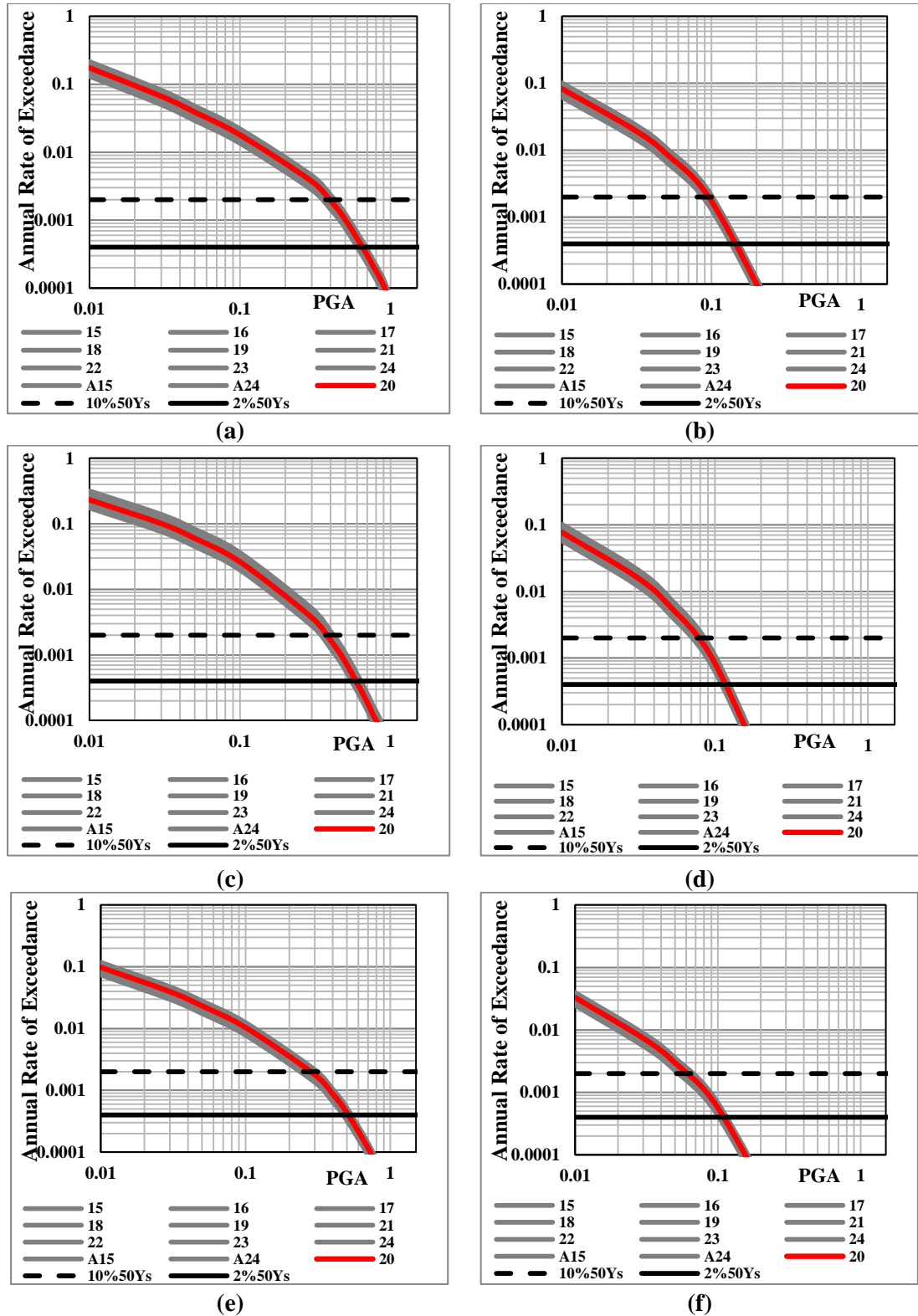


Figure 3.13: Effect of changing the slip rates (ranging between 15 and 24 mm/yr) on the hazard for Model 3a with $R_{rup} = 5$ km for figures (a), (c), (e) and $R_{rup} = 50$ km for figures (b), (d) and (f). Figures (a) and (b) show the set of sites located near the center, figures (c) and (d) show the results for east located sites and figures (e) and (f) are located at the west part of the source.

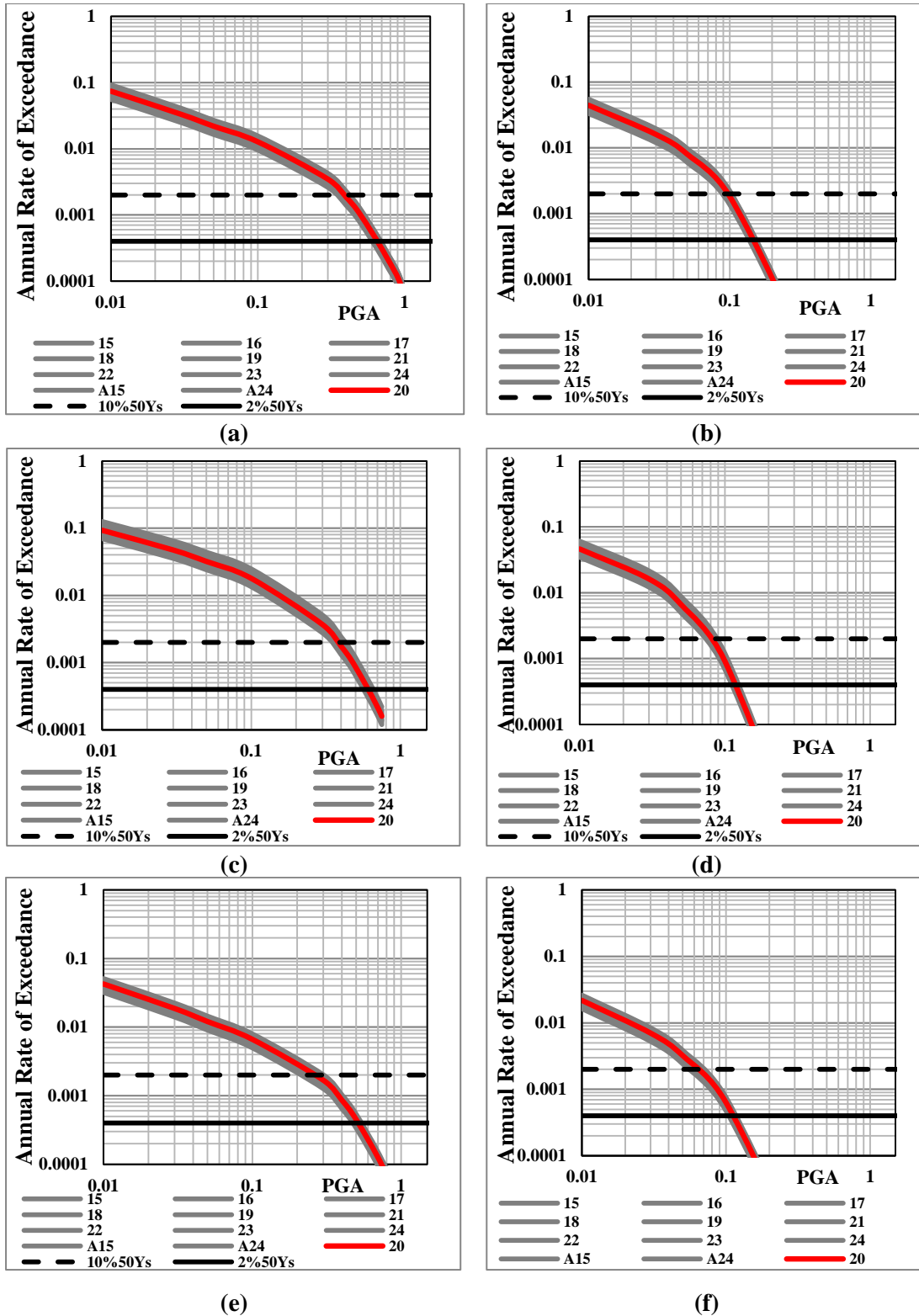


Figure 3.14: Effect of changing the slip on the hazard for Model 3b with $R_{rup} = 5$ km for figures (a), (c), (e) and $R_{rup} = 50$ km for figures (b), (d) and (F). Figures (a) and (b) show the set of sites located near the center, figures (c) and (d) show the results for east located sites and figures (e) and (f) are located at the west part of the source.

Response of the hazard results to the change in the annual slip rate is similar to that

of Model 2: the change in the annual slip rate has a significant effect on the hazard results for the near field sites. For the example site with $R_{rup}=5$ km, the annual slip rate changes the 475 and 2475 years design PGAs approximately by $\pm 0.1g$. In Model 2, annual slip rate does not change the 475 and 2475 years return period ground motions if the rupture distance is larger than 15 km. Figures 3.23(a) and 3.24(a) both show that the hazard results are not completely independent of the annual slip rate for all rupture distances if the planar sources are used in PSHA. Still, the effect is smaller for the far field sites: the design PGA changes only by $\pm 0.05g$ with the change in the slip rate according to Figure 3.24(a).

3.3.2. Sensitivity analysis for the effect of fault width

Sensitivity of the hazard curve to the fault width is evaluated by changing the fault width between 8 km and 20 km and comparing the hazard curves with the base case hazard curve for the near-fault and far-field sites. Figure 3.15(a-b) and Figure 3.16(a-b) show the hazard curves for Model 3a and Model 3b, respectively. Increasing the fault width changes both sides of the moment balance equation: accumulated seismic moment increases since the area of the fault zone increases (Eq. 2.6), however the released seismic moment also increases since the characteristic magnitude of the fault segments is dependent on the fault area (Eq. 2.7). Figures 3.23(b) and 3.24(b) indicate that the effect of the fault width on the hazard outcome is comparable with the effect of annual slip rate. Even if it is small, the effect of the change in the fault width on the hazard is still observed for far field sites in planar fault sources. On the other hand, when the buffer zones are added to the fault lines as in Model 2, the effect of fault width is less significant.

3.3.3. Sensitivity analysis for the effect of scenario weights

Similar to Model 2, arbitrary combinations of fault rupture scenario weights are employed in the logic tree to examine the effect of scenario weighting factors on the hazard curve for Model 3a (Figure 3.17(a-b)) and Model 3b (Figure 3.18(a-b)). As expected, the scenario weights do not have a substantial impact on the hazard results when the TE magnitude recurrence model is preferred (Figure 3.23(c)). When the composite magnitude distribution is used, then the hazard is sensitive to the changes in the larger rates of large magnitude events coming from different combinations of fault rupture scenarios.

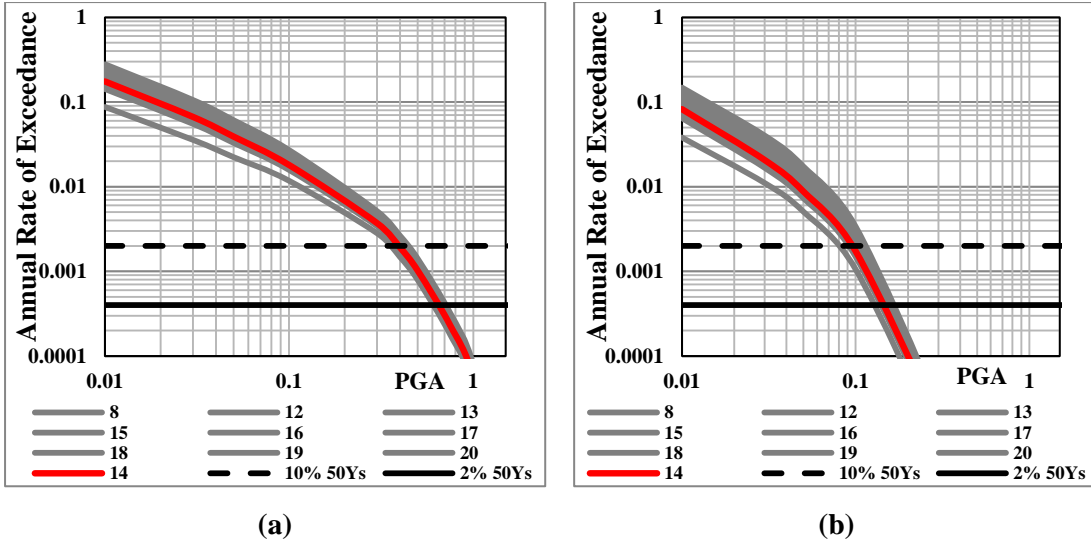


Figure 3.15: Effect of changing the fault width of Model 3a (ranging between 8 km and 20 km) on the hazard at a site with (a) $R_{rup} = 5$ km and (b) $R_{rup} = 50$ km. In these figures the solid red line represents the hazard curve for the base case and the broken and solid black lines represent the hazard levels of 10% and 2% chance of being exceeded in 50 years.

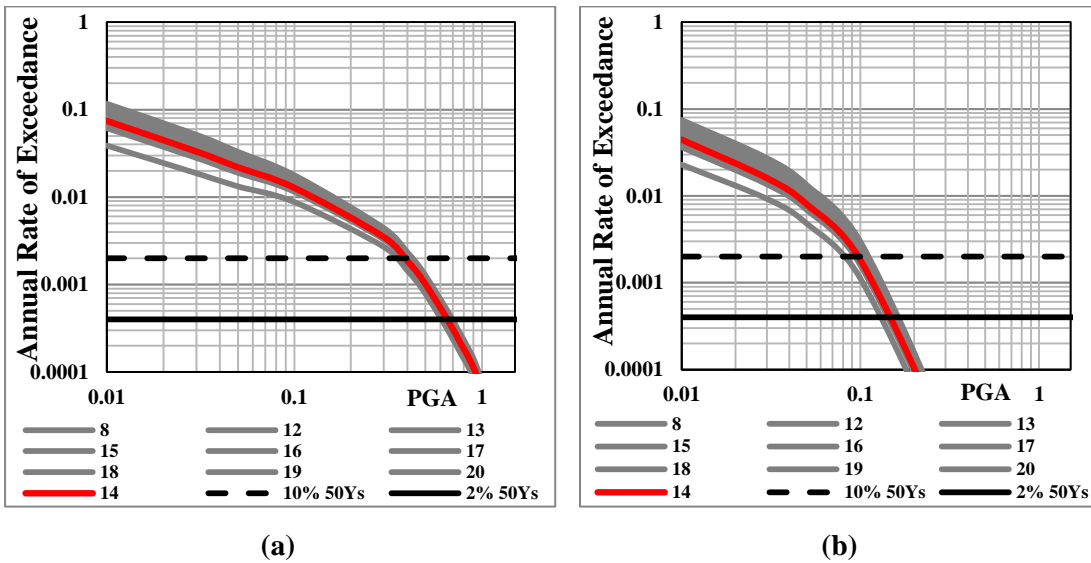


Figure 3.16: Effect of changing the fault width of Model 3b (ranging between 8 km and 20 km) on the hazard at a site with (a) $R_{rup} = 5$ km and (b) $R_{rup} = 50$ km. In these figures the solid red line represents the hazard curve for the base case and the broken and solid black lines represent the hazard levels of 10% and 2% chance of being exceeded in 50 years.

Figure 3.24(c) shows that the scenario weights can change the design PGA values approximately $\pm 0.10g$ for 475 and 2475 years return periods for the near-fault sites, but this effect diminishes as the rupture distance increases. Sensitivity of the hazard may not be reflected properly in Figure 3.24(c) since we limited the scenario weight combinations to make sure that none of the multi-segment scenarios are excluded from the system.

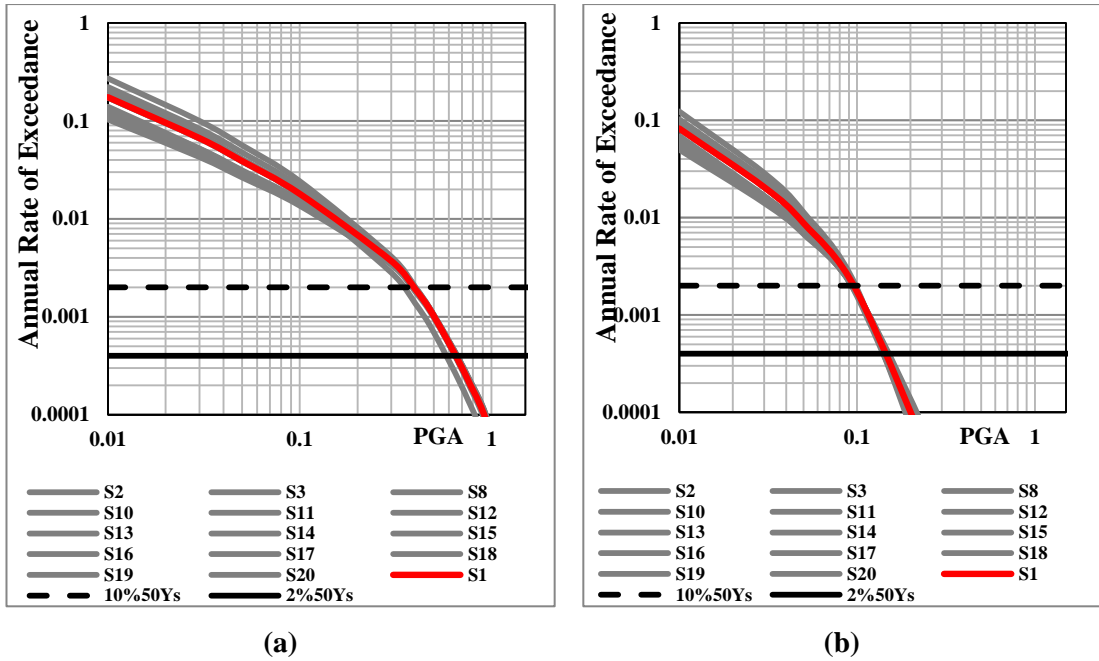


Figure 3.17: Effect of changing the scenario weights of Model 3a on the hazard at a site with (a) $R_{rup} = 5$ km and (b) $R_{rup} = 50$ km. In these figures the solid red line represents the hazard curve for the base case and the broken and solid black lines represent the hazard levels of 10% and 2% chance of being exceeded in 50 years.

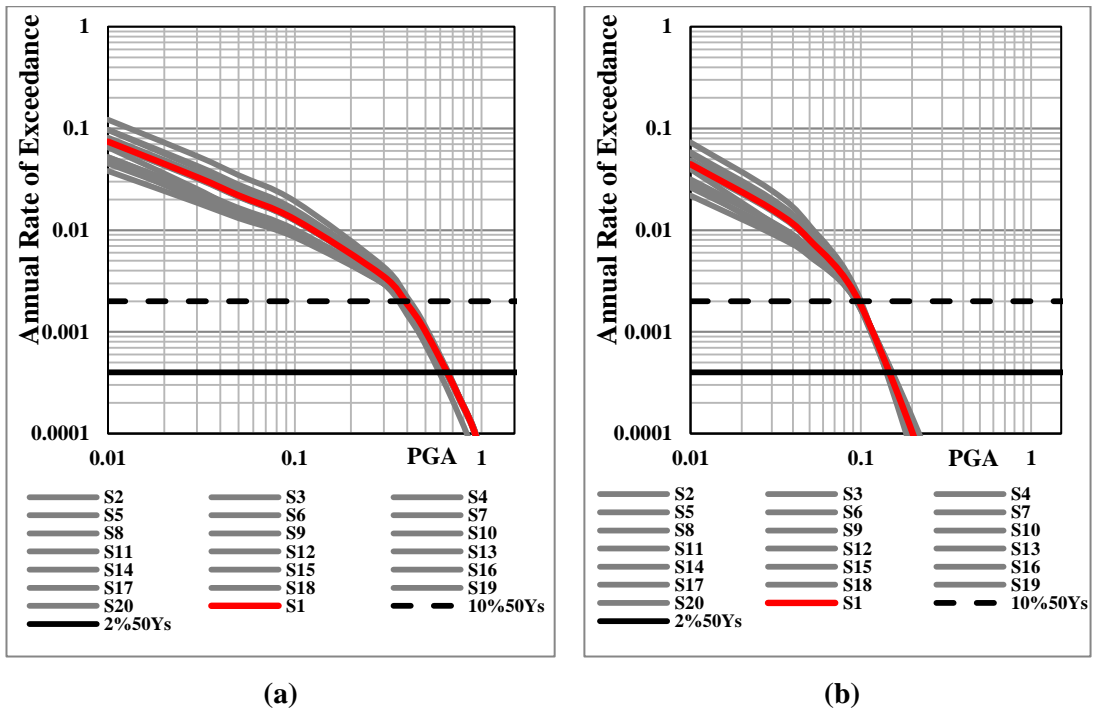


Figure 3.18: Effect of changing the scenario weights of Model 3b on the hazard at a site with (a) $R_{rup} = 5$ km and (b) $R_{rup} = 50$ km. In these figures the solid red line represents the hazard curve for the base case and the broken and solid black lines represent the hazard levels of 10% and 2% chance of being exceeded in 50 years.

The change in the ground motions can be higher for more extreme weight combinations defined by the hazard analysts.

3.3.4. Sensitivity analysis for maximum and characteristic magnitudes

Final set of sensitivity analysis are conducted by changing the M_{max} values for Model 3a and M_{char} values for Model 3b within the same range (7.2-8.2) and the results are compared with the base case (solid red line) in Figures 3.19(a-b) and 3.20(a-b), respectively.

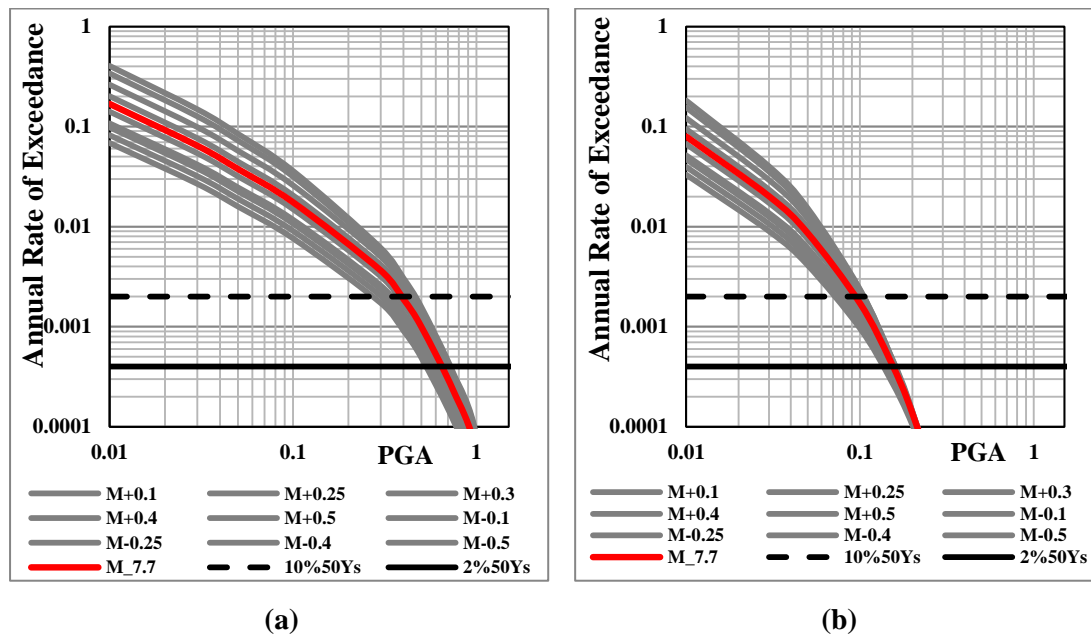
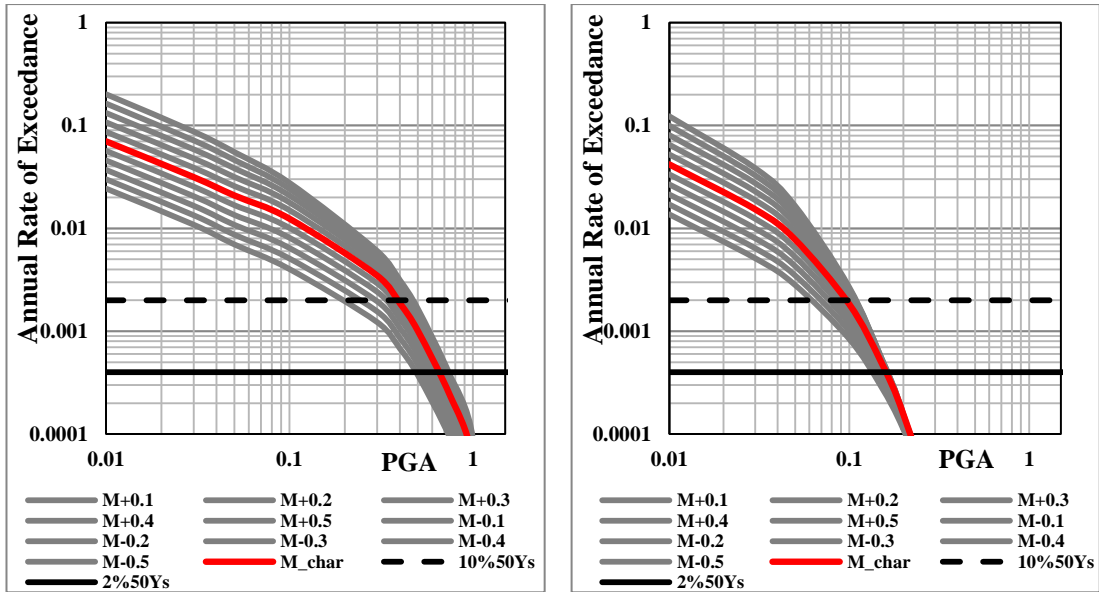


Figure 3.19: Effect of changing the M_{max} of Model 3a on the hazard at a site with (a) $R_{rup} = 5$ km and (b) $R_{rup} = 50$ km. In these figures the solid red line represents the hazard curve for the base case and the broken and solid black lines represent the hazard levels of 10% and 2% chance of being exceeded in 50 years.

As presented in Figures 3.19 and 3.20, the effect of the upper extreme of the magnitude distribution is larger in the composite model when compared to the TE model. Especially for the near fault sites, the design ground motions may be reduced by approximately 10% with 0.5 magnitude units decrease in the M_{max} value of the TE distribution, whereas the effect is close to 25% when the M_{char} value of the composite model is reduced by the same amount. For both cases, the effect diminishes as the rupture distance increases, especially when $R_{rup} > 50$ km.



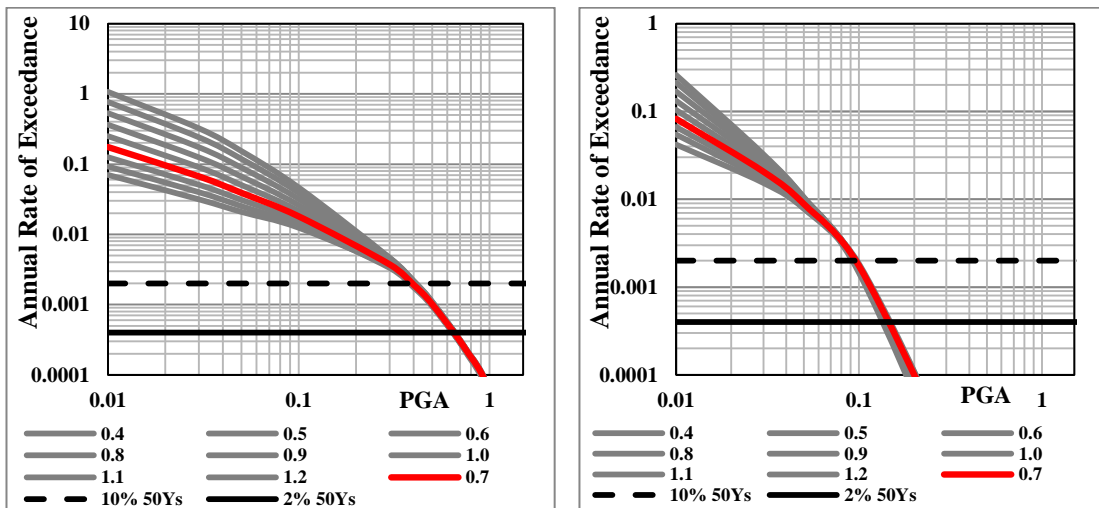
(a)

(b)

Figure 3.20: Effect of changing the M_{char} of Model 3b on the hazard at a site with (a) $R_{rup} = 5$ km and (b) $R_{rup} = 50$ km. In these figures the solid red line represents the hazard curve for the base case and the broken and solid black lines represent the hazard levels of 10% and 2% chance of being exceeded in 50 years.

3.3.5. Sensitivity analysis for the effect of b-value and M_{min}

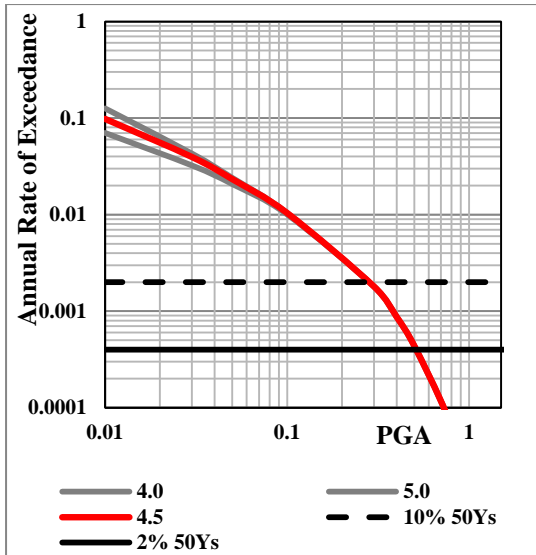
Further sensitivity analyses for Models 3a and 3b are conducted to evaluate the effect of the b-value, the parameter that defines the slope of the exponential tail of the Youngs and Coppersmith (1985) composite model.



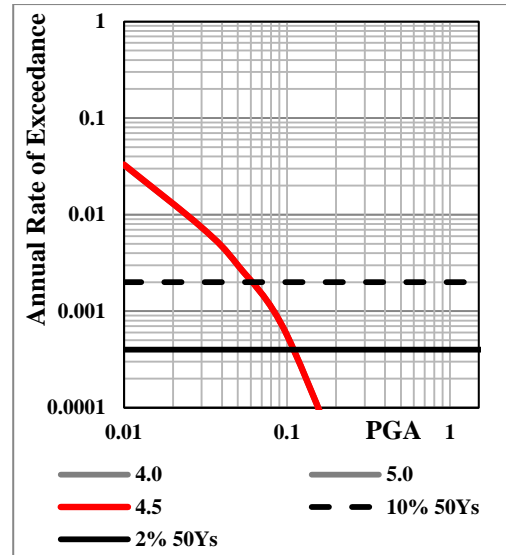
(a)

(b)

Figure 3.21: Effect of changing the b value on the hazard at a site with (a) $R_{rup} = 5$ km and (b) $R_{rup} = 50$ km and M_{min} at a site with (c) $R_{rup} = 5$ km and (d) $R_{rup} = 50$ km for Model 3a. In these figures the solid red line represents the hazard curve for the base case and the broken and solid black lines represent the hazard levels of 10% and 2% chance of being exceeded in 50 years.



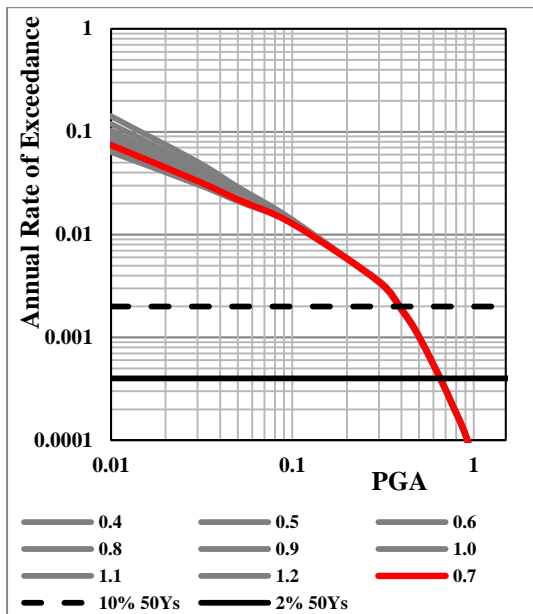
(c)



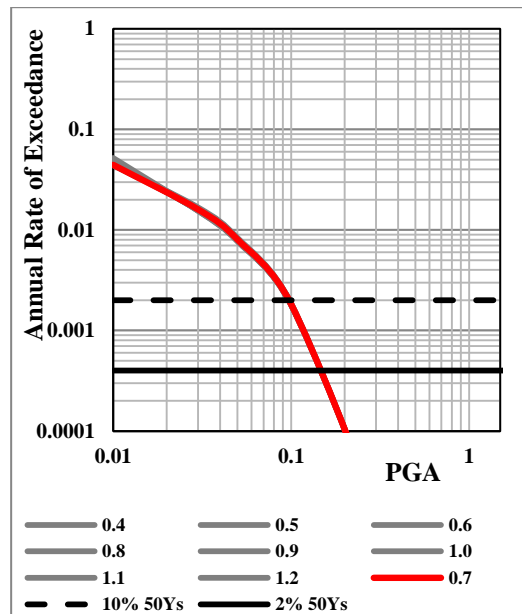
(d)

Figure 3.21: (Continued)

In the analysis, the b-value is again changed within the range of 0.4 and 1.2. The hazard curves are compared with the base case hazard curve for the near-fault site (Figures 3.21(a) and 3.22(a)) and for the far-field site (Figures 3.21(b) and 3.22(b)).



(a)



(b)

Figure 3.22: Effect of changing the b value on the hazard at a site with (a) $R_{rup} = 5$ km and (b) $R_{rup} = 50$ km and M_{min} at a site with (c) $R_{rup} = 5$ km and (d) $R_{rup} = 50$ km for Model 3b. In these figures the solid red line represents the hazard curve for the base case and the broken and solid black lines represent the hazard levels of 10% and 2% chance of being exceeded in 50 years.

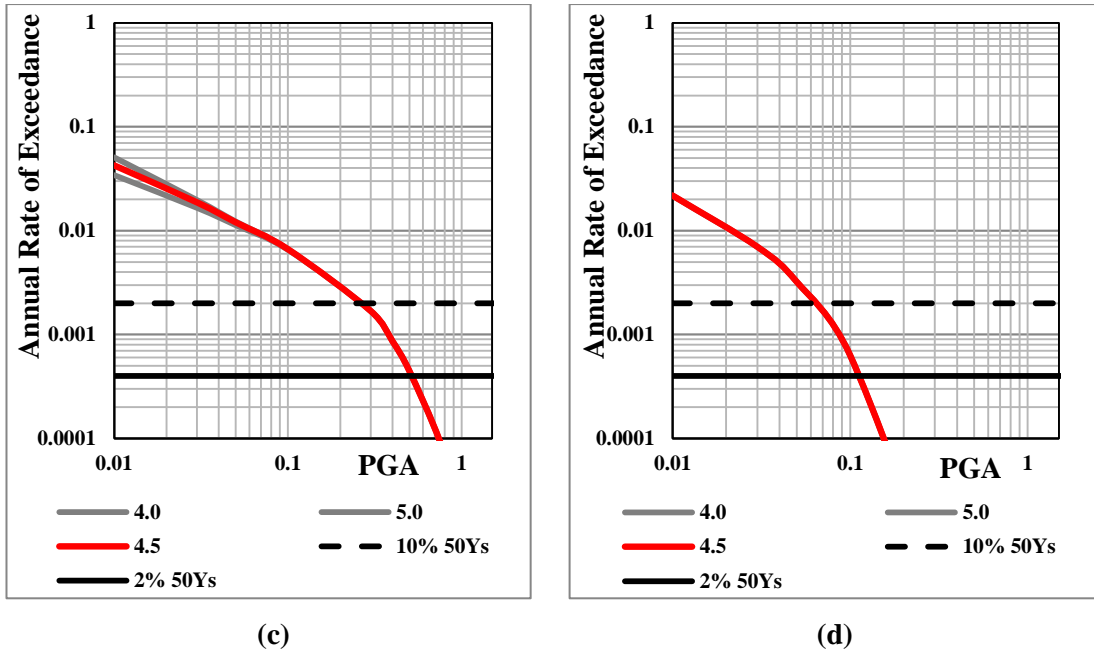


Figure 3.22: (Continued)

Figure 3.21 and Figure 3.22 show that Model 3a is more sensitive to the changes in b-value. The effect of the b-value is visible in the small hazard levels for the near fault sites; however, the hazard curve is insensitive to the changes in the b-value at the hazard levels accepted by the building codes. The effect of the b-value on the hazard outcome for the far-field site is negligible for all hazard levels as expected. Another parameter that does not change the ground motions for 475 and 2475 years return periods is M_{min} as shown in Figures 3.22(c-d) and 3.23(c-d). In both models three M_{min} values were selected (4.0, 4.5 and 5.0) but the differences in hazard levels accepted by the building code were insignificant. Both parameters only control 6% of the released seismic moment by the exponential tail of the model, therefore have no substantial effect on the results.

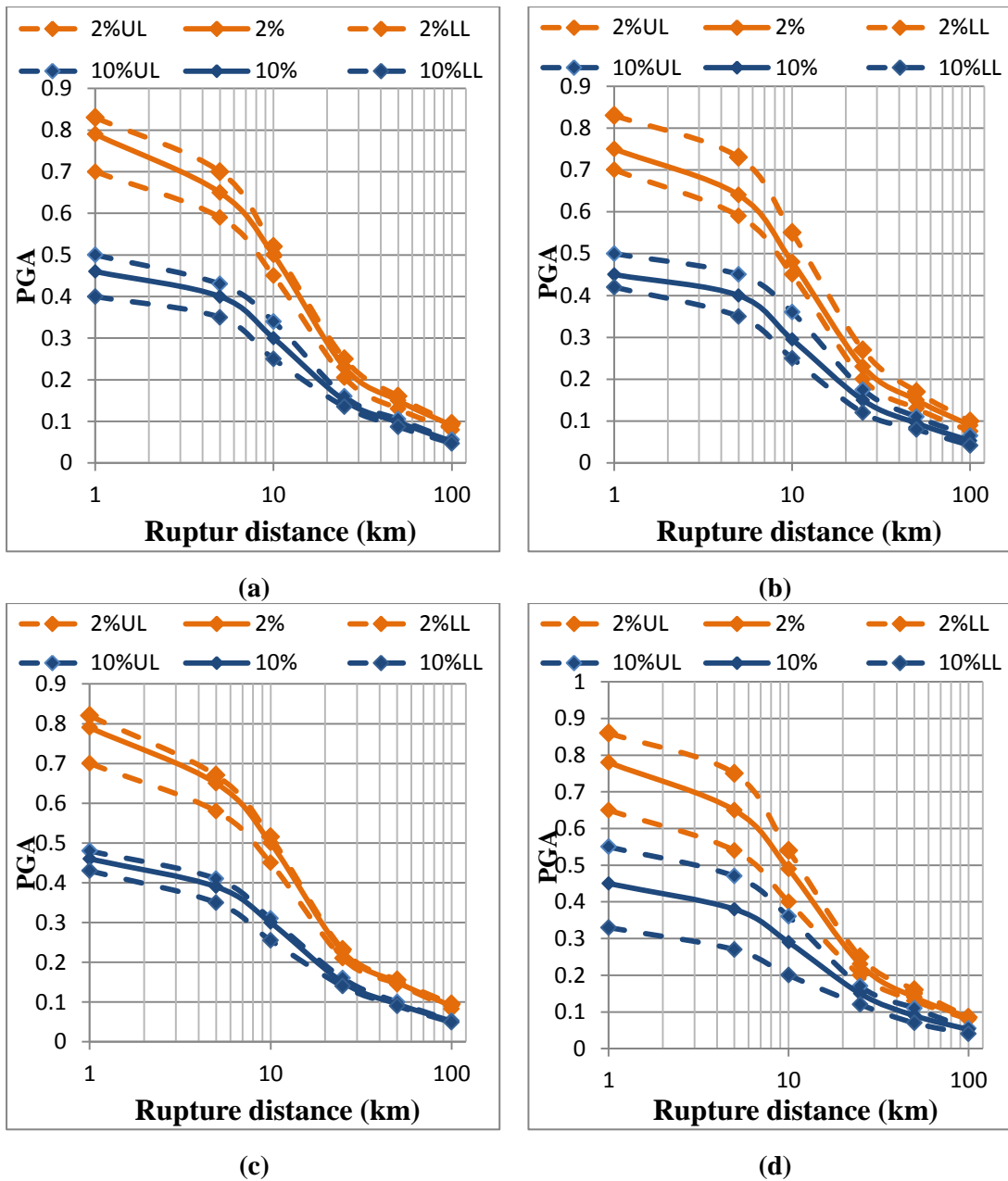


Figure 3.23: Sensitivity of the hazard to different parameters of Model 3a: (a) annual slip rate, (b) fault width (c) scenario weighing factors, and (d) M_{char} . The broken orange and blue lines show the upper and lower limits on PGA for 2% and 10% chance of being exceeded and the solid lines represent the PGA vs distance values for base case.

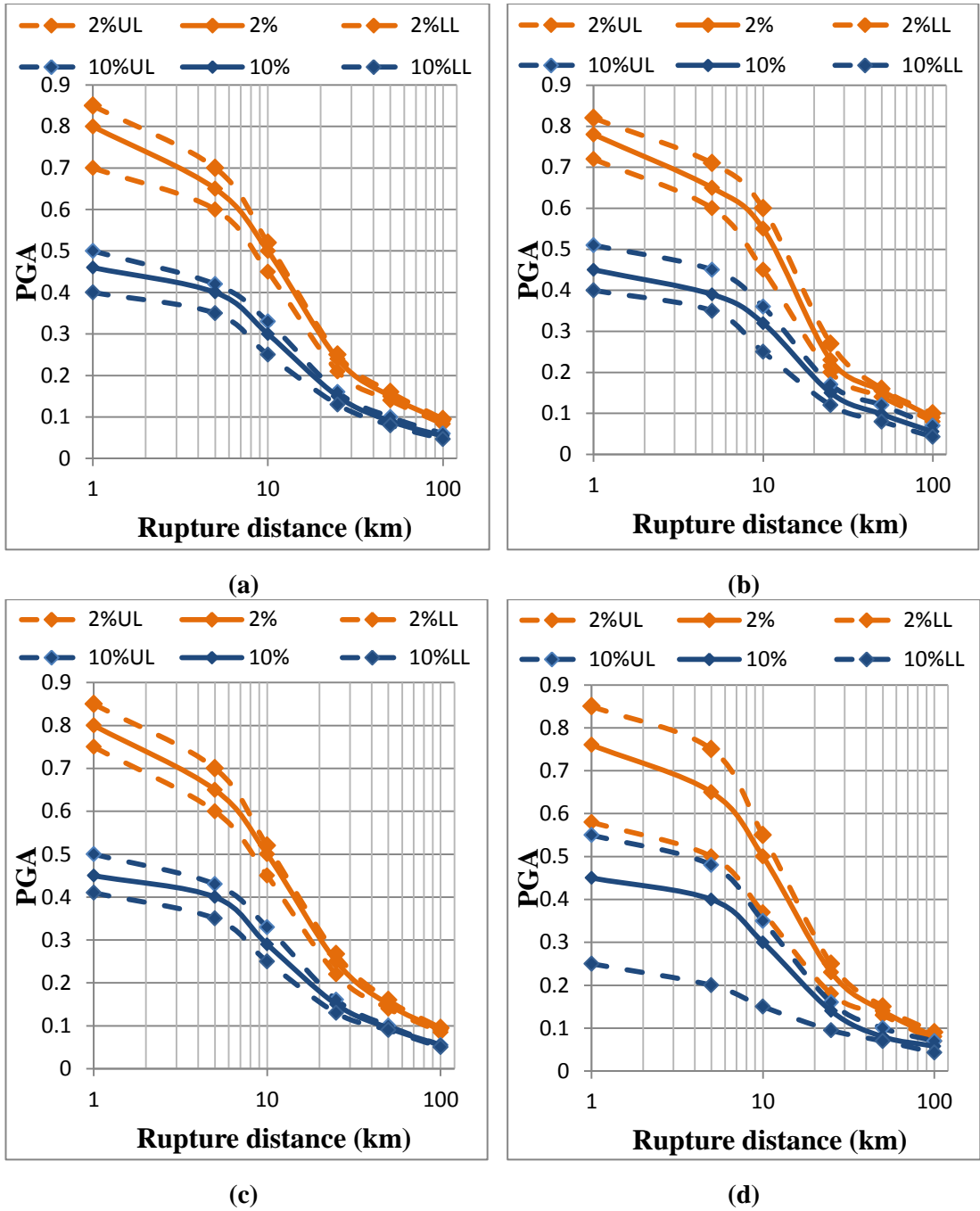


Figure 3.24: Sensitivity of the hazard to different parameters of Model 3b: (a) annual slip rate, (b) fault width (c) scenario weighing factors, and (d) M_{char} . The broken orange and blue lines show the upper and lower limits on PGA for 2% and 10% chance of being exceeded and the solid lines represent the PGA vs distance values for base case.

CHAPTER 4

DESIGN GROUND MOTIONS BASED ON DIFFERENT SEISMIC SOURCE MODELS: A COMPARISON WITH TURKISH EARTHQUAKE CODE (2007) REQUIREMENTS

Effect of the seismic source models on the 475 and 2475 years return period PGA for near fault ($R_{rup}=5$ km) and far field ($R_{rup}=50$ km) sites was evaluated on Chapter 2. To be able to examine the same effect for other spectral periods and for different locations, 22 example sites are selected as shown in Figure 4.1 for further analyses. 3 different sets of sites are chosen to show the effect of annual slip rate: Sites 1-5, Site 16 and Site 21 are close to the Ezinepazarı Segment, representing low slip rate conditions (8 mm/year) whereas other sites are located parallel to central and eastern segments with higher annual slip rates (17-19 mm/year). Spatial distribution of the sites are selected carefully to enable the comparison of design spectra from PSHA with the Turkish Earthquake Code (TEC, 2007) requirements in Zones 1-4 (In Figure 4.1, the TEC-2007 zones are shown by different colors). Table 4.1 present the TEC-2007 seismic zone that the selected sites are located and closest distance between the site and the fault plane.

A common method for developing design spectra based on the PSHA results is using the Uniform Hazard Spectrum (UHS). The UHS is developed by computing the hazard independently at a set of spectral periods and then computing the ground motion for a specified probability level at each spectral period. Since the hazard is computed independently for each spectral period, the UHS does not represent the spectrum of any single earthquake. The term “uniform hazard spectrum” is used because the spectral acceleration value at each period has an equal chance of being exceeded (Gülerce and Abrahamson, 2010). The procedure used in developing the UHS is illustrated in Figure 4.2.

Only two different seismic source characterization models discussed in Chapter 2 are employed in the PSHA runs for developing the UHS: Model 1 (areal seismic source zone with TE magnitude distribution model and Model 3b (planar seismic source zone with composite magnitude distribution model). For both seismic source model options, two GMPEs, TR-Adjusted Boore and Atkinson (2008) and TR-Adjusted Campbell and Bozorgnia (2008), are used in the analysis with equal weights (50%) in logic tree to decrease the computational time. In the PSHA runs, rock site conditions are assumed ($V_{S30}=760$ m/s). Three hazard curves are obtained for PGA and the spectral accelerations at $T=0.05$, $T=0.1$, $T=0.2$, $T=0.3$, $T=0.5$, $T=0.75$, $T=1$, $T=2$, $T=3$, $T=4$ and $T=5$ seconds spectral periods as shown in Figure 4.2.

Table 4.1: Closest distance to the fault and seismic zones of the selected sites

Sites	Distance to the Fault (km)	Seismic Zone (TEC-2007)
Site 1	96.481	Zone 3
Site 2	81.945	Zone 2
Site 3	39.807	Zone 1
Site 4	20.849	Zone 1
Site 5	39.012	Zone 2
Site 6	72.868	Zone 3
Site 7	34.761	Zone 1
Site 8	24.966	Zone 1
Site 9	49.882	Zone 2
Site 10	82.943	Zone 4
Site 11	58.747	Zone 3
Site 12	23.741	Zone 1
Site 13	29.915	Zone 1
Site 14	73.018	Zone 2
Site 15	39.521	Zone 2
Site 16	68.777	Zone 3
Site 17	71.661	Zone 3
Site 18	55.563	Zone 2
Site 19	5.0 (East)	Zone 1
Site 20	5.0 (Center)	Zone 1
Site 21	5.0 (West)	Zone 1
Site 22	94.480	Zone 4

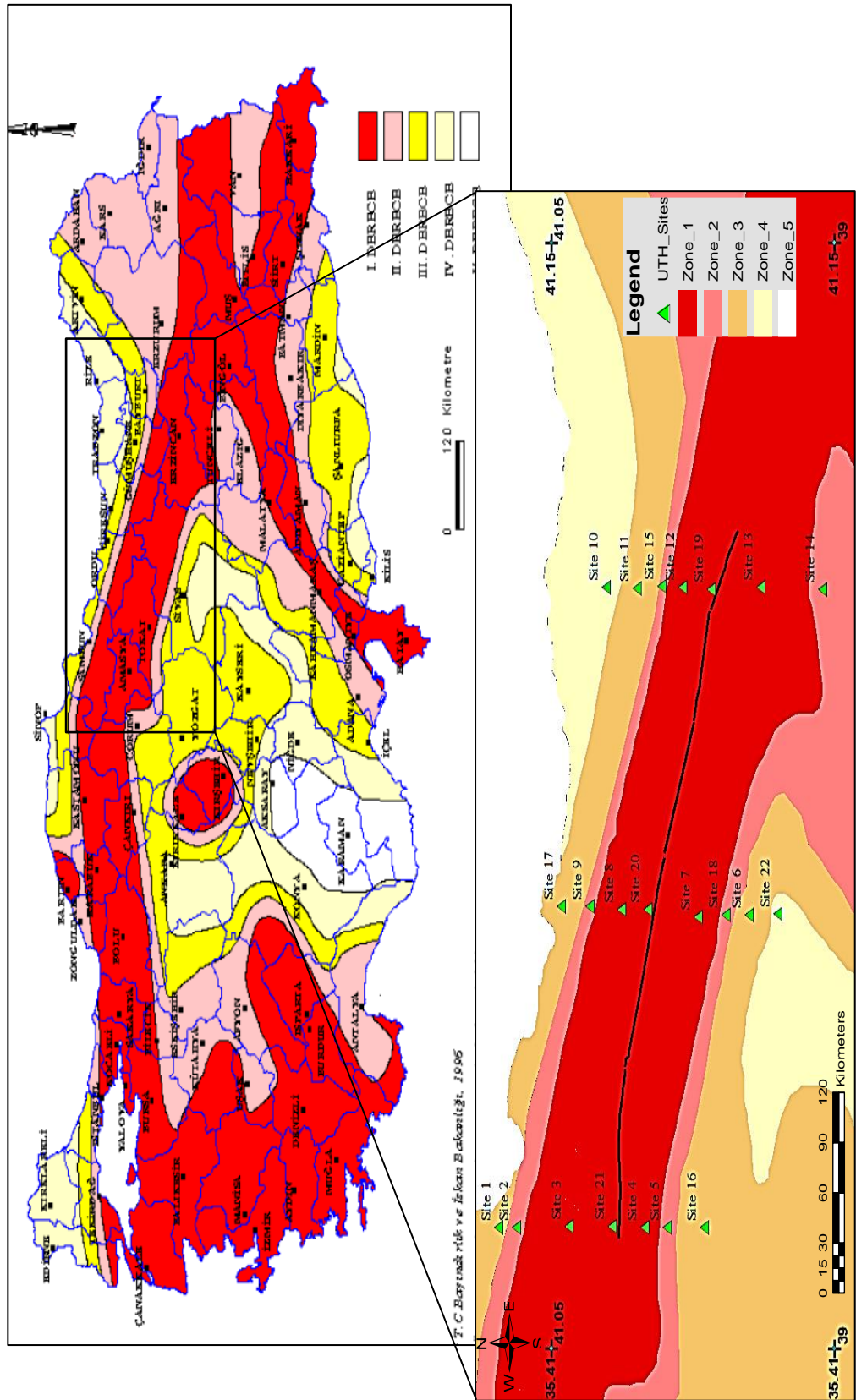


Figure 4.1: Location of the selected sites with respect to the first, second, third and fourth seismic zones depicted in Seismic Zoning Map of Turkey

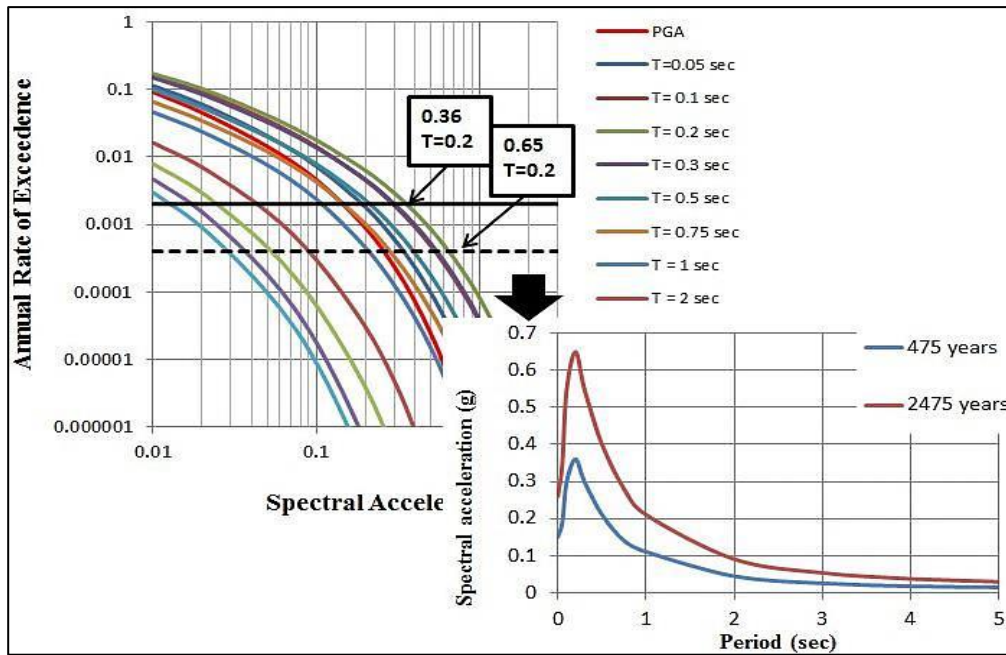


Figure 4.2: The procedure used in developing the UHS.

UHS for 475 and 2475 years return periods are developed for both source models and shown by solid and broken lines in Figure 4.3, respectively. TEC-2007 design spectrum for rock site condition (soil class Z1 for $V_{S30} = 760$ m/s) is also plotted in Figure 4.3 by black solid lines. Figure 4.3 presents the 475 and 275 years return period UHS for sites located on a perpendicular line passing through the central segment as shown in Figure 4.1. Independent of the source to site distance, Model 1 results in lower spectral accelerations when compared to Model 3b for 475 years return period. Especially for near fault sites, the spectral accelerations between 0.1-1 spectral periods given by Model 1 are more than 50% lower than those of Model 3b (e.g. Figure 4.3(a)). The difference in the ground motions levels given by two models decreases as the distance between the site and source increases (e.g. Figure 4.2 (h)). Figure 4.3 indicates that the UHS for almost all sites (except for Site 20 with $R_{rup}=5$ km) are lower than the TEC-2007 design spectrum both for Model 1 and Model 3b. It is notable that the Zone 1 of TEC-2007 is unrealistically large and completely neglects the change in the ground motions within the 50 km buffer around the tectonic structure. Currently, a site that is 35 km away from the fault (Site 7, Figure 4.3(c)), and a site that is only 5 km away from the fault (Site 20, Figure 4.3(a)) have to use exactly the same design envelope. However, the UHS for these sites are significantly different than each other. The difference is substantial for Model 3b, but less significant for Model 1. According to Figure 4.3(a), the UHS is very close to the

TEC-2007 requirements in the near field; it is even higher than the plateau of TEC-2007 envelope between 0.1-0.2 seconds where the UHS peaks.

To provide a better view of the differences within the same zone, a zone by zone comparison of the developed UHS and the TEC-2007 design spectrum is presented in Figure 4.4 (a-h) for 475 year return period. Gray lines in Figure 4.4 (a-h) show the UHS for 475 year return period for all sites within the same zone according to TEC-2007 and black solid line represents the TEC-2007 requirements as design spectrum. In the left hand side figures (Figures 4.4(a, c, e, g)) the UHS is obtained by Model 3b and in right hand side figures (Figures 4.4(b, d, f, h)) Model 1 is employed. According to Figure 4.4(a), the spectral accelerations for 2 near fault sites (Site 19 and Site 20, located 5km away from the fault) are 1.25 and 1.5 times higher than the TEC-2007 requirements for 0.1-0.3 seconds periods range. However for the other sites in the same zone, the UHS are below the TEC-2007 design spectrum and the UHS spectral accelerations decrease as the distance between the site and source increases (starting from 0.72g to 0.23g for 0.2 second spectral period). For Zones 2 and 3 (Figure 4.4 (c-f)) the UHS based on both source models are far below the TEC-2007 requirements. The disagreement between the UHS and TEC-2007 recommendations is smaller for Zone 4 (Figure 4.4 (g-h)).

Figure 4.5 is prepared to show the contribution of the annual slip rate to the differences in the design spectrum. The UHS for Sites 19, 20 and 21, all located within the same distance (5 km) from the fault line, are shown in Figure 4.5. These points are close to the segments of 1939 Erzincan Earthquake rupture zone with different annual slip rates. The UHS for Sites 19 and 20 (located near the eastern and center parts of the 1939 Erzincan Earthquake rupture zone) are significantly larger than the UHS of Site 21 which is located near the Ezinepazari Segment with lower annual slip rate. Differences are substantial for all return periods: the 475-years spectral acceleration for 0.2 second spectral acceleration for Site 21 is 0.7 times lower than TEC-2007. The results presented for Site 21 is completely unrealistic since the source models developed for other parallel branches of NAF Zone are excluded. However, Figure 4.5 indicates that the design spectrum is very strongly correlated with the annual slip rate when the planar fault models are employed whereas; distance to the source boundary dominates the design spectrum when areal source models are employed.

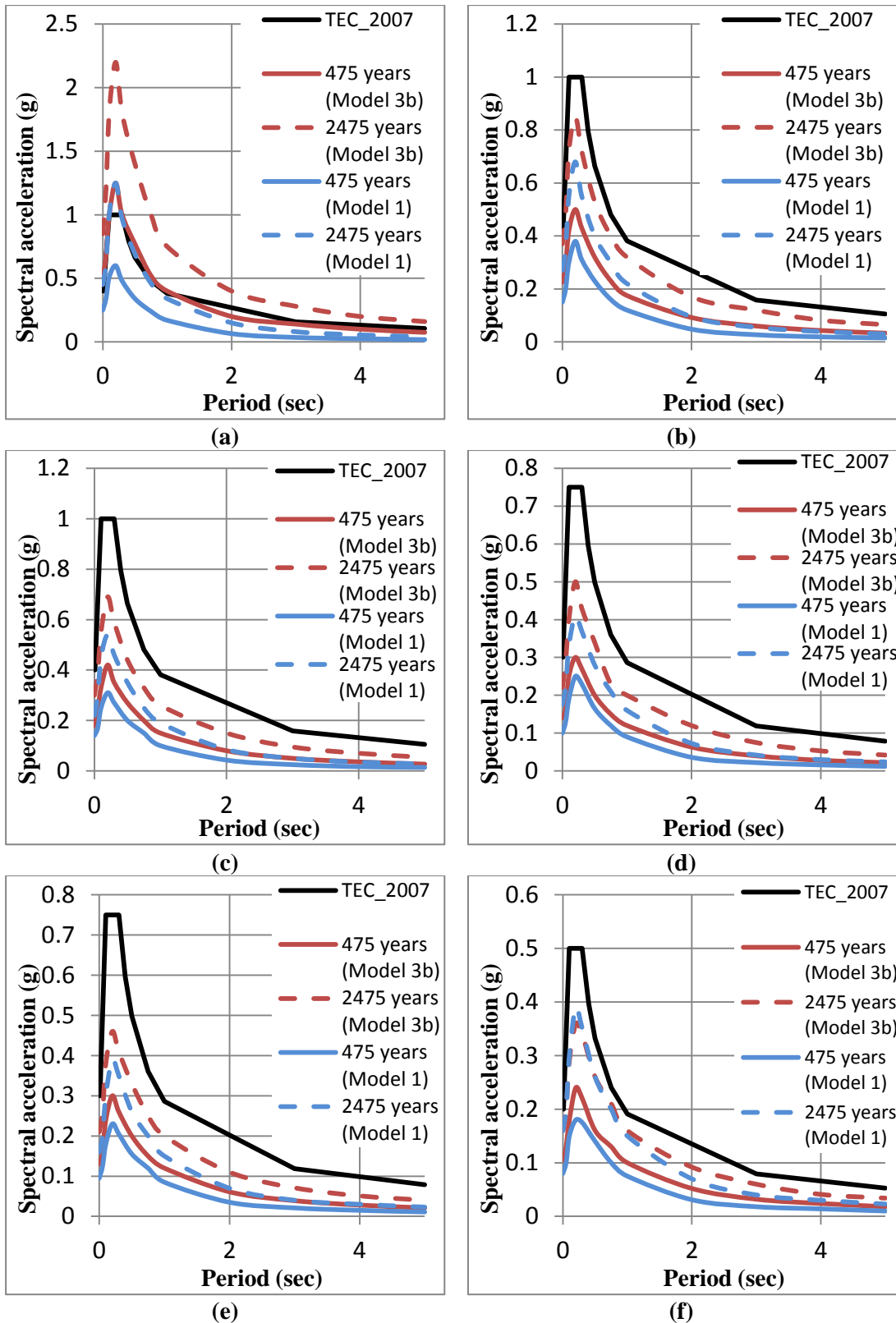
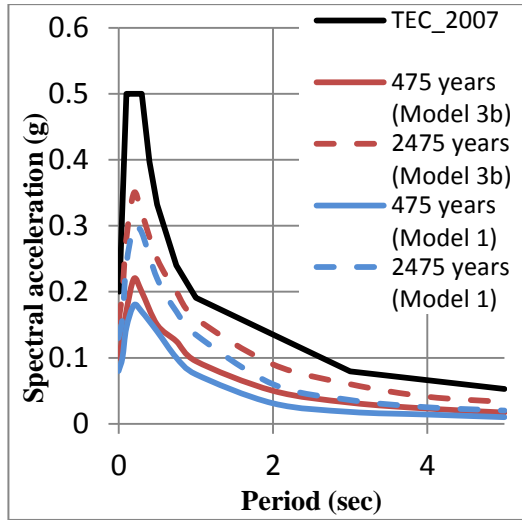
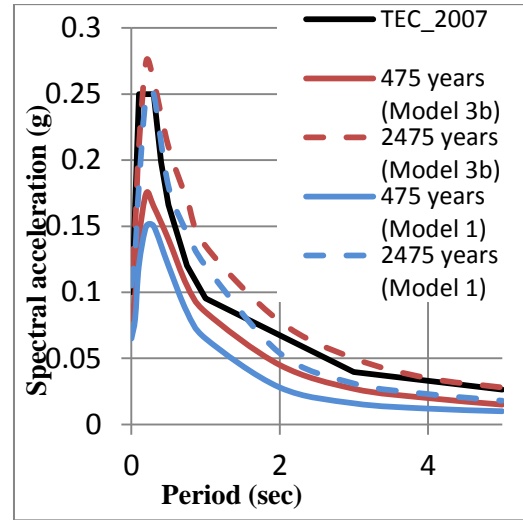


Figure 4.3: UHS for the (a): Site 20, (b): Site 8, (c): Site 7, (d): Site 9, (e): Site 18, (f): Site 6, (g): Site 17, (h): Site 22 , all located near the center part of the Niksar-Erzincan segment of NAF Zone. The red solid and broken lines represent the UHS for Model 3b and the blue solid and broken lines represent the UHS for for 475 and 2475 year return period for Model 1. The black solid line represents the TEC-2007 for each site.

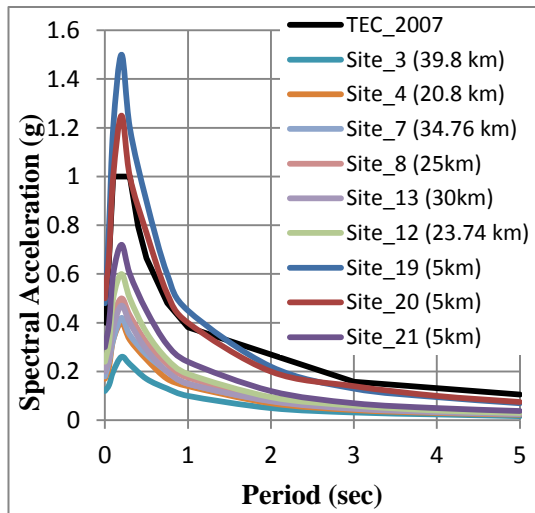


(g)

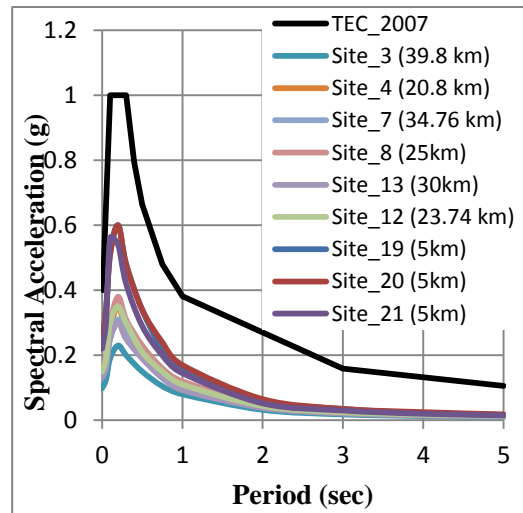


(h)

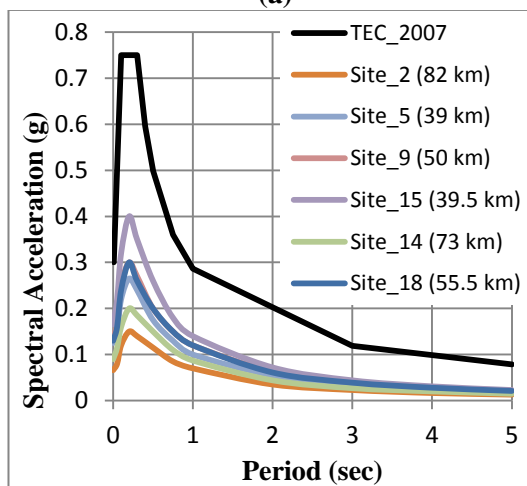
Figure 4.3: (Continued)



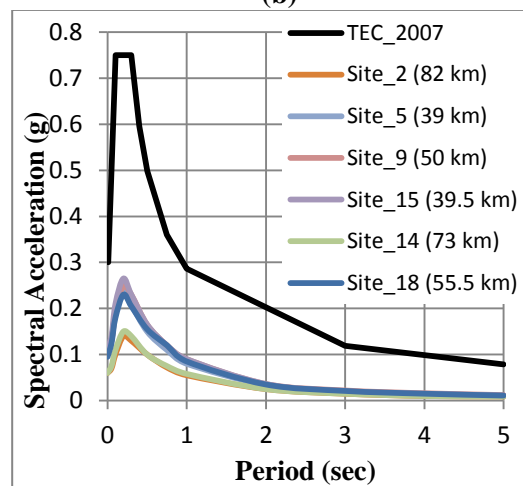
(a)



(b)



(c)



(d)

Figure 4.4: UHS for the sites located within the boundaries of (a): Zone 1, (c): Zone 2, (e): Zone 3, (g): Zone 4 for Model 3b and, (b): Zone 1, (d): Zone 2, (f): Zone 3, (h): Zone 4 for Model 1.

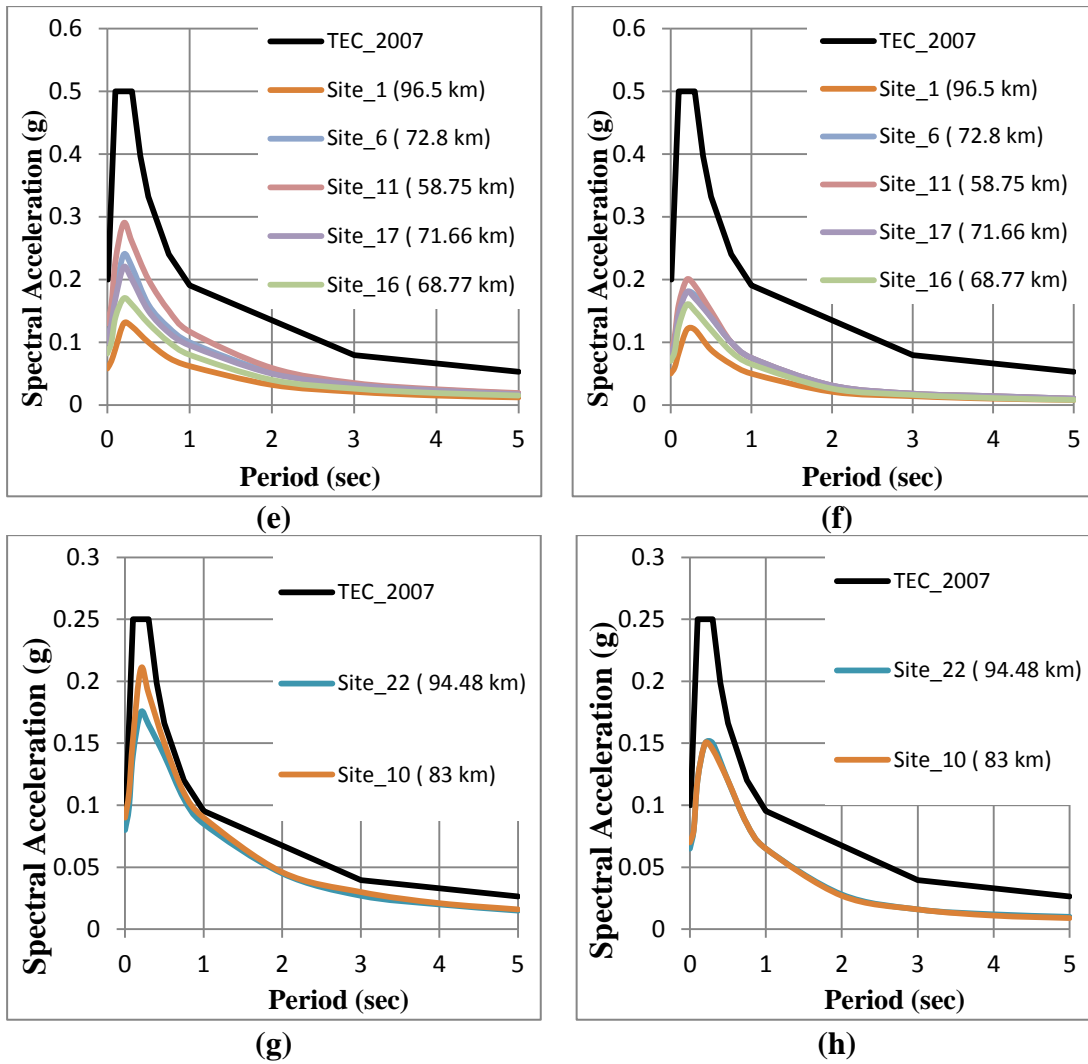


Figure 4.4: (Continued)

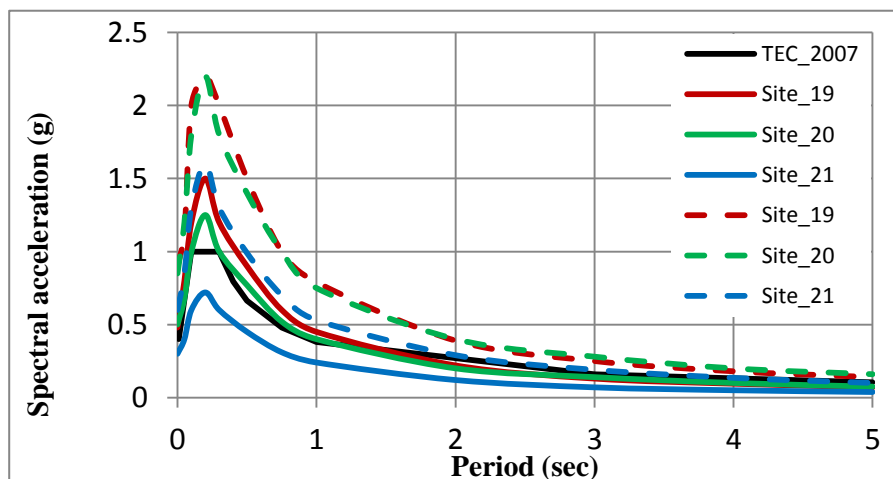


Figure 4.5: UHS for Site 19, 20 and 21 of this study. The solid and broken lines represent the UHS for 475year and 2475 year return periods respectively. The black solid line represents the TEC-2007 design spectrum for rock site conditions.

CHAPTER 5

SUMMARY AND DISCUSSION

The primary objective of this study was to quantify the effects of different approaches in seismic source modeling on the PSHA results and design ground motions in the near-fault and far-field regions. Four different seismic source models are developed by using areal or planar source geometries (or a combination of both) and by employing different magnitude distribution models based on the widespread applications in the current PSHA practice. Niksar-Erzincan segment of NAF zone is selected in this example since almost all fault parameters required to develop a full fault rupture model are available for this well-defined tectonic structure.

Analysis results show that the variances in the hazard results obtained by different seismic source models are closely correlated with the source to site distances and the desired hazard level. For near-fault regions, design ground motions estimated by adopting areal source zones in the PSHA are significantly and systematically smaller than the results of PSHA based on fault models. Therefore, seismic source models composed of merely areal source zones should be excluded from the PSHA logic trees if adequate information related to the fault zone for developing planar source models is available. Analysis results also indicated that when the source models that combine the characteristic behavior of faults and exponential distribution of small-to-moderate magnitudes either by defining fault lines and surrounding buffer zones (Model 2) or planar faults alone (Model 3b) are developed, the hazard results are quite stable both in the near-fault and far-field regions. However, the threshold magnitude should be selected carefully to prevent the overlap of assigned rates to moderate magnitude earthquakes in the buffer zone and in single or multi-segment fault sources. In that sense, using planar fault models without buffer zones and

combining the rates by employing the composite magnitude recurrence model should be preferred.

One of the most valid arguments in preferring the simplified areal source zones for active tectonic structures instead of planar fault geometries is the missing fault parameters or data such as fault width (or seismogenic depth), annual slip rate, recurrence characteristics, and segmentation models. While building the planar source models, several assumptions and/or simplifications had to be made to define the fault parameters and the associated uncertainty. The hazard analysts should be utterly familiar with all aspects of the PSHA framework to develop a common sense on the sensitivity of the hazard outcome to different source models and model parameters. Unfortunately, most of the PSHA studies are published as consultancy reports and are not open to public; therefore, experience from previous practice is not effectively transferred to current PSHA works. In this study, we also aimed to provide some insight on the effect of source or fault parameters on the final hazard outcome by presenting series of sensitivity analyses. Following interpretations can be made based on the sensitivity analysis results:

- If an areal source zone is preferred, then the seismicity (or the instrumental catalogue) dominates the behavior of the source model and the recurrence model parameters (especially the b-value) bring in the largest uncertainty to the PSHA results. Therefore, the factors affecting the b-value such as the source zone boundaries, catalogue completeness intervals, catalogue declustering, and regression methodology should be properly considered and the involved uncertainty should be included in the logic tree.
- When the planar fault models are used, then the large rates of moderate-to-large magnitude events dominate the hazard curve, especially for the hazard levels used for standard engineering applications. Therefore, the uncertainties introduced by the fault parameters such as fault width, annual slip rate, scenario weights, etc. are significantly larger than the uncertainties involved in the seismicity parameters. The recurrence parameters (a- and b-values) lose their significance completely in planar fault models.
- Analysis results showed that the effect of fault width, scenario weights and annual slip rate on the final hazard curve is comparable for all models including planar fault geometries. These parameters may change the hazard results by 15-

20% in the near fault regions but they are almost negligible for far field sites ($R_{rup} > 40$ km). It should be noted that the sensitivity analysis conducted here only includes a “reasonable” range of variation for these parameters. The effect would have been higher if the parameters are stretched out to extreme values.

- Among the other catalogue and fault characteristic parameters, the effect of maximum magnitude (or M_{char}) on the hazard curve is more significant than others for planar source models. Results presented here confirmed that a logic tree including proper fault segmentation models that considers multi-segment ruptures and the uncertainty in magnitude-rupture area relations is inevitable in PSHA.

To examine the effect of seismic source model on the ground motions for other spectral periods, 22 example sites are selected and the UHS for 475 and 2475 years return periods based on areal (Model 1) and planar (Model 3b) source models are compared with the TEC-2007 requirements. Following interpretations can be made based on these comparisons:

- The results showed that, the effect of selected source model is consistent for all spectral periods. Similar to design PGA levels, the design spectral accelerations between 0.01-1 second spectral periods obtained by areal source model are more than 50% lower than given by planar fault source, especially for near fault sites.
- The Earthquake Zone 1 defined in TEC-2007 is unrealistically large and completely ignores the change in the design ground motions within the 50 km buffer around the NAF Zone. The UHS for almost all sites are lower than the TEC-2007 design spectrum both for Model 1 and Model 3b. The difference between the UHS and TEC-2007 recommendations is substantial for planar fault models, but less significant for areal sources.
- The difference between the UHS and TEC-2007 design spectrum decrease as the distance between the site and source increases. For Zones 2 and 3 the UHS based on both source models are far below the TEC-2007 requirements but the disagreement between the UHS and TEC-2007 recommendations is smaller for Zone 4.
- Even if it is not explicitly mentioned in TEC (2007), the PGA values at 10% probability of exceedance in 50 years were adopted from Gülkan et al. (1993)

for each seismic zone and Gülkan et al. (1993) utilized one of the early-stage ground motion prediction equations and truncated the ground motion variability with approximately $\pm 1\sigma$. However, in this study two different GMPEs are adapted and the ground motion variability is truncated with $\pm 3\sigma$.

- TEC2007 considers the very stiff clay and silty clay soils with drift wave velocities between 300-700 m/s (Group (B)) as rock site conditions. In this study the rock site conditions are defined by $V_{S30} = 760$ m/s, which may be another reason for the difference between these results.

It is noteworthy to mention that no comprehensive sensitivity analysis on the effects on the hazard estimates by changing the selected GMPEs are conducted in this study. However, Vakilinezhad et al. (2013) showed that selecting different GMPEs induce substantial changes in the final hazard estimates.

REFERENCES

- Abrahamson, N. (2006). Seismic hazard assessment: problems with current practice and future developments. *First European Conference on Earthquake Engineering and Seismology*, Geneva, Switzerland, 3-8 September 2006.
- Abrahamson, N., & Silva, W. (2008). Summary of the Abrahamson & Silva NGA Ground-Motion Relations. *Earthquake Spectra*, 24(1), 67–97.
- Aki, K. (1965). Maximum likelihood estimate of b in the formula $\log N = a - bM$ and its confidence limits. *Bull. Earthq. Res. Inst.*, 43, 237-239.
- Akkar, S., Çağnan, Z., Yenier, E., Erdoğan, Ö., Sandıkkaya, M. A., & Gülkan, P. (2010). The recently compiled Turkish strong motion database: preliminary investigation for seismological parameters. *Journal of Seismology*, 14(3), 457–479.
- Ambraseys, N.N., and Finkel, C.F. (1987). The Anatolian earthquake of 17 August 1668. In: Lee, W.H.K., Meyers, H., and Shimazaki, K. (eds.). *Historical Seismograms and Earthquakes of the World: Academic Press, New York*, 173-180.
- Atakan, K., A. Ojeda, M. Meghraoui, A. A. Barka, M. Erdik, and A. Bodare (2002). Seismic hazard in Istanbul following the 17 August 1999 Izmit and 12 November Duzce earthquakes. *Bull. Seism. Soc. Am.*, 92, 466-482.
- Barka, A. (1996). Slip distribution along the North Anatolian fault associated with the large earthquakes of the period 1939 to 1967. *Bulletin of Seism. Soc. of Am.*, 86, 1238–1254.

- Bender, B. (1986). Modeling source zone boundary uncertainty in seismic hazard analysis, *Bull. Seism. Soc. Am.*, 76, 329–341.
- Bender, B. (1987). Effects of observational errors in relating magnitude scales and fitting the Gutenberg-Richter parameter β . *Bull. Seism. Soc. Am.*, 77, 1400-1428.
- Bender, B., and Perkins, D. (1993). Treatment of parameter uncertainty and variability for a single seismic hazard map. *Earthquake Spectra*, 2(9), 165-195.
- Bernreuter, D. L., J. B. Savy, R. W. Mensing, and J. C. Chen (1989). Seismic hazard characterization of 69 nuclear power plant sites east of the Rocky Mountains. *U.S. Nuclear Regulatory Commission Report*, NUREG/CR-5250.
- Bernreuter, D., Savy, J., & Mensing, R. (1987). Seismic hazard characterization of the eastern United States: Comparative evaluation of the LLNL and EPRI studies. *May 1987, Report*, 288 p.
- Bommer, J. J., Stafford P. J., and Akkar S. (2010). Current empirical ground-motion prediction equations for Europe and their application to Eurocode 8. *Bulletin of Earthquake Engineering*, 8 (1), 5 -26.
- Boore, D. M., and Atkinson, G. M. (2008). Ground-motion prediction equations for the average horizontal component of PGA, PGV, and 5%-damped PSA at spectral periods between 0.1 s and 10.0 s. *Earthquake Spectra*, 24 (1), 99-138.
- Bradley, B. (2013). A New Zealand-Specific Pseudospectral Acceleration Ground-Motion Prediction Equation for Active Shallow Crustal Earthquakes Based on Foreign Models. *Bulletin of the Seismological Society of America*, vol. 103 no. 3 1801-1822.
- Campbell, K. W., and Bozorgnia, Y. (2008). NGA ground motion model for the geometric mean horizontal component of PGA, PGV, PGD and 5%-damped linear elastic response spectra for periods ranging from 0.1 s to 10.0 s. *Earthquake*

Spectra, 24 (1), 139 -171.

Chiou, B. S.-J., and Youngs, R. R. (2008). An NGA model for the average horizontal component of peak ground motion and response spectra. *Earthquake Spectra*, 24 (1) , 173 -215.

Cornell, C. (1968). Engineering seismic risk analysis. *Bulletin of the Seismological Society of America*. Vol. 58 no. 5, 1583-1606.

Crowley, H. and Bommer, J.J. (2006) Modelling seismic hazard in earthquake loss models with spatially distributed exposure. *Bulletin of Earthquake Engineering*, vol.4. , 279-273.

Dewey, J. W. (1976). Seismicity of Northern Anatolia. *Bulletin of the Seismological Society of America*, 66(3), 843–868.

Emre, Ö., Duman, T.Y., Duman, S., Özalp, S. (2013). Active Fault Map of Turkey with an Explanatory Text, Publications of the Mineral Research and Exploration (MTA), Ankara.

Emre, O., Kondo, H., Ozalp, S., Elmaci, H., and Kurcer, A. (2010). Fault geometry and slip distribution associated with the 1939 Erzincan Earthquake (M: 7.9), North Anatolian Fault. *EGU General Assembly Conference Abstracts*, 12, 2551.

EPRI/SOG (1987a). Seismic hazard methodology for the Central and Eastern United States, Vol1: Methodology. NP-4726, Research Projects P101-38, -45,-46, 2556-14. Prepared by Risk Engineering, Inc., Geomatrix Consultants, Inc., Woodward-Clyde Consultants and Cygna Corporation for Seismicity Owners Group and Electric Power Research Institute, 3412 Hillview Ave., Palo Alto, CA 94304.

EPRI/SOG (1987b). Seismic hazard methodology for the Central and eastern United States Vol IV: Applications, NP-4726, Research Project P101-47. Prepared by Jack R. Benjamin and Associates, Inc., 444 Castro St., Mountain View, CA

94701.

Erdik, M., Demircioglu, M., Sesetyan, K., Durukal, E., & Siyahi, B. (2004). Earthquake hazard in Marmara Region, Turkey. *Soil Dyn. and Eq. Engineering*, 24(8), 605–631.

Erdik, M., Doyuran, V., Akkaş, N., & Gülkan, P. (1985). A probabilistic assessment of the seismic hazard in Turkey. *Tectonophysics*, 117(3-4), 295–344.

Erturaç, M., & Tüysüz, O. (2012). Kinematics and basin formation along the Ezinepazar-Sungurlu Fault Zone, NE Anatolia, Turkey. *Turkish Journal of Earth Sciences*. Vol.21, 497-520.

Field, E. H., T. E. Dawson, K. R. Felzer, A. D. Frankel, V. Gupta, T. H. Jordan, T. Parsons, M. D. Petersen, R. S. Stein, R. J. Weldon II, and C. J. Wills (2009). Uniform California earthquake rupture forecast, version 2 (UCERF 2), *Bull. Seismol. Soc. Am.*, 99, no. 4, 2053–2107.

Gardner, J., and Knopoff, L. (1974). Is the sequence of earthquakes in southern California, with aftershocks removed, Poissonian. *Bull. Seismol. Soc. Am.*, 64(5), 1363-1367.

Grunthel, G., Bosse, C., Sellami, S., Mayer-Rosa, D., Giardini, D. (1999). Compilation of the GSHAP regional seismic hazard map for Europe, Africa and the Middle East. *Ann Geofis*, 42(6), 1215–1223.

Gülerce, Z., Kargioğlu, B., and Abrahamson, N. A. (2015). Turkey-Adjusted NGA-W1 Horizontal Ground Motion Prediction Models. *Earthquake Spectra*.

Gülerce, Z., Erkan Yılar, Mert Levendoğlu, Marjan Vakilinezhad, Barış Güner, Fuat Şaroğlu, A. Arda Özacar and Nuretdin Kaymakçı, Seismic Hazard Maps for 1939-1944 Earthquake Rupture Zones on NAF (*in preparation for Earthquake Spectra*).

Gülerce, Z., & Ocak, S. (2013). Probabilistic seismic hazard assessment of Eastern

- Marmara Region. *Bulletin of Earthquake Engineering*, 11,1259–1277.
- Gülkan, P., Kocuyigit, A., & Yüçemen, M. (1993). En Son Verilere Göre Hazırlanan Türkiye Deprem Bölgeleri Haritası. *ODTU Deprem Muhendisligi Arastırma Merkezi*, Rapor No. 93–01 (In Turkish).
- Gürsoy, H., Tatar, O., Akpınar, Z., Polat, A., Mesci, L., & Tunçer, D. (2013). New observations on the 1939 Erzincan Earthquake surface rupture on the Kelkit Valley segment of the North Anatolian Fault Zone, Turkey. *Journal of Geodynamics*, 65, 259–271.
- Gutenberg, B., & Richter, C. F. (1944). Frequency of earthquakes in California. *Bull. Seismol. Soc. Am.*, 34, 185–188.
- Hanks, T. C., & Kanamori, H. (1979). A moment magnitude scale. *Journal of Geophysical Research*, 84(B5), 2348.
- Hartleb, R. D. (2003). A 2000-Year-Long Paleoseismologic Record of Earthquakes along the Central North Anatolian Fault, from Trenches at Alayurt, Turkey. *Bulletin of the Seismological Society of America*, 93(5), 1935–1954.
- Hecker, S., Abrahamson, N. A., and Wooddell, K. E. (2013). Variability of Displacement at a Point: Implications for Earthquake-Size Distribution and Rupture Hazard on Faults. *Bulletin of the Seismological Society of America*, 103(2A), 651–674.
- Hubert-Ferrari, A. (2002). Morphology, displacement, and slip rates along the North Anatolian Fault, Turkey. *Journal of Geophysical Research*, 107(B10), 2235.
- Hubert-Ferrari, A., King, G., Woerd, J. v. d., Villa, I., Altunel, E., & Armijo, R. (2009). Long-term evolution of the North Anatolian Fault: new constraints from its eastern termination. *Geological Society, London, Special Publications*, 311(1), 133–154.

- Idriss, I. (2008). An NGA empirical model for estimating the horizontal spectral values generated by shallow crustal earthquakes. *Earthquake Spectra*, 24 (1), 217-242.
- Ishibe, T., and Shimazaki, K. (2012). Characteristic Earthquake Model and Seismicity around Late Quaternary Active Faults in Japan. *Bulletin of Seism. Soc. of Am.*, 102(3), 1041–1058.
- Kagan, Y. Y. (1996). Comment on“ The Gutenberg-Richter or characteristic earthquake distribution, which is it?” by Steven G. Wesnousky. *Bulletin of the Seismological Society of America*, 86, 274–285.
- Kalafat, D., Güneş, Y., Kara, M., Deniz, P., Kekovali, K., Kuleli, H.S., Gülen, L., Yilmazer, M., Özel, N.M., (2011). *A revised and extended earthquake catalogue for Turkey since 1900 ($M \geq 4.0$)*.
- Kalkan, E., Gülkan, P., Yilmaz, N., Çelebi, M. (2009). Reassessment of probabilistic seismic hazard in the Marmara Region. *Bull. Seism. Soc. Am.*, 99(4), 2127–2146.
- Ketin, I. (1948). Über die tektonisch-mechanischen Folgerungen aus den großen anatolischen Erdbeben des letzten Dezenniums. *Geologische Rundschau*, 36-36(1), 77–83.
- Kramer, S.L. (1996). Geotechnical Earthquake Engineering. *Prentice Hall, Upper Saddle River, New Jersey*. 653 pp.
- McClusky, S., Balassanian, S., Barka, A., Demir, C., Ergintav, S., ..., Vies, G. (2000). Global Positioning System constraints on plate kinematics and dynamics in the eastern Mediterranean and Caucasus. *J. Geophys. Res.*, 105, 5695–5719.
- McGuire, R. K. (1977). Effects of uncertainty in seismicity on estimates of seismic hazard for the east coast of the United States. *Bull. Seism. Soc. Am.*, 67, 827- 848.
- McGuire, R. K. (2004). Seismic hazard and risk analysis. EERI Monograph MNO-

10. *Earthquake Engineering Research Institute*, Oakland, California.

McGuire, R. K. and Shedlock, K. M. (1981). Statistical uncertainties in seismic hazard evaluations in the United States. *Bull. Seism. Soc. Am.*, 71 (4), 1287-1308.

McKenzie, D. (1972). Active Tectonics of the Mediterranean Region. *Geophysical Journal International*, 30(2), 109–185.

Pacific Gas & Electric Company (2010). Verification of PSHA code Haz43. GEO.DCPP.10.03 Rev 0.

Probabilistic Seismic Hazard analysis for Swiss Nuclear Power Plant Sites (PEGASOS project) (2004). *Open-File report*, V1.

Petersen, M., Frankel, A., and Harmsen, S. (2008). Documentation for the 2008 update of the United States national seismic hazard maps. *USGS Open-File Report*, 2008–1128.

Reilinger, R., McClusky, S., Vernant, P., Lawrence, S., Ergintav, S., Cakmak, H., ..., Karam, G. (2006). GPS constraints on continental deformation in the Africa-Arabia-Eurasia continental collision zone and implications for the dynamics of plate interactions. *Journal of Geophysical Research*, 111 (B05), 411.

Reiter, L. (1990). *Earthquake Hazard Analysis: Issues and Insight*. Columbia University Press, New York.

Scasserra, G., & Stewart, J. (2009). A comparison of NGA ground-motion prediction equations to Italian data. *Bulletin of the Seismological Society of America*, 99(5), 2961-2978 .

Schwartz, D., & Coppersmith, K. (1984). Fault behavior and characteristic earthquakes: Examples from the Wasatch and San Andreas fault zones. *Journal of Geophysical Research: Solid Earth*, 89(B7), 5681–5698.

- Shoja-Taheri, J., Naserieh, S., & Hadi, G. (2010). A test of the applicability of NGA models to the strong ground-motion data in the Iranian plateau. *Journal of Earthquake Engineering*, 14, 278-292.
- Stafford, P., Strasser, F., & Bommer, J. (2008). An evaluation of the applicability of the NGA models to ground-motion prediction in the Euro-Mediterranean region. *Bull Earthquake Eng.*, 6, 149-177.
- Stein, R. S., Barka, A. A., and Dieterich, J. H. (1997). Progressive failure on the North Anatolian fault since 1939 by earthquake stress triggering. *Geoph. J. Int.*, 128, 594–604.
- Stirling, M. (1996). Fault trace complexity, cumulative slip, and the shape of the magnitude-frequency distribution for strike-slip faults: a global survey. *Geoph. J. Int.* 124 (3), 833-868 .
- Tatar, O., Poyraz, F., Gürsoy, H., Cakir, Z., Ergintav, S., Akpınar, Z.,..., Yavaşoğlu, H. (2011). Crustal deformation and kinematics of the Eastern Part of the North Anatolian Fault Zone (Turkey) from GPS measurements. *Tectonophysics*, 518-521, 55–62.
- Turkish Earthquake Code (2007) Specification for structures to be built in disaster areas. Ministry of Public Works and Settlement, Ankara.
- Vakilinezhad, M., Levendoğlu, M., Gülerce, Z. and Şaroğlu, F., (2013). Effect of Fault Characteristics on the Probabilistic Seismic Hazard Assessment Results, *Proceedings of International Conference on Earthquake Engineering*, 29-31 May 2013, Skopje.
- Weichert, D. (1980). Estimation of the earthquake recurrence parameters for unequal observation periods for different magnitudes. *Bull. Seismol. Soc. Am.*,70, 41337-1346.

- Wells, D. L., and Coppersmith, K. J. (1994). New Empirical Relationships among Magnitude, Rupture Length, Rupture Width, Rupture Area, and Surface Displacement. *Bulletin of the Seismological Society of America*, 84, 974–1002.
- Wesnousky, S. G. (1994). The Gutenberg-Richter or characteristic earthquake distribution, which is it? *Bulletin of the Seismological Society of America*, 84(6), 1940–1959.
- Working Group on California Earthquake Probabilities (2003). Earthquake probabilities in the San Francisco Bay Region: 2002–2031. *U.S. Geological Society Open File, Report*, 03–214.
- Yavaşoğlu, H., Tari, E., and Tüysüz, O. (2011). Determining and modeling tectonic movements along the central part of the North Anatolian Fault (Turkey) using geodetic measurements. *Journal of Geodynamics*, 51(5), 339–343.
- Yılmaz-Öztürk, N. (2008). Probabilistic Seismic Hazard Analysis: a sensitivity study with respect to different models. Middle East Technical University , PhD Dissertation.
- Youngs, R. R., and Coppersmith, K. J. (1985). Implications of fault slip rates and earthquake recurrence models to probabilistic seismic hazard estimates. *Bull. Seismol. Soc. Am.*, 75, 939–964.
- Yılar, E. (2014). A sensitivity Study for Probabilistic Seismic Hazard Assessment of Sinop Nuclear Power Plant Site. Middle East Technical University, MS Thesis Dissertation.